Targeting the tumor microenvironment with co-delivery system using electrospun nanofibers

A proof-of-concept study in 3D tumor heterospheroids

Master Thesis - Biomedical Engineering (Bioengineering Technologies)
Research Group: BST- Targeted Therapeutics, TNW Faculty

Ornela Petrai (s2193515)

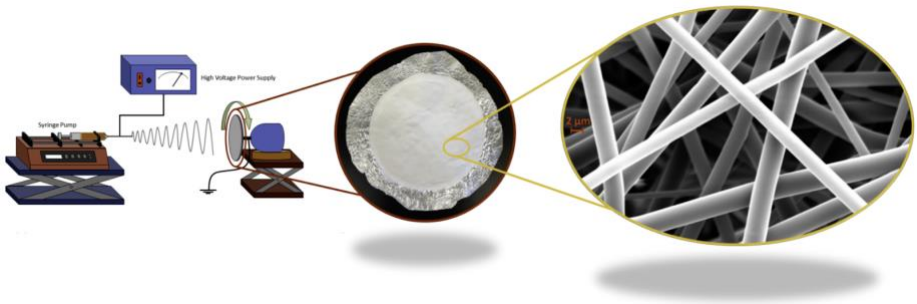

Graduation Committee

Committee Chair: Prof. Dr. Jai Prakash
Supervisor: Prof. Dr. Jai Prakash
Committee member UT: Dr. Andreas Poot
External member: Dr. Andries van der Meer
Co-supervisor: Ahmed Mostafa

UNIVERSITY OF TWENTE.

Abstract

Cancer is one of the most severe diseases, and many studies have been conducted to investigate possible treatments for it. Cancer is characterized by abnormal cell growth and the ability to invade tissue and distant organs. It is a lethal disease that can eventually cause death if the tumor has progressed beyond the stage that can be removed. Recent treatment mainly includes radiation therapy, surgery, targeted cancer treatment, and chemotherapy are the most used methods for treating various types of cancer. However, these methods usually lead to failures or not complete removal of the tumor site. What is needed is to combine treatment by administrating various drugs that are examined to inhibit and kill tumor cells and minimize the recurrence of cancer once it has been removed.

This project mainly focuses on breast cancer treatment even though the same method can be applied to various cancer types. Understanding the importance of the tumor microenvironment (TME) by promoting tumor migration, proliferation, and metastasis and enhancing the drug resistance that is occurred by stromal cells, we also focused on the TME activity. We explored the potential of electrospun nanofibers loaded with two different drugs, one chemotherapy which kills cancer cells, and one antistromal drug which inhibit the cancer-associated fibroblasts that are the most abundant cell type within TME. Electrospinning does not only provide an easy way for controlled drug delivery but also provides local drug delivery, which extends the delivery of the drug at the specific site, minimizing the cytotoxicity to the normal cells and maximizing the drug efficacy.

We explore the drug activities on 2D cultured cells and heterospheroids prepared with 3T3 fibroblasts and 4T1 breast tumor cells. Although the potential of paclitaxel is already known, the potential of FRAX597 still needs to be investigated. After the development of electrospun nanofibers and their characterization, dual-drug nanofibers were tested on heterospheroids. Drug-loaded nanofibers caused a significant decrease in the size and growth rate of spheroids. Notably, FRAX597 showed some promising results in cancer treatment, which killed tumor cells more efficiently than chemotherapy. In conclusion, co-therapy nanofibers can inhibit breast cancer cells based on the synergistic action of paclitaxel and the PAK1 inhibitor, FRAX597.

Preface

Almost three years after attending the University of Twente, I have finalized my master thesis project by earning so much knowledge, experience and meeting so many new friends. First of all, I wish to express my deepest gratitude to Prof. Dr. Jai Prakash for the opportunity to join the Targeted Therapeutics and conducting my master thesis under his supervision. Furthermore, I would like to thank Dr. Andreas Poot and Dr. Andries Van der Meer for being a member and the external member of my graduation committee.

Moreover, I would like to thank Ahmed Mostafa for his supervision and all the help he provided during these months. Furthermore, I am grateful to all the people whose assistance was a milestone in completing this project. So, special thanks to Hetty ten Hoopen and Marc Ankone for their help during my master thesis. Also, I would like to say a huge thank you to all the targeted therapeutic group, especially to Alessia, Marina, and Kunal, for all the support and help. Last but not least, special thanks to my parents, my sister, and my boyfriend, Filippos, for their unconditional love and support.

Table of Contents

Abbreviations

TME	Tumor Microenvironment
ES	Electrospinning
ECM	Extracellular matrix
NFs	Nanofibers
PCL	Poly-ε-caprolactone
CAFs	Cancer Associated Fibroblasts
PTX	Paclitaxel
FRAX 597	Fraxinellone 597
PLGA	Poly lactic-co-glycolic acid
PLLA	Poly (L-lactic acid)
PEG	Poly-ethylene glycol
DOX	Doxorubicin
EMT	Epithelial-mesenchymal transition
TAMs	Tumor Associated Macrophages
a-SMA	Alpha-smooth muscle actin
TAAs	Tumor associated adipocytes
TGF-β	Transforming growth factor β
PAKs	p21-activated kinases
DMF	N, N- Dimethylformamide
DCM	Dichloromethane
GRM	Growth Rate Measurements

1. Introduction

Cancer is the leading cause of death worldwide, accounting for approximately 10 million deaths; in 2020, the most common cancer was breast cancer, with 2.26 million cases and 695.000 deaths globally [1]. Every woman at any age after puberty can develop breast cancer, but with increasing rates in later life [1].

Early detection programs and different models of treatments for invasive cancer improved survival in the 1980s. Most cancers are treated surgically, with complete or partial removal of the tumor. However, other treatments can be applied, such as radiation therapy, chemotherapies, and targeted therapeutics. Targeted therapeutics' main goal is to deliver drugs at the site of interest by minimizing the toxicity and maximizing the therapeutic efficacy.

However, local or regional cancer recurrence happens in an average of 9% of cases within 5-10 years after surgery. Tumor recurrence happens because a small group of cancer cells remains after the tumor resection. Thus, a need to develop systems that effectively eradicate the residual tumor cells and hamper the local cancer relapse is noticeable.

Various drug delivery vehicles, including gels, films, particles, and fibers with extended drug discharge kinetics, have been explored as localized drug delivery systems. Among them, electrospun nanofibers have achieved remarkable attention during the last two decades due to their ideal characteristics for use as localized drug delivery devices containing micro-scale or nano-scale diameters, controllable surface morphology, very high surface area with high porosity, high drug loading, and entrapment capacity, synchronous delivery of various therapeutic agents and cost-effectiveness.

Remarkably, the tumor microenvironment (TME) is a promising target to reduce tumor progression and metastasis. Within TME, both cancer and nor cancerous cells can be targeted. Chemotherapeutic agents such as paclitaxel, doxorubicin, 5-Fluorouracil, capecitabine, and gemcitabine are widely used to inhibit cancer cells. However, non-cancerous cells can also be inhibited by drugs and molecules. Saridegib, vismodegib, paricalcitol, and FRAX597 are some of the molecules for targeting and inhibiting cancer-associated fibroblasts' activity. Cancer-associated fibroblasts, which are the most abundant cells within TME, can promote tumor functions and increase chemoresistance. Thus, their inhibition is crucial for increasing the treatment and inhibition of cancer.

1.1 Cancer - Epidemiology

Cancer is the leading cause of death worldwide, accounting for 13 million new cases, and almost 10 million cancer deaths occurred in 2020 [2]. The cause of cancer may be genetic factors or external factors such as physical (ultraviolet radiation), chemical (components of tobacco smoke), and biological (infections from viruses, bacteria, and parasites) carcinogens [3]. Cancer includes a large group of diseases expressed by uncontrolled cell growth and division. It is characterized by uncontrolled proliferation and abnormal differentiation; cancer cells do not follow the typical cell cycle, leading to apoptosis. They lose the contact of inhibition as cancer cells ignore signals to stop dividing and do not die. Furthermore, cancer cells can lose cohesiveness and adhesiveness by spreading to distant sites, circulating through blood and lymphatic vessels [4].

The global cancer burden expects to be 28.4 million cases in 2040, a 47% rise from 2020 [2]. Thus, it is really important to build a sustainable infrastructure for the dissemination of cancer prevention measures, and the provision of cancer treatment is critical for global cancer control.

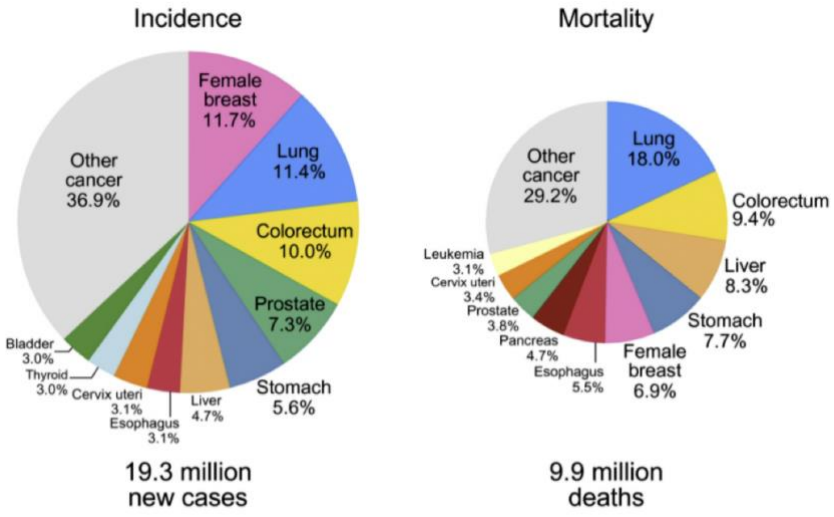

Figure 1: *Distribution of cases and deaths for the most common cancers in 2020* [2].

1.2 Current ways of cancer treatment

The increasing molecular and tumor biology knowledge has notably changed cancer treatment paradigms during the past 20 years. Cancer treatment allows surgery, radiation, medications, and other therapies to cure, shrink, or stop cancer progression. Cancer treatments can be classified into primary, (neo)adjuvant and, palliative treatment. The main goal of primary treatment is to remove cancer altogether. The most commonly used way to remove entire cancer from the body is surgery. Adjuvant treatment aims to kill any cancer cells that may remain after primary treatment to reduce the chance that cancer will recur. Common adjuvant treatments can be chemotherapies, radiation therapy, and hormone therapy [5] [6]

Similarly, neoadjuvant therapy can also be applied before the primary treatment to make the treatment more straightforward and effective. Furthermore, palliative treatment may be applied for relieving side effects of treatment of symptoms of cancer. Surgery, radiation, chemotherapy, and hormone therapy can all be used to relieve symptoms [5] [6].

As is already mentioned, many procedures and drugs are available to treat cancer. Some of them characterized ’local’ treatments such as surgery and radiation therapy to treat a specific tumor or area of the body. In contrast, drug treatments like chemotherapy, immunotherapy, and targeted therapy are named ‘systemic’ treatments to affect the entire body [5]. Next, the different ways of can treatments will briefly describe.

Surgery seems to be the most common treatment for many types of cancer. It is used to prevent, diagnose (biopsy) and treat cancer. During the operation, the mass of cancerous cells and some of the nearby tissue will be taken out [5] [6].

Radiation therapy uses high-energy particles or waves (x-rays, gamma rays, electron beams, or protons) to destroy or damage cancer cells. Radiation breaks DNA and prevents cancer cells from growing and diving, and leads to cell death. The main goals of radiation therapy are to cure or shrink early-stage cancer, to stop cancer from coming back (recurring) somewhere else, to treat symptoms caused by advanced cancer, and to treat recurred cancer [5] [6].

Chemotherapy includes drugs that are used for cancer therapy. Chemotherapy aims to cure cancer by destroying or shrinking and stop cancer from growing and spreading. In some cases that curing or controlling the tumor is not efficient. Chemotherapy is used for easing symptoms caused by cancer to improve the patient's quality of life [5] [6].

Targeted therapy applies drugs to stop cancer from growing and spreading. The difference between targeted therapy and chemotherapy is the targeted action. Traditional chemotherapy is cytotoxic to most cells by damaging healthy cells, while targeted therapy aims to affect the cancer cells and harm the normal cells less. Targeted treatment focuses on specific targets in cancer cells. The drug tries to prevent cancer cells from spreading [5] [6].

Immunotherapy relies on a patient's immune system to fight cancer. It can boost or change the way that the immune system works in order to attack cancer cells. Immunotherapy works by preventing or reducing the growth of cancer cells, inhibiting cancer from spreading, and promoting the immune system's competence to kill cancer cells. **Targeted therapy** uses drugs to stop cancer from growing and spreading. The difference between targeted therapy and chemotherapy is the targeted action. Traditional chemotherapy is cytotoxic to most cells by damaging healthy cells, while targeted therapy aims to affect the cancer cells and harm the normal cells less. Targeted treatment focuses on specific targets in cancer cells. The drug tries to prevent cancer cells from spreading [5] [6].

Hormone therapy is used to treat cancers powered by hormones such as breast, prostate, and ovarian cancers. This treatment blocks or alters hormones using surgeries or drugs to reduce or even stop the growth of cancer cells [5] [6].

Photodynamic therapy uses drugs that are sensitive to a particular type of light. These drugs stay in the cancer cells longer while light from a laser or other light source is directed at the cancer cells. The light promotes drugs to kill the cancer cells [6].

Hyperthermia, laser, and **cryotherapy** can also be applied for cancer treatment. Hyperthermia uses heat which is delivered from a machine outside the body to damage and kill cancer cells. Laser therapy uses a narrow and focused beam of light to destroy cancer cells, while cryotherapy applies cold gas to freeze and kill cancer cells [6].

1.3 Cancer treatment failures and side effects

In the previous section, the different cancer treatments have been analyzed to reduce and kill cancer cells to treat, control, or ease the cancer symptoms, providing an improved quality

of life. However, there are some disadvantages to these therapies. Here, the cancer treatment failures and side effects of the cancer treatment will be described.

Surgery may provide multiple side effects. Generally, the more complex the surgery is, the greater the risk of side effects. Surgery is an invasive treatment with bleeding, blood clots, damage to nearby tissues, drug reactions, pain, infection, and slow recovery rate to be the main drawbacks. Still, sometimes surgery is not enough to kill cancer cells and avoid recurrence [7].

Radiation therapy also has some disadvantages. Its side effects divide into early and late. The early happens during therapy or shortly after, and the late develop after months or even years. The common side effects are fatigue, skin problems, hair loss, and low blood counts [7].

Chemotherapies are drugs that try to kill cancer cells which are usually growing very fast. When chemotherapies travel throughout the body, they can also affect normal, healthy cells growing fast. Chemotherapies can occur side effects such as fatigue, hair loss, bleeding, infection, anemia, appetite, weight, mood changes, organ failures, and fertility problems [7].

Targeted therapeutics most common side effects are skin problems, high blood pressure, bleeding or blood clotting problems, slow wound healing, heart damage, and autoimmune reactions [7].

Immunotherapy disadvantages started from the limit of this therapy to be applied in various cancers. Moreover, there are common side effects such as fever, weakness, nausea, diarrhea, and low blood pressure [7].

Hormone therapy is a cancer treatment method applied to specific cancer types and is usually combined with additional treatment. The main side effects are fatigue, blood clots, memory problems, weight changes, and a higher risk of other cancer types [7].

Most of the proposed therapies are invasive treatments, and even if the side effects are not always lethal, the quality of life of patients will negatively change. In the last years, nanomedicine has developed promising drug delivery methods to prevent or eliminate the side effects of controversial treatments. Controlled delivery systems are promising aspects of minimizing the side effects and maximizing the drug delivery to the cancer site. However, targeting the site of interest may still be challenging as the tumor cells are surrounded by normal cells that make the chemotherapy penetration difficult, and also, the chemotherapeutic agents could also damage these normal cells. This complex environment that includes cancer cells, as well as non-cancerous cells, is essential to be studied in order to gain an efficient cancer treatment. This environment is named tumor microenvironment, and it will be further analyzed in the next section.

1.4 Tumor microenvironment and cancer-associated fibroblasts

In 1889, Stephen Paget referred to cancer cells as ‘seeds’ that grew inauspicious ‘soil’ the microenvironment of organs. In the last decades, the tumor microenvironment has been extensively studied[8]. The tumor microenvironment (TME) comprises proteins produced by cancerous and non-cancerous or stroma cells. It includes cells from immune, inflammatory and adipose systems, endothelial, mesenchymal, and fibroblasts cells [9], cancer-associated fibroblasts (CAFs), tumor-associated macrophages, pericytes [10], vascular cells, and extracellular matrix (ECM) [11]. TME is a cellular milieu that interacts with tumor cells and promotes tumor growth, proliferation, invasion, vascularization, and metastasis [12]. TME can regulate positively or negatively cancer [13], and the transformation of cells in the TME depends on genetic and environmental factors [8].

TME is a target environment for developing new anticancer drugs [14]. Within TME, there are different products such as metabolites, hypoxia, interstitial pressure, and pH changes that drive tumor growth and proliferation [14]. TME influences the penetration and distribution of therapeutic agents and produces factors and signals to regulate tumor cells [15]. Poor drug penetration and the increased drug resistance are the main complications of ineffective cancer treatment. CAFs are the main components of the TME that forms the 'soil' [15]. They can enhance drug resistance by providing tumor proliferation and supporting ECM, making drug penetration harder, and inserting adhesion-mediated drug resistance [16].

Cancer-associated fibroblasts (CAFs) are derived from many types of cells such as resident tissue fibroblasts, adipocytes, bone marrow-derived mesenchymal stem cells, hematopoietic stem cells, epithelial and endothelial cells [8]. CAFs are characterized as heterogeneous cell populations and are identified as smooth muscle actin α-SMA positive cells, while fibroblast activation protein alpha (FAP-/) and podoplanin have been considered biomarkers of CAFs population [17].

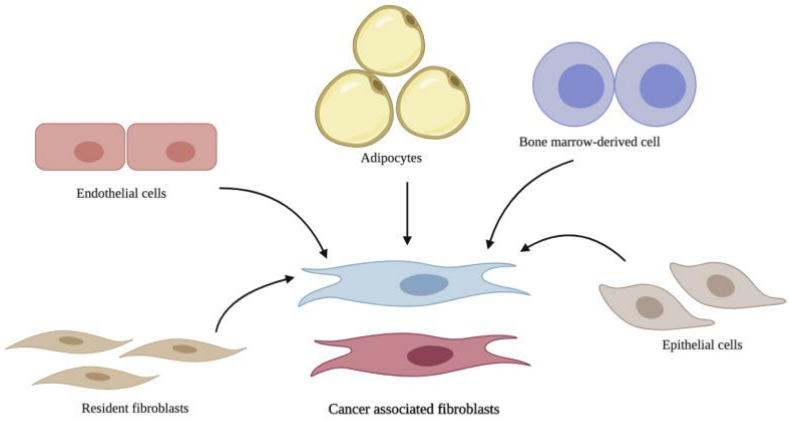

Figure 2: *Schematic diagram that shows that CAFs can be derived from resident fibroblasts, endothelial cells, adipocytes, bone marrow-derived cells, and epithelial cell types.*

Fibroblasts can be either in a quiescent or activated state. The origin of most fibroblasts is the primitive mesenchyme that arises from the mesoderm after gastrulation. Fibroblasts can also be derived from a part of the ectoderm, the neural crest. In normal physiology, fibroblasts produce the connective tissue ECM which plays an essential role in tissue repair. During the wound healing procedure, ECM produces transforming growth factor β (TGF-β). Fibroblasts at this stage are named myofibroblasts. Moreover, fibroblasts promote angiogenesis by producing vascular endothelial growth factor A (VEGFA) and promote cytokines and chemokines for immune system function. To summarize, quiescent fibroblasts are not only producers of ECM but also communicate with other cell types during tissue homeostasis and repair [18].

Compared to quiescent fibroblasts, CAFs are larger. They can produce several growth factors and cytokines, such as transforming growth factor-β (TGF-β) and vascular endothelial growth factor (VEGF), which benefit angiogenesis and improve the immunosuppressive cells to support immune evasion [14]. Additionally, compared to the quiescent fibroblasts that express vimentin, an intermediate filament protein, CAFs express alpha-smooth muscle actin (α-SMA). This protein describes the smooth muscle cells. Moreover, fibroblast-specific protein 1, fibroblast activation protein, palladin, platelet-derived growth factor and receptor, fibronectin, and others expressed in CAFs may express differently in different CAF populations within TME [10].

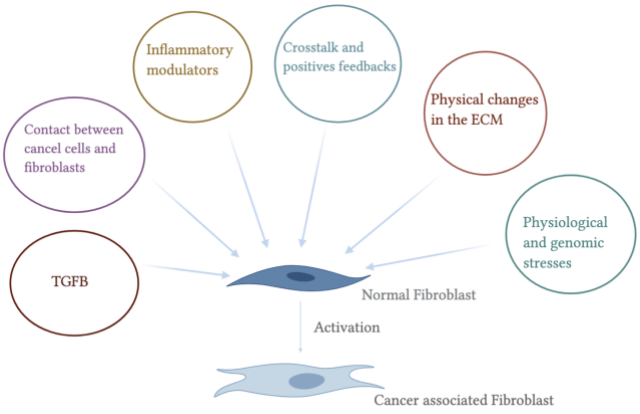

Figure 3: *Schematic diagram of various mechanisms of CAFs activation.*

Figure 3 presents the multiple mechanisms which may lead to CAF activation. TGF-β family ligands and lipid mediator lysophosphatidic acid trigger the activity of factors to drive the expression of CAFs marker α-SMA. Contact between cancer cells and fibroblasts may promote signaling pathways like Notch signaling in breast cancer, which promotes CAFs activation. Moreover, several inflammatory factors such as interleukin-1 (IL-1) acting through NF-kB and IL-6 through signal transducer can promote CAF activation. In addition, crosstalk and positive feedback, for example, Janus kinase - STAT signaling, boosts further CAFs activation. An additional mechanism that may lead to CAFs activation is the physical changes in the ECM and tissue stiffness, but also genomic and physiological stresses can result in changes in fibroblasts. For example, DNA mutation and double-stranded DNA breakage promote IL-6, and TGF-β family ligand may trigger CAFs activation. However, fibroblasts and activated fibroblasts can share some common transcription mechanisms, complicating the way the activation can be promoted [18].

1.5 Targeting the Tumor Microenvironment

Targeting the TME is a potential tool in controlling tumor progression [16]. Despite significant advances in anticancer drug development, the effective treatment of breast cancer is still prevented by the appearance of metastasis and therapy resistance. Anticancer therapy mainly focuses on the tumor cells; however, targeting the TME is a promising and potent instrument in regulating tumor progression.

Among the TME, CAFs are the main component of stromal cells within breast cancers and affect cancer resistance. Even though the origin of CAFs has not been understood, CAFs are demonstrated to play a crucial role in tumor development by supporting tumor survival, angiogenesis, and immune suppression [19]. In addition, CAFs promote tumor functions and increase chemoresistance. During the treatment with anticancer drugs, tumor cells are impaired through many pathways which change the TME. Chemotherapy activates CAFs to secrete cytokines that trigger pathways that inhibit the destruction of tumor cells [20].

Tumor survival is based on the energy sources such as glutamine and glucose and the interaction with numerous cells in the TME. CAFs contribute to that process by sharing and exchanging metabolites among cancer cells, which triggers a cascade pathway that results in

drug resistance. On the other hand, cancer cells also undergo some reactions to adapt to the poor glucose level. They switch their metabolic activity production to aerobic glycolysis. Tumor cells under aerobic glycolysis also lead stromal cells to apply aerobic glycolysis, leading to drug resistance [20]. Tissue stroma and extracellular matrix (ECM) also play an active role in cancer and drug resistance. ECM consists of many macromolecules such as collagen, laminin, fibronectin, and heparan sulfate proteoglycans (HSPGs). ECM maintains organ homeostasis and ensures cell-cell contact. In tumors, ECM is remodeling by several families of matrix-degrading enzymes. The remodeled ECM enhances the therapy resistance [21].

1.5.1 Drugs for targeting the TME

There are many ways to target the TME, and **Figure 4** are represented some therapeutic strategies for targeting. Among them, inhibitors of VEGF, PDGF signaling, anti-CAFs, anti-lymphatic targeting, anti-inflammatory, and anti-tumor targeting have been used to target different cells in TME.

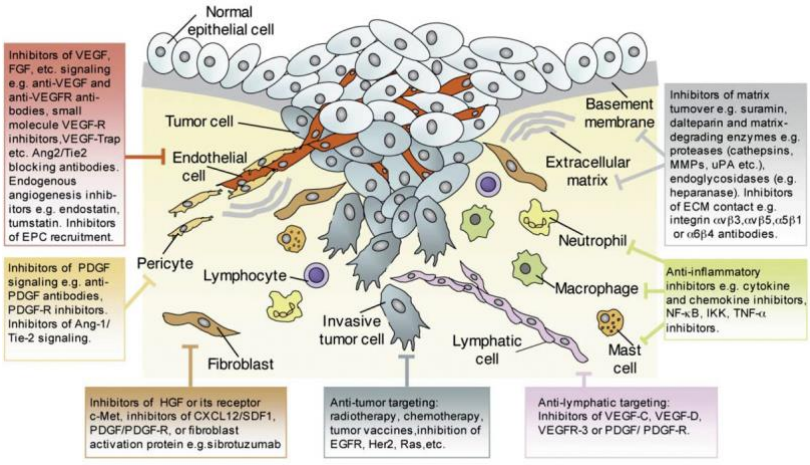

Figure 4: Therapeutic strategies to target different cells in TME [21].

Targeting the TME includes:

1. <u>Targeting tumor cells with traditional therapies such as chemotherapy</u>

Cancer is a heterogeneous disease, and choosing the appropriate chemotherapeutic drugs is crucial for the treatment. Chemotherapeutic drugs are separated into classes, including antimetabolites, immunologic therapy, alkylating agents of DNA, and antimitotic drugs. Antimetabolites are responsible for inducing apoptosis and are further classified into inhibitors of dehydrogenases, topoisomerases, nucleosides, and kinases. Among them, commonly used are methotrexate (dehydrogenase inhibitor) and DOX (class of topoisomerase II inhibitors). Further, 5-Fluorouracil, Capecitabine, and Gemcitabine are essential therapeutic drugs and nucleoside inhibitors associated with the silencing of transcription and translation in breast cancer [21]. The drawback of those is the complication during therapy because of the high level of toxicity [22]. Immunotherapy is also applied for cancer treatment. Some immunotherapies are Herceptin which blocks the extracellular domains of HER2 receptor tyrosine kinase, and ado-trastuzumab, which delivers inhibitory agents into breast cells with an increased level of HER2. Human epidermal growth factor receptor 2 (HER2) is overexpressed in around 20–30% the breast cancer[23].

Further, DNA alkylating agents interact with DNA and block DNA replication, and they are classified into platinum-based agents (cisplatin, carboplatin, oxaliplatin), nitrogen mustards

(cyclophosphamide, chlorambucil), and organophosphorus compounds (thiotepa)[22]. Also, taxanes (paclitaxel, cabazitaxel, and docetaxel) and alkaloids (vinblastine) are chemotherapy drugs derived from plants. Vinblastin acts as a microtubule-disruptive agent inhibiting tubulin polymerization, while taxanes are the most applied chemotherapies between patients with metastatic and early-stage breast cancer [22]. PTX, an antimitotic and anticancer drug, is clinically used to treat breast cancer and its mechanism of action is briefly presented in **Figure 5** [22].

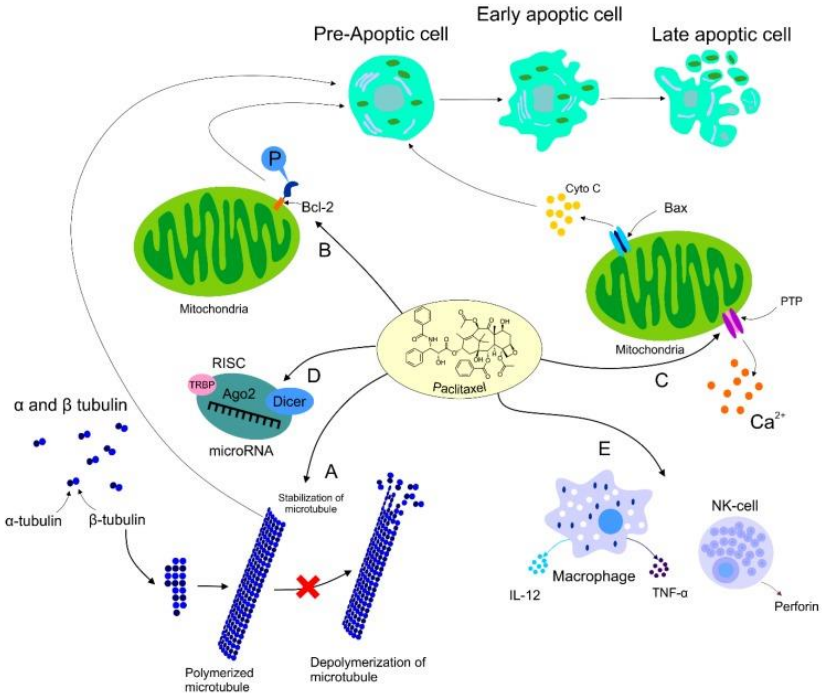

Figure 5: *Mechanism of action of PTX. PTX action results in stabilization of microtubule, cell arrest, and apoptosis (A). PTX activates the immune response leading to tumor eradication (B). PTX also inactivates Bcl-2 via phosphorylation of the anti-apoptotic protein causing apoptosis (C). Moreover, PTX modulates the tumor progression by regulating some specific miRNA (D), and PTX plays a vital role in the area of immunomodulation by stimulating and suppressing of immune cells associated with the tumor growth (E) [22].*

However, cancer treatment with PTX can lead to increased resistance and chemotherapy failure. The ATP-binding cassette, spindle assembly checkpoint (SAC), associated with the checkpoint function in PTX sensitivity, the alterations in the expression of microtubule-associated proteins (MAP), and molecular regulation mechanisms connected with miRNA expression play a crucial role in chemoresistance. However, the complex nature of chemoresistance is still not completely understood [22].

2. Targeting cancer-associated fibroblasts in the TME

TME is composed of various cells and secreted factors that are targets for anticancer therapy. Apart from heterogeneous cancer cells, immune cells (T and B lymphocytes, TAMS, DCs), stromal cells (CAFs, pericytes, mesenchymal stromal cells), blood cells, and tissue-specific cell types such as adipocytes are all composed of TME. All these cell types secrete

ECM components, cytokines, and growth factors contributing to tumor progression and therapeutic response. Many therapies have been developed and used, mainly focused on targeting TAMs, DCs, T cells, tumor vasculature, ECM, and CAFs (**Figure 6**) [24]. **Table 1** summarized the drugs and their mechanism of action and their target area for specific TME components.

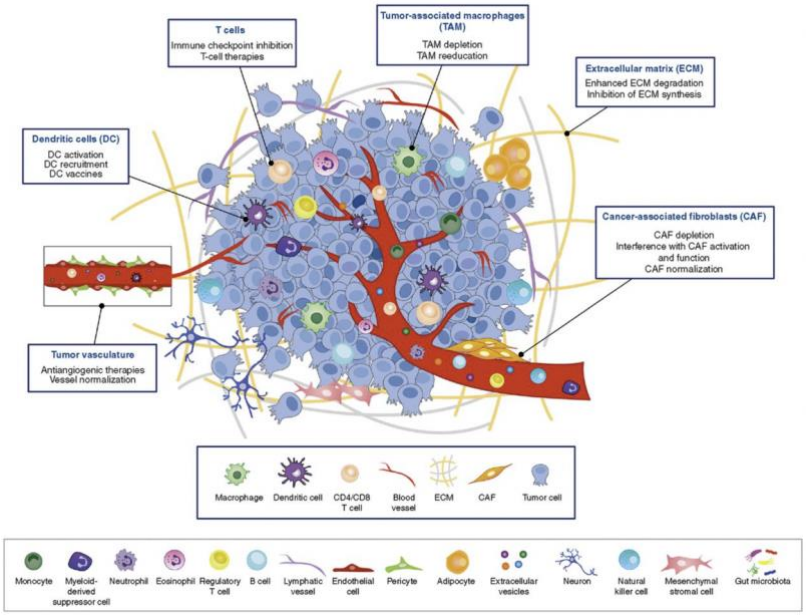

Figure 6: *TME composition and therapeutic strategies against them. With blue boxes are summarized therapies against TAMs, DCs, T cells, ECM and CAFs [24].*

Table 1: Drugs, target area and mechanism of actions for TAMs, DCs, immune cells, tumor vasculature and CAFs [24], [25].

Cell types	Target	Drugs	Mechanisms
TAMs	CSF1R	BLZ945	Reduces macrophage survival or leads to macrophage reeducation
Immune	PD-L1	Atezolizumab	Binds to PD-L1 to stop the interaction between PD-1 and PD-L1 in order to restore antitumor T-cell functions
Vasculature	VEGF/VEGFR	Aflibercept	Antiangiogenic therapy
CAFs	FAP-expressing cells	PT630, RO6874281, and sibrotuzumab	Interferes with CAF function, promotes T cell responses
CAFs	FGFR	Erdafitinib (JNJ-42756493)	Prevents CAF activation
CAFs	CXCR4	AMD3100	Interferes with CAF signaling
CAFs	Demosplastic melanoma	FRAX 597	Remodeling fibriotic TME

Small molecules with antifibrotic effects have also been studied to treat the TME. Mendruil Liu et al., in 2019, developed aminoethylanisamide (AEAA, ligand of sigma receptors) – targeted nanoemulsion system to deliver FRAX597 to CAFs. In that study, desmoplastic melanoma was used as a tumor model. After FRAX597 treatment, the amount of α-SMA+ CAFs significantly reduced, and FRAX597 provided inhibition on tumor growth and remodeled TME [26].

FRAX597 is a small-molecule pyridopyrimidinone that targets group 1 PAKs through binding to the ATP. However, studies provided that FRAX597 does target not only group 1 PAKs but also inhibits other kinases such as RET, YES1 TEK, and CSF1R [27]. Yeo et al., in 2016, showed that FRAX597 decreased proliferation and migration in pancreatic cancer cell lines in vitro and in vivo testing on an orthotopic murine model when combined with gemcitabine. This combination therapy further decreased tumor volume compared to therapy with each drug separately [27]. Moreover, Yeo et al., in 2017, reported that at 1 uM concentration [28], FRAX597 induced pancreatic stellate cells apoptosis. FRAX 597 inhibited PAK1 expression and activity and a-SMA expression under normoxia and hypoxia[28]. Antitumor effect of FRAX597 (1uM) has also been reported by Licciulli et al. by inhibiting the tumor proliferation and growth of *NF2*-null Schwann cells in vivo [29].

In conclusion, according to the above studies, FRAX597 is a promising antifibrotic drug with great antitumor and antistromal effects. However, there are only a few reports about the pharmacology of FRAX597 because most studies are focused on its anti-bacterial, anti-inflammatory, and neuroprotective properties [30],[31],[32]. Although the molecular mechanism of FRAX597 in cancer has not been characterized [25], it has been confirmed as an efficient PAK1 inhibitor. Importantly, p21-activated kinase 1 (PAK1) has also been identified as a regulator of CAF activation [28], so FRAX597 seems to be an attractive drug to inhibit CAFs activation.

1.6 Local drug delivery system

Advancements in nanomedicine and biomaterials have facilitated enhanced local delivery systems for cancer therapy, enhancing treatment efficacy while minimizing toxicity [33]. The advantages of local drug delivery systems are:

i. the enhancement of the stability of encapsulated chemotherapeutic agent and conservation of its chemotherapeutic effect [33]
ii. the controlled sustained and extended drug release behavior in combination with low systemic drug concentration [33]
iii. the loading capacity and release of poorly soluble chemotherapeutic agents [33]
iv. the specific targeting of the tumor and fewer medicine wastes [33]
v. the total amount of drug which needs to be loaded is decreased [33]
vi. the minimized systemic toxicities and adverse effects on normal cells [33]
vii. the used devices are usually biodegradable, so there is no need for surgical removal of the device [34]

A local delivery system contains foams, films, wafers, scaffolds, and fibers. Wang et al. have developed biodegradable poly- (D, L-lactic-co-glycolic acid) (PLGA) microporous foams to deliver prolonged paclitaxel release. PLGA microporous foam showed early burst release

over one month with zero-order kinetics in *vitro*. Foams with different ratios of paclitaxel and PLGA provided increased apoptotic activity in cell culture experiments due to the sustained release of the drug [34]. Furthermore, films are used in preclinical studies for post-surgical cancer treatment. Colson and coworkers have prepared poly (glycerol monostearate co-ε-caprolactone) polymer films (PGC-C18) for paclitaxel delivery to inhibit local tumor relapse. The tumor resection site implanted with PGC-C18 films showed a 3000-fold higher concentration of paclitaxel than that of systemic injection after ten days of treatment [34]. In the early 1980s, Langer and Brem developed GLIADEL wafers to deliver the drugs directly to the brain via bypassing the blood-brain barrier. In 2003, these wafers were upgraded with bis-chloroethyl nitrosourea (BCNU), and the survival time was increased from 336 days to 404 days in glioma patients [34]. Additionally, Chen et al. have developed therapeutic gels inside which CaCO3 nanoparticles were inserted to promote the local release of anti-DD47 antibodies. The authors also showed the improved inhibition of relapses of the tumor (tumors were not visible in 50 % of mice [34].

Last but not least, nanofibers are widely used for local drug delivery systems due to their high drug loading capacity, flexible conformation, large surface area, and adjustable size and shape. In 2010, for the first time, Carcaboso et al. developed poly(lactic acid) electrospun polymer nanofibers with SN-38 microcrystals for the localized treatment of pediatric solid tumors. Drug-loaded nanofibers assured significantly higher and more prolonged drug concentrations than cisplatin solution without increasing toxicity [34]. Since then, many chemotherapeutic agents such as cisplatin, doxorubicin, paclitaxel, 5-fluorouracil, docetaxel, and curcumin have been encapsulated into electrospun nanofibers for local chemotherapy after surgical resection. However, it is essential to note that electrospun nanofibers used for drug delivery systems are still preclinical and clinical trials [33].

Many studies are using electrospun nanofibers for local drug delivery. Zhang et al. developed a multi-layered nanofiber mat to inhibit the recurrence of cervical cancer in mice. The outer layer of the nanofiber mat was electrospun with dichloroacetate, which can selectively target the cancer cells and the inner layer was electrospun with Oxaliplatin, which is an anticancer drug. PLLA (poly-L-lactide) was used to separate and protect the two drug layers and allow their release. 50% - 80% of the postoperative recurrence of liver cancer was observed in patients. Jing and co-authors have used the electrospun nanofibers co-loaded with curcumin and cisplatin to treat the mice with cervical cancer. In that study, apoptosis was induced, and the growth of cervical cancer was inhibited. They concluded that combinational therapy was relatively more effective than systemic combination therapy [34]

Due to their high drug loading capacity, electrospun nanofibers can encapsulate and deliver multiple chemotherapeutic agents. Next, some examples of dual drug-loaded NFs delivery in different solid tumors will be discussed. Liu et al. (2015) developed sodium DCA and diisopropylamine dichloroacetate (DADA)-loaded PLA NFs tested on colorectal cancer, while Zhang et al. (2016) developed 5-Fluorouracil and oxaliplatin-loaded PLA NFs for colon cancer treatment. Additionally, Yang et al. (2014) fabricated DOX and curcumin-loaded mPEG-PCL micelles-loaded PVA NFs to treat cervical cancer, while Yuan et al. (2016) developed DOX and DOX-loaded mesoporous silica in PLLA NFs, to treat residual breast cancer cells [33].

The treatment of cancer cells with drug-loaded nanofibers can increase the concentration of drugs at local sites and decrease drug dosage. In that way, sustained delivery can be facilitated directly to the disease site, and the side effects usually associated with the systemic administration can be minimized. The nanofibers can provide a sustained release of drugs at the local sites to be implanted directly into the solid tumor cells for treatment [35].

1.7 Electrospinning technique and characteristics

The main characteristics of cancer cells are uncontrolled growth, immortality, and metastasis. The most adapted treatments for cancer treatment are conventional surgery, radiotherapy, and chemotherapy. These treatments are usually limited by the side effects and toxicity level at therapeutic concentrations [36].

Compared with conventional drug therapies, the benefit of controlled delivery systems is maintaining the drug in the desired therapeutic range, which reduces the toxicity and increases the therapeutic agent's effectiveness. Drug release is regulated by drug diffusion or chemical mechanisms such as the degradation of the polymer. Moreover, nanofibers materials provide localized drug delivery which enhances drug delivery to a specific target. With the localized drug delivery, the amount of the needed drug and the frequency of drug administration is reduced because all the amount of the loaded drug will reach the target area.[36].

Electrospun nanofibers (NFs) are used for local drug delivery systems after surgical operations to remove solid tumors [38]. The therapeutic agents may (i) attach to the surface of fibers chemically or physically or (ii) mixed with the polymers [36].

1.7.1 Electrospinning Setup and the variables

Electrospinning is a potential and cost-effective technology to produce nano- and microfibers by applying electric force. A basic electrospinning setup consists of a high-voltage power supply, a needle spinneret, and a collector. When high voltage is applied, the polymer solution at the needle tip disfigures into a cone shape or, as it is named Taylor cone due to the electrostatic forces [37].

The electrospinning technique is based on an electrostatic field, and when this reaches the critical voltage Vc, the charged jet excludes from the tip of the needle. That critical voltage Vc is expressed by Taylor's calculation[37].

$$V_c^2 = 4\frac{H^2}{h^2}\left(\ln\left(\frac{2h}{R}\right) - 1.5\right)(1.3\pi R\gamma)(0.09) \quad \text{(Taylor,1969)}$$

where H is the distance from the needle to the collector, h is the length of the liquid column, R is the inner radius of the spinneret, and γ is the surface tension of the spinning solution[1]. The factor 0.009. is added in order to estimate the voltage. Then, after the fiber's elongation and the evaporation of the solvent, the produced fiber is collected on the collector [37].

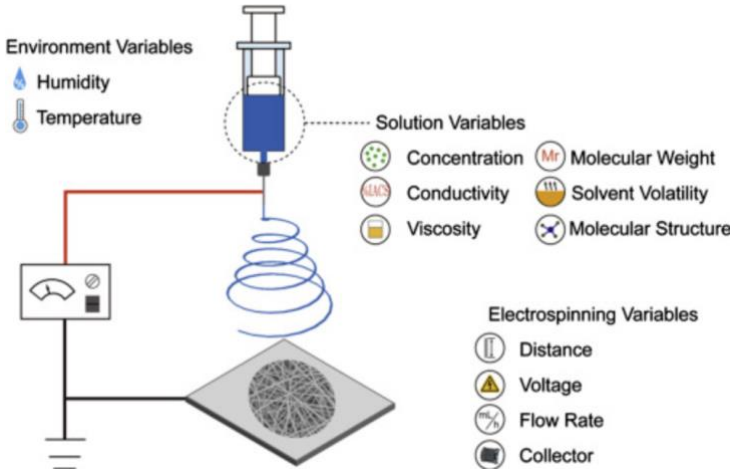

Figure 7*: Schematic diagram of the electrospinning set up and the environment, solution and electrospinning variables [37].*

Although electrospinning is an easy method to develop continuous fibers, some variables influence this progress. In **Figure 7**, the environment, solution, and electrospinning variables are presented. The optimization of these parameters is a determinative factor for the properties of the produced fibers.

1.7.2 Electrospinning Variables

i. Applied Voltage

The applied voltage plays an important role in the electrospinning process. Increasing voltage can increase the volume solution in the tip of the needle and greater stretching of the polymer, resulting in thinner fibers. Moreover, using high voltage with a low-viscosity solution, the results can be multiple jets and smaller fiber diameter [37].

ii. Tip-to-collector distance

The distance between tip and collector affects the jet path and the time that the solution needs to reach the collector. A typical distance ranges from 10 to 15 cm, which is sufficient for the solvent to vaporize and produce fiber. Increasing the distance from the tip to collector, the polymer can stretch further and the fiber diameter can be decreased However, the fiber diameter will increase beyond the typical distance due to weakened field strength, as shown in **Figure 8** [37].

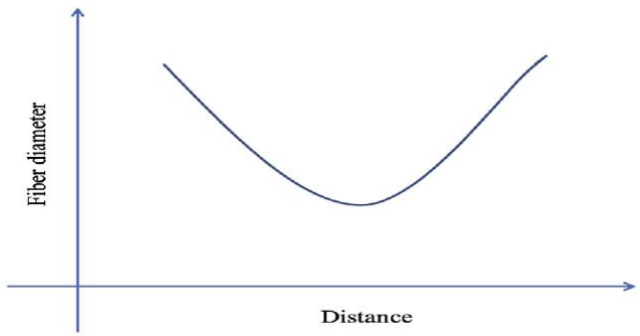

Figure 8*: Schematic function between fiber diameter and electrospinning distance [37].*

iii. Solution Flow Rate

It is important to balance the rate that the solution is drawn off the nozzle tip and the solution distributed on the collector. When the solution flow rate is too high, beaded fibers will be produced, increasing the fiber diameter [37].

1.7.3 Solution Variables

i. Solution Conductivity

Increasing solution conductivity increases the stretching of the solution and lengthens the jet pathway, leading to improved fiber quality by reducing beads and making thinner fiber diameter[37].

ii. Solution Viscosity

In general, the higher the solution, the greater the fiber diameter. However, increasing the solution viscosity, the stretching of the solution to the desired fiber diameter can be more complex [37].

iii. Solvent volatility

A solution that consists of a solvent with low volatility can produce wet fibers or not fiber. On the other hand, solutions with the very high volatility of the solvent resulted in solidification of the solution at the tip. Thus, the solvent volatility should be in a certain region [37].

1.7.4 Environment Variables

i. Humidity

Higher or lower humidity may both result in larger fiber diameter. For higher humidity, the further elongation of the polymer is prevented, and the produced fibers have a larger diameter. In comparison, the lower humidity results in quicker solvent vaporization, which leads to an increase in the solidification of the polymer and ends up with a larger fiber diameter. [37].

ii. *Temperature*

It is reported that higher temperature results in thinner fibers because higher temperature results in faster solvent vaporization and decrease the polymer viscosity [37].

1.8 Electrospinning techniques for drug delivery

There are two electrospinning categories for drug delivery systems, the coaxial and the uniaxial electrospinning. The uniaxial includes the simple blending electrospinning by which the drug-loaded NFs can be developed in two different methods. At the first method, the drug is dissolved in the polymer-solvent solution, and then this solution with the drug is electrospun using a single nozzle (**Figure 9**). After electrospinning the polymer-solvent solution at the second method, the drug will be added by surface modification. Notably, the drug is loaded on the NFs surface through electrostatic interaction, hydrogen bond interaction, van der Waals interactions, and hydrophobic interactions. Among the uniaxial electrospinning methods,

simple blending electrospinning is the easiest and most common method. On the other hand, the coaxial electrospinning provides drug-loaded NF with the drug packed in the core layer of the NF. In this method, the drug is dissolved into a polymer solution and is electrospun by an inner nozzle, while there is an extra polymer-solvent solution electrospun by an outer nozzle (**Figure 9**), providing the outer area of the produced NFs, which keeps the drug and its biological properties unharmed [38].

The main electrospinning techniques that are used for drug delivery are blending, coaxial, and emulsion electrospinning (**Figure 9**). Blending electrospinning is a simple and easy technique to electrospun solutions with drugs dissolved in polymer-solvent solutions. Both hydrophobic and hydrophilic drugs can be electrospun, as well as many others biomolecules. The degradation of the NFs observes the release of the drug through pores and surface diffusion. The advantages of blending electrospinning are the cost efficiency, ease of use, and the possibility of using many different polymer-solvents solutions and drugs [39]. However, the simple blending electrospinning method has some limitations in drug delivery, such as the sensitivity of the drug molecules/biomolecules that are denatured in the organic solvents resulting in the loss of their biological activity, the encapsulation efficiency of the drug is low, the distribution of the drug is not controllable, and the initial drug release is burst [38].

Coaxial electrospinning provides NFs with a core-shell structure [40]. Both synthetic and natural polymers can prepare core-shell NFs with promising physicochemical properties [41]. Moreover, this method allows the encapsulation of the drug in the core of the NF, which can result in a controlled drug release system. The obtained NFs can be loaded with many drugs, proteins, and biomolecules, and it is beneficial that the core structure protects the loaded substances without any effect on their biological activity [39]. The protection of the drug encapsulated in the inner core is the advantage of this method over the simple blending electrospinning [39].

Emulsion electrospinning is based on making droplets of one solution which is insoluble in another. It requires the same setup as blend electrospinning. The biological agents and the polymer-solvent solution are dissolved in different solution which the one is polar, and the other is non-polar [42].

Figure 9 : *The difference in the loading of the polymer-solvent solution (dark green) with the therapeutic agent (light green) for blend, coaxial, and emulsion electrospinning and the difference in the resulting structure of the nanofibers [43].*

1.9 Electrospinning Polymers

Polymeric nanofibers are the commonly used material that was obtained from the electrospinning technique. Electrospun polymers can be divided into natural and synthetic polymers. Natural polymers that have been electrospun into nanofibers mainly involve polysaccharide nanofibers such as cellulose and its derivatives, hyaluronic acid nanofibers such as collagen, gelatin, and nucleic acids nanofibers. Furthermore, synthetic polymers such as poly-ε-caprolactone (PLC), polylactide-co-glycolide (PLGA), polyethylene glycol (PEO), polyvinyl alcohol (PVA), polyvinyl alcohol (PVA), poly-l-lactic acid (PLLA) have been already electrospun [44]. More than fifty different polymers and many solvents have already been electrospun into nanofibers with diameters ranging from 1 nm to 1 mm. **Table 2** highlights some electrospinning types with the solvents anticancer drugs [44].

Table 2: Electrospinning types of anticancer agents, polymers and solvents [44].

Drug	Polymers	Solvents	Electrospinning type
PTX	Chitosan/PEO/HA	Aceticacid/dH_2O	Single nozzle
PTX	PLGA	DCM/DMF	Single nozzle
DOX	PLLA	Chloroform-methanol-DMSO	Single nozzle
DOX hydrochloride	PEG-PLA	Chloroform	Emulsion
Hydroxycamptothecin	HPCD	DMSO	Emulsion
Cisplatin	PLA/PLGA	DCM	Single nozzle
Curcumin	Cellulose acetate	Acetone/dimethylacetamide	Single nozzle
Titanocene Dichloride		DCM	Single nozzle

Poly-ε-caprolactone (PCL) is a semi-crystalline hydrophobic polymer with much interest in the biomedical field. The thermal, mechanical, and physical properties in combination with biodegradability and biocompatibility have made it extensively studied in drug delivery systems. Polycaprolactone's degradation time depends on its morphology and molecular weight, while biodegradability provides easy removal of polymer metabolites from the body by metabolic processes [45]. All the above characteristics, in addition to its slow rate of degradation and non-toxic degradation byproducts [46], provide unique properties to PCL as a material for electrospinning procedures.PCL solubility has been investigated in numerous studies and different solvents, either single solvents (chloroform, acetic acid) or binary solvents (chloroform/ methanol, dichloromethane/dimethylformamide, formic acid/ethanol, formic acid/ chloroform) [47]. Notably, the electrospinning procedure of the PCL polymers depends on the type and the concentration of solvents, electrospinning variables, concentration, solubility, and conductivity of the polymer[47].

2. Research objective

This thesis focuses on developing and exploring the therapeutic effect of FRAX597 and PTX loaded NFs as a novel therapeutic strategy to inhibit the tumor-promoting effect of CAFs and kill tumor cells more effectively.

In order to perform this study, 4T1 breast cancer cells will be used. Although local drug delivery system applies to various cancer, this study will be focused on the co-therapy-loaded nanofibers applied to breast cancer cells. The results can be used and optimized for other cancer types also.

We aimed to develop with simple blending electrospinning single drug-loaded NFs and dual-drug-loaded NFs. We manage to test the therapeutic drug effects on 2D cultured cells and to investigate the inhibitory activity of FRAX597 in activated fibroblasts. Moreover, we tested nanofibers' efficacy on 3D heterospheroids prepared with fibroblast (NHI3T3) and breast (4T1) cancer cells. We investigated the effects of the novel nanofibers measuring the growth rate of heterospheroids treated with drug-loaded NFs compared to treatment with free drugs (with single or multiple doses).

3. Research approach

This project can be divided into different stages (**Figure 10**), starting with optimizing the electrospinning variables to obtain a uniform and smooth surface of nanofibers with the desired properties. After the optimization, the next step is developing drug(s)-loaded nanofibers and characterizing their surface morphologies. Furthermore, NIH3T3 (3T3) and 4T1 breast cancer cell viabilities were measured when treated with FRAX597 and paclitaxel. From these assays, IC50 graphs for FRAX597 and paclitaxel were obtained. Additionally, drug(s)-loaded nanofibers were tested on 3T3 and 4T1 cells for 72 hr, and the metabolic activity was observed. Finally, investigation of FRAX597 ability to inhibit 3T3 activation, immunocytochemistry staining, and migration/ wound healing assays were tested on 3T3 cells and 3T3 activated with TGF-β cells.

Moreover, after the 2D cultured cells' experiments, the study continued with heterospheroids experiments. Heterospheroids experiments provided a more *in vivo* model of breast cancer, prepared with 3T3 fibroblast and 4T1 breast cancer cells. Growth rate measurement studies were examined for heterospheroids treated with free FRAX597, free PTX, free FRAX597/PTX, empty PCL NFs, FRAX597-loaded NFs, PTX-loaded NFs, and FRAX597/PTX-loaded NFs. Different doses of free drug(s) and drug-loaded nanofibers were used to treat heterospheroids. The main scope was to investigate if co-therapy-loaded NFs provided more promising results than single drug-loaded NFs and to compare these results with treatments with chemotherapy and anti-stromal drug.

Additionally, the same procedure was investigated on 4T1 and 3T3 homospheroids to better understand the effect of nanofibers on mono-culture spheroids and investigate how the drug(s)-loaded nanofibers inhibit 3T3 and 4T1 activities (**Supplementary Figures S5-S12**).

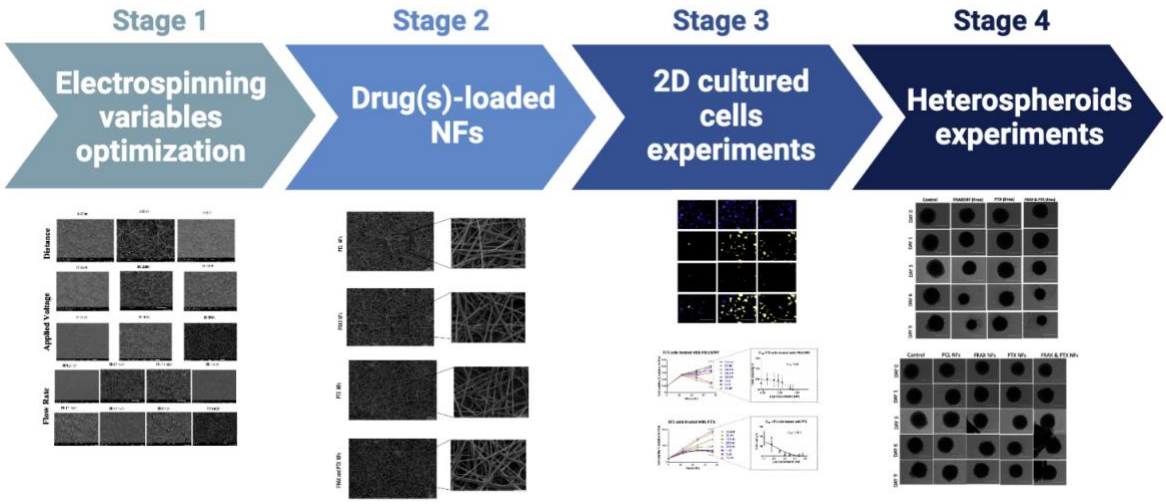

Figure 10: *Study timeline with the project divided into stages. These stages include electrospinning variables optimization, drug-loaded NFs development, experiments performed on 2D cultured cells, and heterospheroids formed with 3T3 fibroblast and 4T1 breast cancer cells.*

4. Methodology

4.1 Chemicals and Materials

Roswell Park Memorial Institute (RPMI)-1640 with- and without glutamine and Dulbecco's Modified Eagle Medium (DMEM) 4.5 g/l with glutamine were purchased from PAA/GE healthcare (Eindhoven, The Netherlands). Dulbecco's phosphate-Buffered Saline (DPBS) was purchased from Lonza Benelux B.V. (Breda, The Netherlands). Fetal bovine serum and Trypsin-EDTA 0.5% were purchased from Life Technologies (Blieswijk, The Netherlands). TGF-b was obtained from PeproTech (Rocky Hill, NJ, USA). Antibodies used were obtained from companies as listed (**Supplementary Table 1**) and fluorescent secondary antibodies from Thermofisher Scientific (Waltham, MA, USA) or Invitrogen (Carlsbad, CA, USA). N, N- Dimethylformamide (DMF) 99.8% ACS and Dichloromethane 99.5% ACS were purchased by VWR Chemicals BDH (North America). Polycaprolactone was purchased from 007 Chemicals B.V. (Deurne, The Netherlands). FRAX597 was purchased from MedChemExpress, Bio-Connect B.V (the Netherlands), and PTX from L.C. Laboratories (USA).

The electrospinning set-up used to develop the nanofibers is given in **Figure 11**, where the main parts of the set-up are the syringe pump, collector, syringe, and electric field.

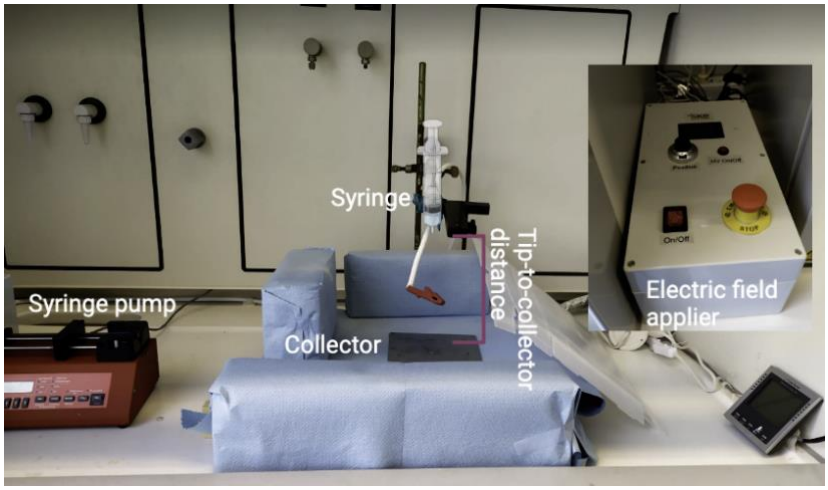

Figure 11: *The electrospinning set-up.*

4.2 Preparation of electrospun solution

a. PCL nanofiber

The polymer solutions were obtained by stirring the polymer in appropriate solvents during 24 hr. 11wt% poly-ε-caprolactone (PCL) (Mw=4500-46000 g/mol) was dissolved in dichloromethane (DCM) and dimethylformamide (DMF) in a ratio 8/2. 10 ml of the PCL prepared solution was placed into a 10 ml syringe and electrospun with 30 kV voltage applied for 1 hr and a flow solution rate of 3 ml/hr. Distance from tip to the collector (metallic collector: 15cm x15 cm) was 10 cm. All experiments were performed under ambient conditions at room

temperature and relative humidity of about 30-50%. Electrospun nanofibers were deposited on a grounded stationary metal collector covered with a piece of aluminum foil. The collected nanofibers were dried at room temperature.

b. FRAX597 nanofiber

FRAX597-loaded nanofibers were obtained by dissolving 0.4 mg 20 mM FRAX597 into the prepared polymer-solvent solution for 24 hr, further. FRAX597-loaded PCL solution was electrospun with the already described variables.

c. PTX nanofiber

PTX-loaded nanofibers were obtained by dissolving 1.232 mg 11,711 mM PTX into the prepared polymer-solvent solution and stirring overnight. PTX-loaded PCL solution was electrospun with the already described variables.

d. FRAX597 & PTX nanofiber

Dual drug-loaded nanofibers were prepared by dissolving in the already prepared polymer solution, 0.4 mg 20 mM FRAX597 and 1.232 mg 11,711 mM PTX. This drug-polymer solution was stirring for 24 hr and electrospun with the described electrospinning variables.

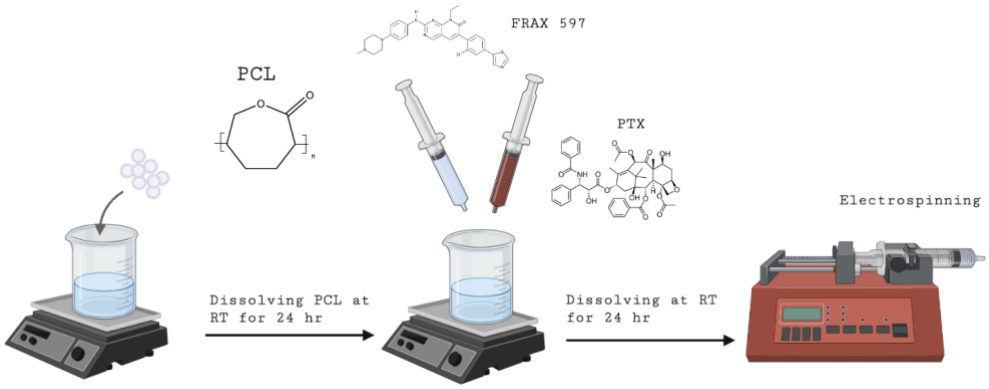

Figure 12: *Schematic representation of drug-loaded NFs synthesis*.

4.3 Scanning electron microscopy

The morphology of the surface and the diameters of the prepared nanofibers were investigated by scanning electron microscopy (SEM). All the images were taken using accelerating voltage 5,00 kV and three different magnifications (x500, x1500, and x4000). The samples were sputter-coated with gold to reduce the charging effect. Fiber diameters were determined by measuring 30-40 diameters of each SEM image with a specific tool from image J, and diameter histograms were prepared using OriginLab OriginPro 2019.

4.5 Cell Culture

NIH3T3 fibroblast and mouse 4T1 breast cancer cells were obtained from American Type Culture Collection (ATCC, Rockville, MD). As instructed by the provider, NIH3T3 cells were cultured in Dulbecco's modified Eagle's medium (DMEM), supplemented with 10% FBS, antibiotics (50 U/ml Penicillin and 50 ug/ml streptomycin), and 2mM L-glutamine. 4T1 cells were cultured in RPMI 1640 medium, supplemented with 10% FBS, antibiotics (50 U/ml Penicillin and 50 ug/ml streptomycin) 2mM L-glutamine. Both cells were grown in cell culture treated 75 cm^2 flasks in a humidified incubator at 37ºC in a humidified 5% CO_2 atmosphere. The cells were passed at ~80 % confluence. The passing of cells was performed as follows: The cells were washed twice with warm Dulbecco's phosphate-buffered saline (DPBS) (Lonza, Basel, CH) before adding 500ul of 1X trypsin/ethylenediaminetetraacetic acid (EDTA) (Gilbo) and incubating for 1 min at 37 ºC. The cell passed to well plates in the designated amounts calculated based on the total number of harvested cells.

2D cell culture experiments

4.6 Cell viability

NIH3T3 cells, 4T1 cells, and their combination were seeded into a 96 well plate at a seeding density of 5.000 cells/well. For NIH3T3 and 4T1 combination, a 50/50 ratio was used. Each day, the cell viability was measured by adding Alamar Blue (Sigma-Aldrich) at a concentration of 10 vol.% of the total media. After incubation for 4 hr, the fluorescence was measured using standard protocols with a Viktor 3 plate reader (Victor 3 model 1420 multi-label counter, PerkinElmer Groningen, NL). The metabolic activity was measured at 0 hr, 24 hr, 48 hr, and 72 hr, respectively.

Cell viability with drug concentrations: After the first metabolic measurement at 0 hr, drug concentrations of free FRAX597 and PTX were added. For both drugs the concentrations were used 50 nM, 100nM, 250 nM, 500 nM, 1 uM, 5uM and 10 uM. Furthermore, the combination of both drugs (FRAX597 and PTX) with the referred concentrations was also measured. The metabolic activity was measured at 24 hr, 48 hr, and 72 hr, respectively.

Cell viability with drug-loaded nanofibers: 1 mm of the developed FRAX597-loaded NF, PTX-loaded NF, and FRAX597/PTX -loaded NF were cut with AcuPuncher (diameter of 1mm). After the first metabolic measurement at 0 hr, each nanofiber was inserted in each well with NIH3T3, 4T1, and NIH3T3 and 4T1 cells. The metabolic activity was measured at 24 hr, 48 hr, and 72 hr, respectively.

4.7 Immunocytochemistry staining - a-SMA & collagen 1

NIH3T3 cells were seeded into a 24 well plate at a seeded density of 25.000 cells/well. After 24 hr, the cells were starved by adding 0% FBS-DMEM medium. After 24 hr at the incubator at 37ºC in a humidified 5% CO2, cells were treated with three different concentrations of FRAX597. TGF-β was used to prepare the concentration 0.5 uM, 1uM, and 5uM of FRAX597 to treat the cells. Further, activation media (5ng/ml TGF-β) replaced 0%

FBS-DMEM medium. The treatment step lasted for 48 hr where the cells were incubated at 37ºC in a humidified 5% CO_2. Then, the cells were washed twice with warm DPBS and fixed with acetone/methanol (50/50) for 30 minutes at -20ºC. After the acetone/methanol was discarded and cells after drying were stored at -20ºC overnight.

The next day, the cells were first dried, and then a hydrophobic circle was made by PAP-pen/ Immedge pen (Life Technologies) for immunostaining to prevent the waste of valuable reagents. The cells were rehydrated in 1x PBS for 5 minutes. 0.5 ug of the first antibodies a-SMA and collagen-1 (diluted in ratio 1/500 and 1/250, respectively) in 2% BSA was added and incubated for 1 hr at room temperature. Then, the cells were washed three times with 1x PBS, and the secondary antibodies, 488 nm donkey anti-mouse and 594 nm donkey anti-goat, were added, diluted in a ratio of 1/100 in 1% BSA. The cells were incubated for 1 hr at room temperature. Then, cells were washed three times with 1x PBS and incubated with DAPI (NucBlue Fixed Cell Stain Ready Probes, Molecular Probes Inc.) and stored overnight at 4 ºC. Images were taken using bright-field microscopy (Nikon Eclipse E400, Nikon, Tokyo, JP)). Quantitative analysis was performed with Image J.

4.8 Migration/wound healing assay

NHI3T3 cells or 4T1 cells were seeded into 12 well plates at a seeding density of 100.000 cells per well and allowed to attach overnight. After 24 hr, the cells were starved with 0%FBS-DMEM medium, and 24 hr later, a scratch was made through the middle of the well using a 200 ml pipette tip to remove cells and washed twice with the starvation medium. The experiment was performed using TGF-β treated and untreated cells. The cells were treated with 0.5 uM, 1 uM, and 5 uM FRAX597. For later localization of the proper position in the well, a horizontal line was made. Images were taken at 0 h and 24 h after activation, respectively, using bright-field microscopy (EVOS microscope, Thermofisher Scientific). Migration of cells was analyzed and quantified using Image J.

3D spheroids studies

4.10 Homospheroids and heterospheroids formation

The spheroids were culture using a 96 suspension well plate, round bottom. The 96 suspension well plates were coated overnight with 1 wt% Pluronic F-127 to avoid attaching the cell to the surface. The coated plates were twice washed with warm DPBS before seeding the cells. 4T1 and NIH3T3 cells were counted and seeded at a density of 6,000 cells/wells. For 4T1 homospheroids and NIH3T3 homospheroids, 6,000 4T1 cells/ml and 6,000 NIH3T3 cells/ml were seeded. Heterospheroids were prepared using 4T1 and NIH3T3 cells in a 1:5 ratio. 4T1 homospheroids and NIH3T3 homospheroids were seeded in RPMI-1640 medium and DMEM medium, respectively, while heterospheroids were seeded in DMEM/RPMI-1640 at 50:50 ration. The spheroids were grown at 37 ºC in a humidified 5% CO_2. After 48 hours, spheroids were fully formed, and bright-field images were taken on days 0, 1, 3, 6, and 9 using bright-field microscopy (Nikon Eclipse E400, Nikon, Tokyo, JP)). Quantitative analysis was performed with Image J to study the growth.

a. Spheroids treatment with free drugs

Homospheroids and heterospheroids were prepared as described before. After 48 hours, that the spheroids were fully formed, bright-field images were taken for day 0, and homo- and heterospheroids were treated with 1 uM FRAX597, 250 nM PTX each diluted in RPMI-1640 and DMEM medium, respectively, and a combination of 1uMFRAX597 and 250 nM of PTX diluted in RPMI-1640 and DMEM at a ratio 50/50. Drug dosages were different for different sets of experiments (**Figure 13**).

b. Spheroids treatment with drug-loaded NFs

Homospheroids and heterospheroids were prepared as described before. 1 mm diameter of drug-loaded NFs were cut with AcuPuncher (diameter of 1mm). After 48 hours that the spheroids were fully formed, brightfield images were taken for day 0 and homo- and heterospheroids were treated with FRAX597-loaded NFs, PTX-NFs (prepared as discussed before), and dual drug drug-loaded NFs (FRAX597&PTX-loaded NFS). Drug-loaded NFs refreshment was different for different sets of experiments (**Figure 13**).

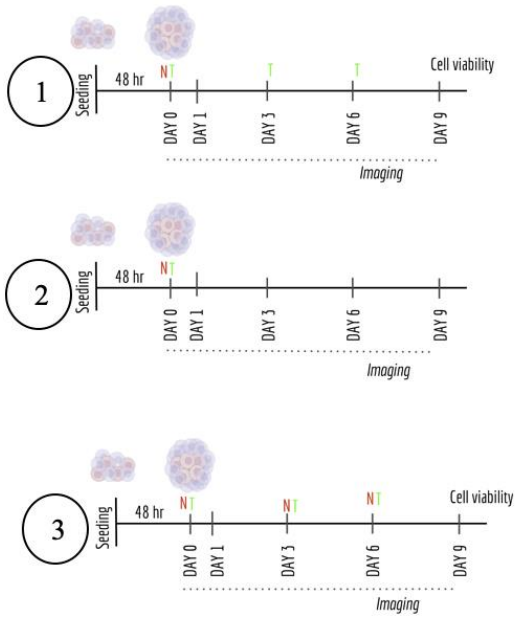

Figure 13: *Different sets of experiments. For all the different sets, free drug and drug-loaded BFs were placed at day 0. (1) Media and free drugs were refreshed on day 3 and day 6, while drug-loaded NFs were not further refreshed, (2) neither free drugs nor drug-loaded NFs were replaced after day 0, (3) both free drugs and drug-loaded NFs were refreshed at days 3 and 6.*

c. Tumor Growth

Post-treated homo- and heterospheroids, prepared as previously mentioned, were observed for a total of 9 days after treatment by imaging the spheroids at day 0,1,3,6 and 9 under a bright-field microscope (EVOS microscope (Thermofisher Scientific). The size was measured by Image J, and the growth was determined using Microsoft Excel using the initiation day (day 0: 48 hours after the deeding day) as reference.

4.11 Spheroid viability- Cell-Titer Glo luminescence Assay

After 9 days of tumor size study, the spheroids were ready for luminescence measurement. One day before the experiments, the Cell-Titer Glo 3D assay (Promega, Madison, Wisconsin, 28 US) was placed at 4˚C to allow a slow defrost of the assay. 30 min before experiments, the assay was placed at room temperature. The spheroids were individually transferred to a 96 well luminescent plate (SPL Life Sciences Co., Naechon-myeon Pocheon-si, KOR) in a total volume of 50 *ml* cell culture medium. An equal amount of Cell-Titer Glo 3D assay was added to the wells before shaking the plate continuously by the shaker for 10 min to lyse the spheroids fully. Afterward, the plate was incubated at room temperature for 30 min. The luminescent signal was measured using standard protocols with a Viktor 3 plate reader (Victor 3 model 1420 multi-label counter, PerkinElmer Groningen, NL).

4.12 Statistical analysis

The results were analysed using GraphPad Prism 9 software (GraphPad Software Inc., San Diego, CA). All values are expressed as a mean ± standard error of the mean (SEM). Statistical significance of the results was performed by a two-tailed unpaired student's t-test for comparison of two treatment groups. Differences were considered significant for a p-value of $*p < 0.05$, $**p < 0.01$, $***p < 0.001$, respectively.

5. Results

5.1 Optimization of electrospinning variables

Applied electric voltage, solution flow rate, and tip-to-collector distance are the main electrospinning variables that need to be optimized before the drug-loaded electrospun NFs process. Various nanofibers provided in **Figure 14** developed with various electrospinning variables provided different surface morphologies summarized in **Table 3**.

Moreover, different percentages of PCL were dissolved in chloroform/methanol and DMF/DCM in different ratios (**Figure S1, Figure S2**).

To conclude, based on the results of the electrospun NFs and the reproducibility, the electrospinning variables (applied voltage: 30 kV, solution flow rate: 3ml/hr and tip-to-collector distance: 10cm) and 11 wt% of PCL dissolved in DCM/DMF in a ratio of 8/2 were obtained.

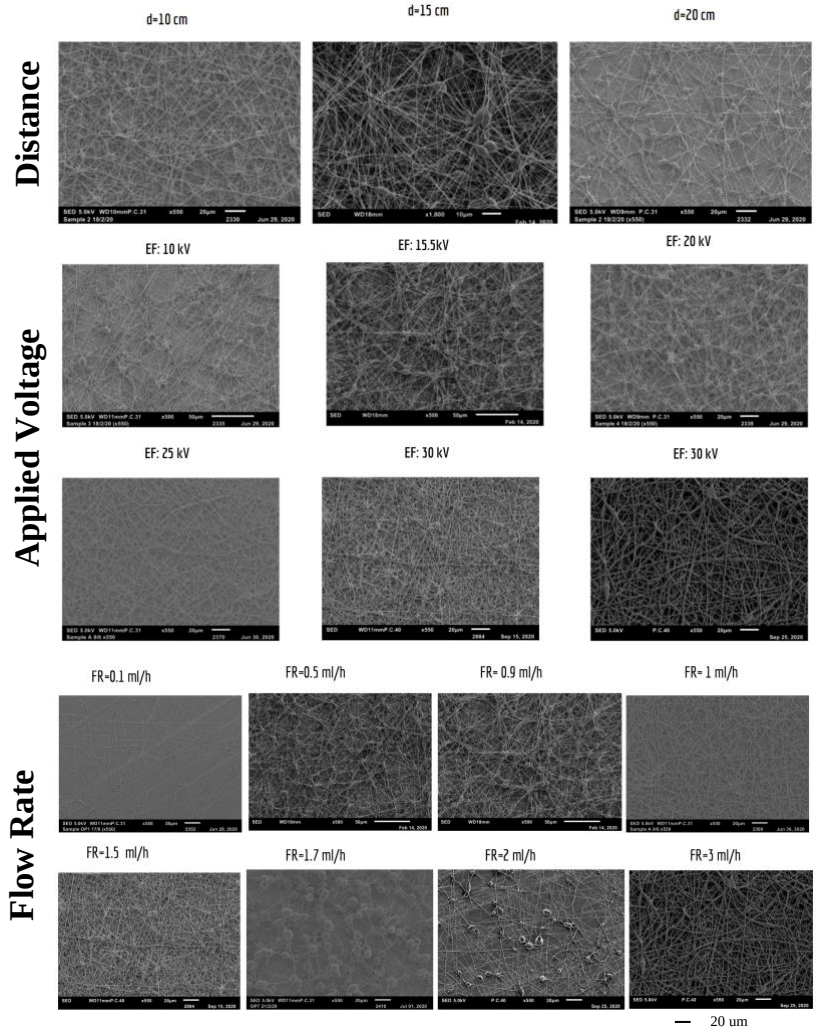

Figure 14: *Scanning electron microscope images provided the electrospinning variables. From above to below, tip-to-collector distance, applied electric voltage, and flow rate solution.*

Table 3: Summarized electrospinning variables and surface morphologies of electrospun nanofibers provided on **Figure 14**.

Type of electrospinning variable	Electrospinning Variables	Surface morphology
Tip-to-collector distance	d=10 cm	Decreased fiber diameter, beaded NFs
Tip-to-collector distance	d=15 cm	Beaded NFs
Tip-to-collector distance	d=20 cm	Beaded NFs with increased diameter
Applied Voltage	EF=10 kV	Beaded NFs
Applied Voltage	EF=15 kV	Beaded NFs
Applied Voltage	EF=20 kV	Beaded NFs
Applied Voltage	EF=25 kV	Beadless NFs
Applied Voltage	EF=30 kV	Beadless NFs
Flow rate solution	FR= 0.1 ml/h	No formation of fibers was observed, the polymer solution did not flow through the tip
Flow rate solution	FR= 0.5 ml/h	Beaded NFs with decreased diameter
Flow rate solution	FR= 0.9 ml/h	Beaded NFs with decreased diameter
Flow rate solution	FR= 1 ml/h	The formation of continuous fibers was observed but no reproducibility
Flow rate solution	FR= 1.5 ml/h	Beaded and thin NFs
Flow rate solution	FR= 1.7 ml/h	Beaded NFs
Flow rate solution	FR= 2 ml/h	Beaded and less NFs formation
Flow rate solution	FR= 3 ml/h	The formation of continuous fibers was observed

5.2 Development of electrospun nanofibers

a) Polymer solution synthesis – PCL NFs

11 wt% poly-ε-caprolactone (PCL) solution with molecular weight 45000-46000 g/mol was dissolved in dichloromethane (DCM) and dimethylformamide (DMF) in a ratio of 8/2 following by stirring for 24 hr at room temperature. The obtained solution was heterogeneous and viscous. The polymer-solvent solution was injected into a 10 ml syringe and irradiated with high voltage energy. The electrospinning variables were 30 kV applied voltage, 3 ml/hr the solution flow rate, 15 cm the distance from the tip of the syringe to the collector. Collector surface area was 15 cm x 15 cm. The electrospinning process lasted 1 hr at room temperature with a relative humidity of 30-50% (**Figure 15**).

b) FRAX597-loaded NFs

11 wt% PCL solution was dissolved in DCM and DMF in a ratio of 8/2 following by stirring for 24 hours at room temperature. After 0.4 mg of 20mM FRAX597 was added, and the drug polymer-solvent solution was further stirring for 24 hr at room temperature. The electrospinning variables were the same as described above (**Figure 15**).

c) PTX-loaded NFs

11 wt% PCL solution was dissolved in DCM and DMF in a ratio of 8/2 following by stirring for 24 hours at room temperature. After 1.232 mg of 11.711 mM, PTX was added, and the drug polymer-solvent solution was further stirring for 24 hr at room temperature. The electrospinning variables were described above (**Figure 15**).

d) FRAX597 & PTX-loaded NFs

Co-therapy nanofibers were synthesized by adding 0.4 mg of 20mM FRAX597 and 1.232 mg of 11.711 mM PTX into the already prepared polymer-solvent solution and then electrospun with the analyzed variables.

Drug-loaded nanofibers

In order to electrospun 2.5 ml of polymer-solvent solution, the minimum of the injected solution is 5 ml to ensure that the electrospun solution is enough, as a small amount of it remains at the walls of the syringe. In general, 120 mg PCL were diluted in 1 ml solvent and electrospun with a 3 ml/hr flow rate. For each fiber development, 5ml of the polymer-solvent solution is needed. That means that the PCL amount for each nanofiber formation is 600 mg PCL. PTX molecular weight is 853.9 g/mol, and the desired PTX concentration of 500 nM will be inserted in a volume of 0.1 ml (each well from 96 well-plate), so the amount of PTX is 0.043 ug (nanofibers with 2 mm diameter). That means that in a 2.5 ml polymer-solvent solution, the amount of PTX is 0.308 mg. It is essential to mention that the used collector's area is 15 cm x 15 cm. Preparing 5 ml polymer-solvent solution, 0.616 mg PTX will be needed, equal to 7.214 10^{-7} moles. For the same number of moles for FRAX597, the amount of FRAX697 is 0.40261 mg, considering that the molecular weight of FRAX597 is 558.1 g/mol. For the experiments, 1 mm and 2 mm of nanofibers were used (**Table 4**).

2mm nanofibers

$E = \pi r^2 = 0.314\ cm^2$, r=2 mm (nanofiber's diameter)

In 2.5 ml polymer-solvent solution were 0.308 mg PTX and 0.4026 mg FRAX597. These were electrospun in a collector (E=225 cm^2). Thus, each 2 mm piece of NFs has 0.429 ug PTX and 0.281 ug of FRAX597.

1mm nanofibers

$E = \pi r^2 = 0.0785\ cm^2$, r=1 mm (nanofiber's diameter)

In 2.5 ml polymer-solvent solution were 0.308 mg PTX and 0.4026 mg FRAX597. These were electrospun in a collector (E=225 cm^2). Thus, each 1 mm piece of NFs has 0.10745 ug PTX and 0.0702 ug of FRAX597.

Table 4: Drugs' amounts and electrospinning variables.

Drug/ Polymer	Amount (mg) in 2.5 ml polymer-solvent solution	Electrospinning Variables	Amount (ug) in 2 mm	Amount (ug) in 1 mm
PTX	0.308	30 kV, 3 ml/hr, 15 cm	0.429	0.10745
FRAX597	0.40261	30 kV, 3 ml/hr, 15 cm	0.281	0.0702

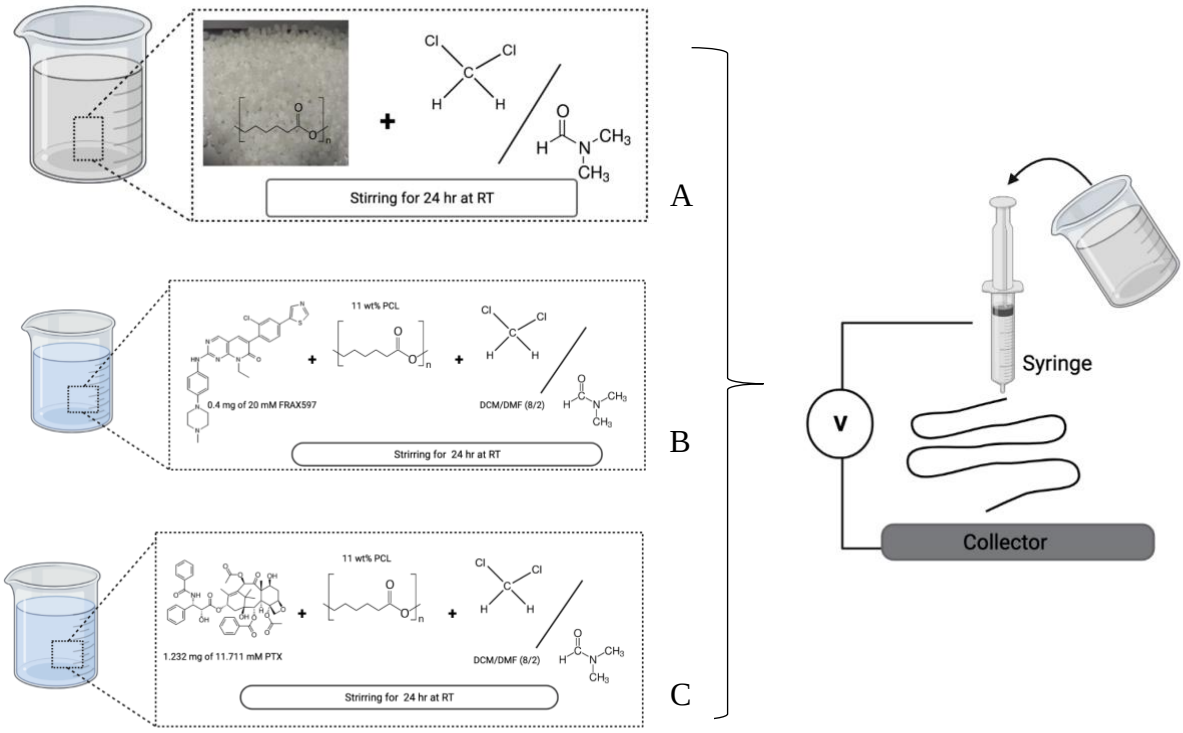

Figure 15: *Schematic illustration for the synthesis of the polymer-solvent solution. (A) FRAX597-loaded NFs (B), PTX-loaded NFs (C) after all the (drug) polymer-solutions were injected into a 10 ml syringe and electrospun under the desired variables.*

Scanning electron microscopy

The morphological characteristics of the electrospun nanofibers were evaluated by scanning electron microscopy. **Figure 16** shows the SEM images of nanofibers development with and without drug, and the diameter distributions are represented with histograms for all the electrospun nanofibers.

Based on the SEM images, electrospun nanofibers seem to be thin without many beads. The few beads that are observed are minor and do not influence the smooth and uniform surfaces. Regarding the diameters, PCL nanofibers have a diameter average of 0.8 – 1 um, FRAX597-loaded NFs have a diameter average of 1-1.2 um, while the diameter average of PTX-loaded NFs ranges from 0.3-0.4 um and 0.4- 0.6 um for the dual drug-loaded NFs. Apart from a slight difference in the nanofibers' diameter, there are no noticeable significant changes in the structure of nanofibers associated with drug absorption.

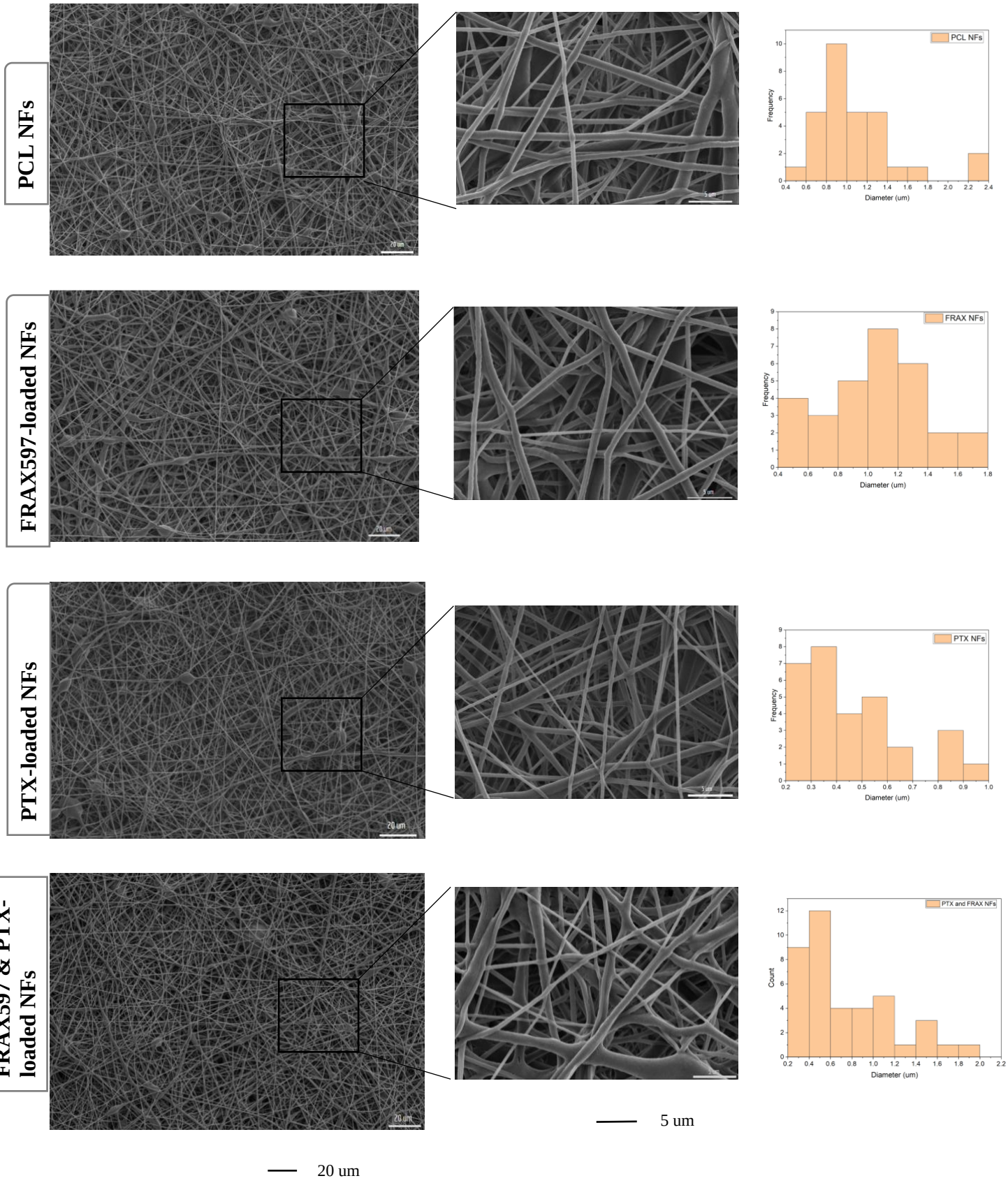

Figure 16: *SEM images of the electrospun nanofibers and the histograms with the diameter distributions.*

5.3 2D cell culture

5.3.1 Cell viability assay with different concentrations of free drug

Firstly, the metabolic activity of NIH3T3 cells (3T3 cells) and breast tumor 4T1 cells was examined with AlamarBlue assay. Both cells were treated at t=0hr with different concentrations of free drugs. 3T3 cells were treated with free FRAX597, and 4T1 cells were treated with free PTX drug at concentrations 50 nM, 100 nM, 250 nM, 500 nM, 1uM, 5 uM, and 10 uM, respectively. Cell metabolic activity assay was conducted at 0 hr, 24 hr, 48 hr, and 72 hr. At 72 hr, the IC50 graphs for 3T3 and 4T1 cells were also calculated in **Figure 17**.

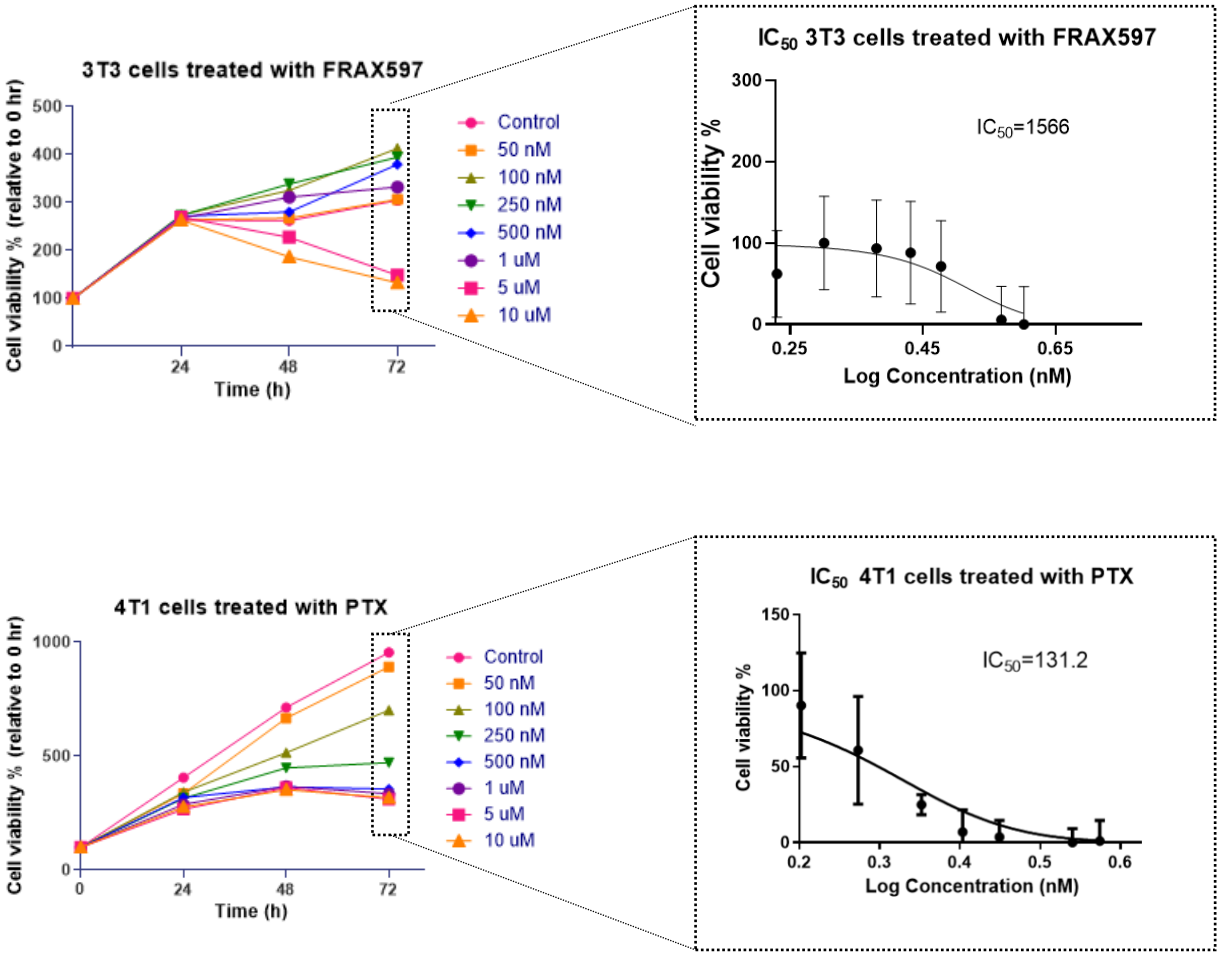

Figure 17: *Cell viability for 3T3 cells treated with FRAX597 and 4T1 cells treated with PTX and the IC50 graphs for t=72 hr. Both cells were seeded at a seeding density of 5000 cells/well, and AlamarBlue assay was conducted at t=0 hr, 24 hr, 48 hr, and 72 hr. (All results are relative to 0hr, cell viability without any treatment). Data represent mean for 3 independent experiments. *p < 0.05, **p < 0.01, ***p < 0.001.*

Regarding the cell viability of 3T3 cells treated with FRAX597, most of drug concentrations seem not to negatively affect the 3T3 growth apart from 5uM and 10 uM FRAX597, where the number of live 3T3 cells started to decline. It is important to note that FRAX597 should be enough to inhibit CAFs activation for our project but not to kill 3T3 cells. That means that the concentrations 5uM and 10 uM are high and results in 3T3 apoptosis. Thus, 1 uM FRAX597 is a promising concentration for inhibiting cancer-associated fibroblasts activation. The above can be confirmed from the IC50 graph, which indicated that 1.566 uM FRAX597 is needed to inhibit in vitro 3T3 cells by 50% (**Figure 17**). Consequently, we hypothesized that 1 uM FRAX597 is an optimal amount to inhibit CAFs activity.

Concerning the metabolic activity of 4T1 cells treated with PTX and the counterpart IC50 graph, PTX concentrations above 100 nM seemed to inhibit the 4T1 cells and induce apoptosis to the tumor cells, with an advanced apoptosis rate at 1uM, 5uM, and 10uM concentrations of PTX. IC50 graph showed that 131.2 nM could inhibit the tumor cells by 50%. However, the graph showed that with 250 nM PTX, cell metabolic activity started to decrease. Therefore, we supposed that 250nM PTX is a propitious concentration that can eliminate tumor cells.

5.3.2 Cell viability assay with drug-loaded nanofibers

Cell viability of 3T3 and 4T1 cells with applied drug-loaded NFs was investigated. 1mm diameter of each developed NFs (PCL, FRAX597-, PTX- and FRA597&PTX- loaded NFs) was added to 3T3 and 4T1 cells, respectively. The drug amount of the electrospun NFs (with surface area = πr^2= 0.0785 cm2) was 0.0702 ug FRAX597 and 0.10745ug PTX. In **Figure 18**, the cell viability was presented, measured at 0hr, 24hr, 48hr, and 72hr. At 72hr, bar graphs were calculated regarding the metabolic activity of 3T3 and 4T1 cells with drug-loaded NFs.

3T3 cells treatment with drug-loaded NFs provided some decrease over time, especially for PTX- and FRAX597&PTX- loaded NFs. However, at 72 hr, the bar graph results didn't significantly differ between the different treatments (**Figure 18**).

The outcome mentioned above was also provided for 4T1 cells treated with drug-loaded NFs for 72 hr. Particularly, cell viability for 4T1 cells treated with PTX- and FRAX&PTX-loaded NFs showed a decreasing rate over time. However, according to the bar graphs results, cell viability measured at 72hr didn't significantly differentiate between the drug-loaded NFs treatment.

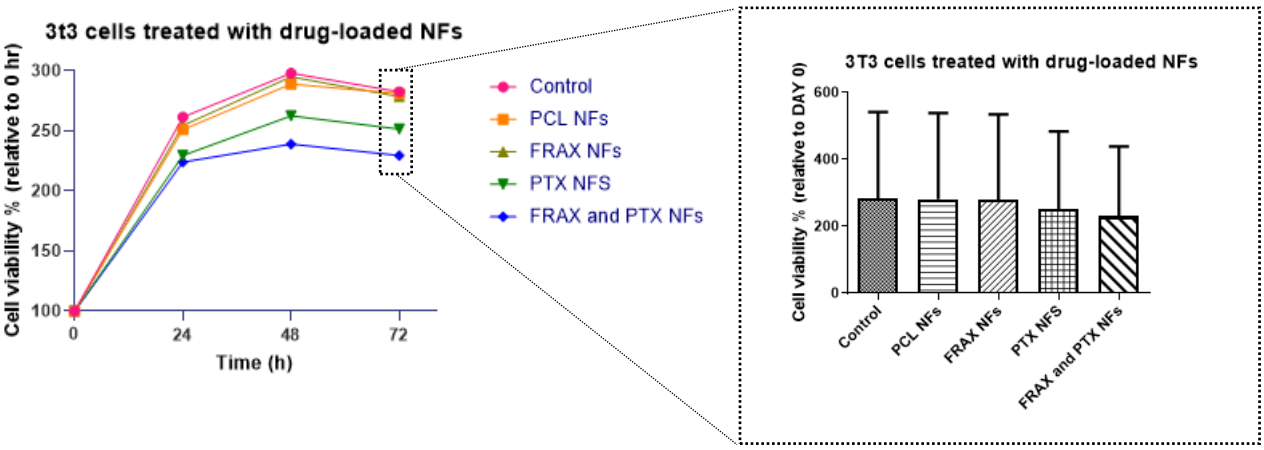

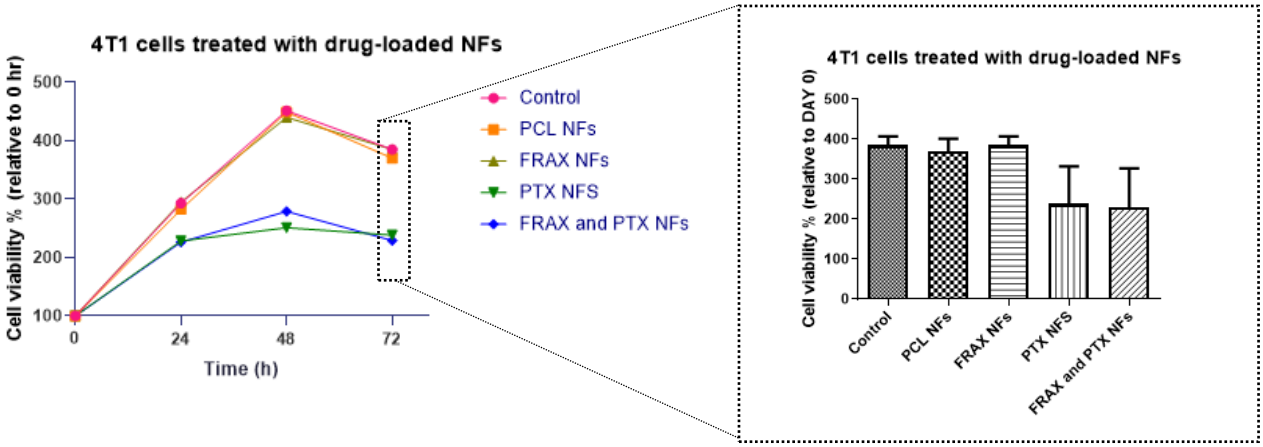

Figure 18: *Metabolic activity of 3T3 and 4T1 cells treated with drug-loaded NFs. PCL, FRAX597-, PTX- and FRAX597&PTX-loaded NFs (diameter:1mm) were added to cells at t=0hr and the cell viability was measure for 0hr,24hr, 48hr and 72hr, respectively. At 72hr, bar graphs were calculated, representing the cell viability regarding the drug-loaded NFs. All results are relative to 0hr cell viability before treatment. Data represent mean for 3 independent experiments. *p < 0.05, **p < 0.01, ***p < 0.001.*

5.3.3 Immunocytochemistry staining – a-SMA & collagen 1

Immunocytochemistry staining was conducted for 3T3 cells in starvation media (0% FBS-DMEM), activated media (TGF-β 5 ng/ml), and activated media with FRAX597 (1uM) treatment. Fluorescence images from the EVOS microscope (**Figure 19 A**) showed blue DAPI staining the number of nuclei and a gross estimation of the cell morphology. The expressions of α-SMA and collagen1 were qualitatively analyzed with green and red staining, respectively. The lowest expression of a-SMA and collagen1 is provided by the 3T3 cells in the starvation media, while the highest expression is presented by activated media as a result of TGF-β activation. This expression was restricted in the presence of FRAX597 (1uM). This outcome is confirmed by the quantitative analysis (**Figure 19 B, C**) for a-SMA and collagen1 expression. FRAX597 at the concentration of 1uM provided decreased expression of a-SMA and Collagen1a, markers that are upregulated on the fibroblast activated state.

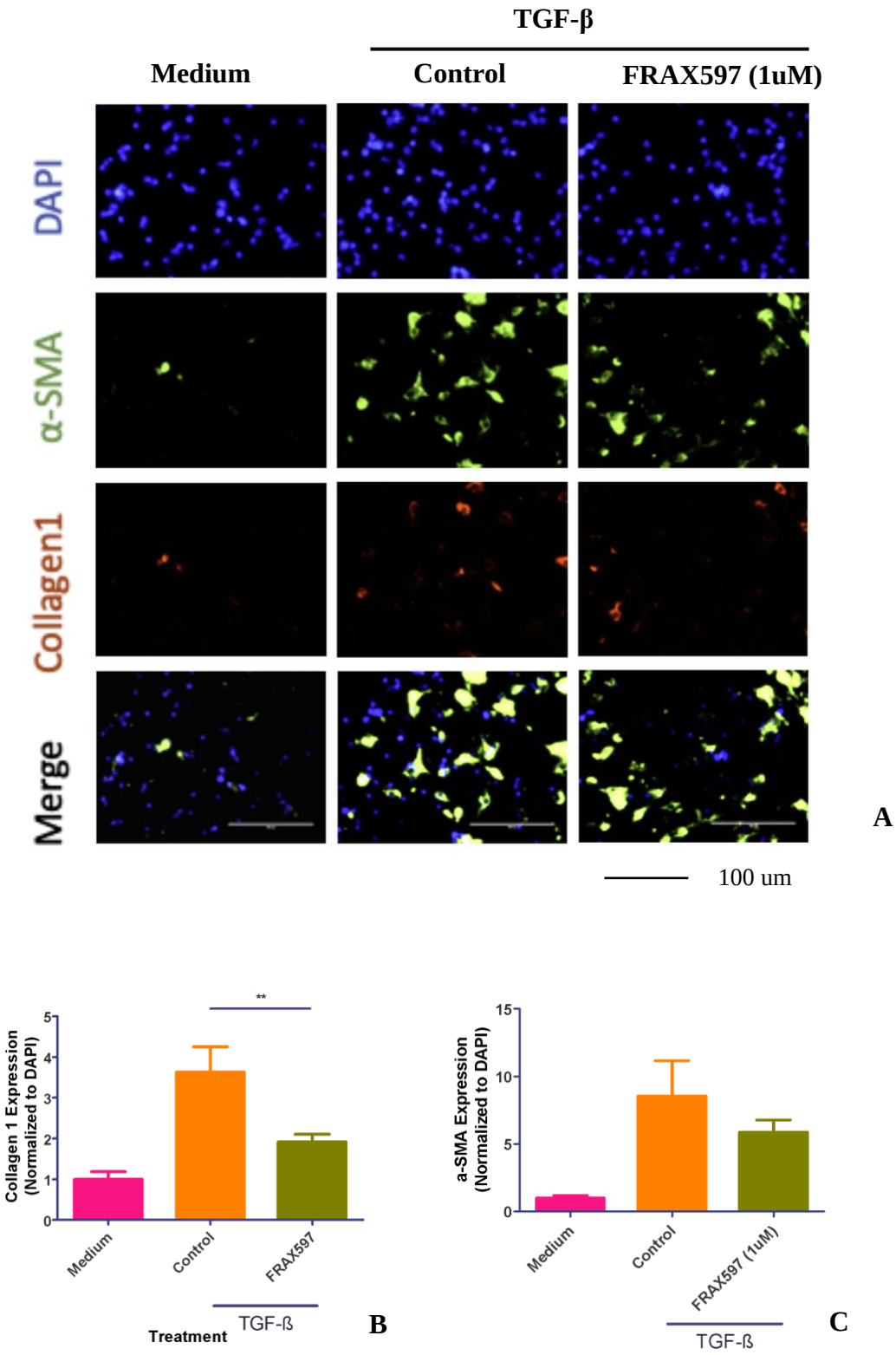

Figure 19: *Immunocytochemistry staining for a-SMA and collagen1 expressions. (A) Fluorescence images by EVOS microscope representing the number of nuclei with DAPI (blue), a-SMA expression (green), and collagen1 expression (red), for 0%FBS-DMEM medium (Medium), 0%FBS-DMEM medium activated with*

*TGF-β (5ng/ml) (Control), and cells treated with 1 uM FRAX597 in activated medium (FRAX597(1uM). Quantitative analysis of (B) collagen1 expression and (C) a-SMA expression. Data represent mean ± SEM for 3 independent experiments. *p < 0.05, **p < 0.01, ***p < 0.001.*

5.3.4 Migration/wound healing assay

The performed wound healing assay revealed that the migration of 3T3 cells could be significantly inhibited after treatment with FRAX597 (**Figure 20 A and B)**. In both cases, TGF-β and non-activated 3T3 cells, a reduction in the migration behavior could be observed when treated with FRAX597 at concentrations 1 uM and 5 uM. The same experiment was conducted for 4T1 cells (**Supplementary Figure S3)**, without significant inhibition of FRAX597 into the 4T1 cell would healing process.

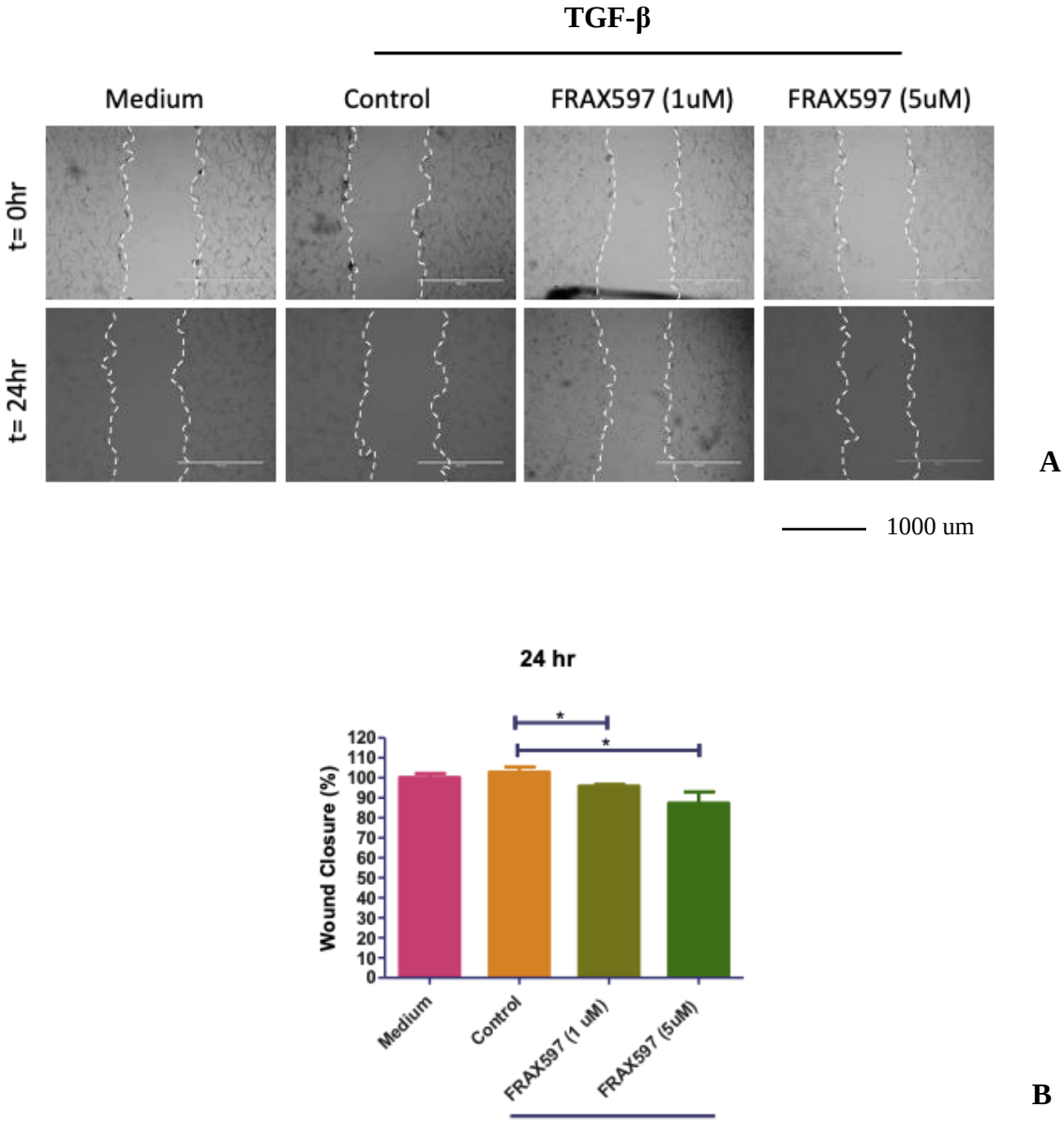

Figure 20: E*ffect of inhibition with FRAX597 (1uM and 5uM) on 3T3 cell migration. Microscopic in of migration/wound closure of 3T3 cells. (A) Wound closure at t= 0hr and t=24hr for medium, TGF-β activated medium (control), and two treatments of FRAX597 applied on activated 3T3 cells. (B) Quantitative analysis of the wound closure after 24hr incubation. Data represent mean ± SEM for 3 independent experiments. *p < 0.05, **p < 0.01, ***p < 0.001.*

5.4 Effect of FRAX597 and PTX applied on heterospheroids

In the previous section, we confirmed that the pre-treatment of 3T3 cells with FRAX597 showed an inhibitory effect and loss of a-SMA and collagen1 in 2D 3T3 cultured cells. To create a more in vivo mimicking treatment model of cancer, 3T3 and 4T1 heterospheroids were made, containing fully untreated 3T3 and 4T1 cells. The heterospheroids were treated with free drugs and drug-loaded NFs, 2 days after the initiation of the experiment. Furthermore, multiple doses of free drug and drug-loaded NFs were used to treat the heterospheroids. The experiments were divided into sets.

5.4.1 Multiple doses of free drug and drug-loaded NFs

For the first set of experiments, free drug and drug-loaded NFs were refreshed every 3 days. For 9 days of imaging, three drug doses and three doses of drug-loaded NFs were used (Figure **22B**). On day 9, luminescent cell viability (**Figure 21**) observed that free FRAX597 provided a minor metabolic activity following free FRAX597 and PTX. Cell viability for heterospheroids treated with drug-loaded NFs didn't provide any significant difference between the different way of treatment.

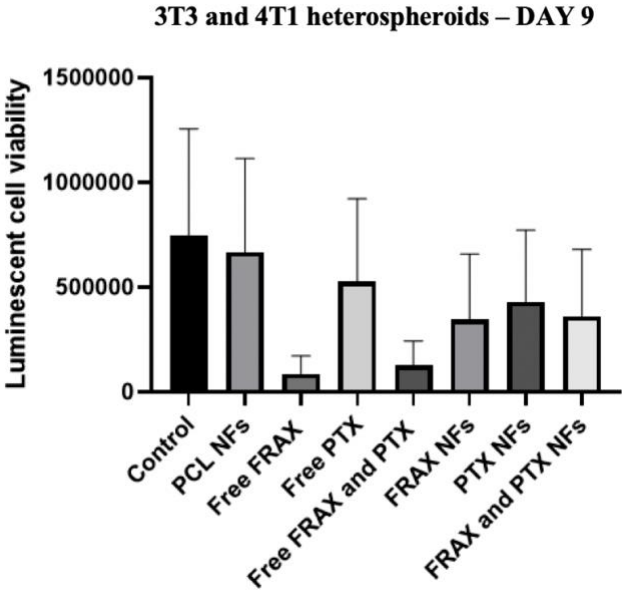

Figure 21: *Luminescent cell viability with CellTiter-Glow assay for 3T3 and 4T1 heterospheroids performed on DAY 9.*

Growth rate measurement of heterospheroids for 9 days showed that free drugs provided more reduction in spheroids growth than drug-loaded NFs (**Figure 22C**). However, there were

no significant differences observed neither for free drug nor for nanofibers treatment (**Figure 22D**).

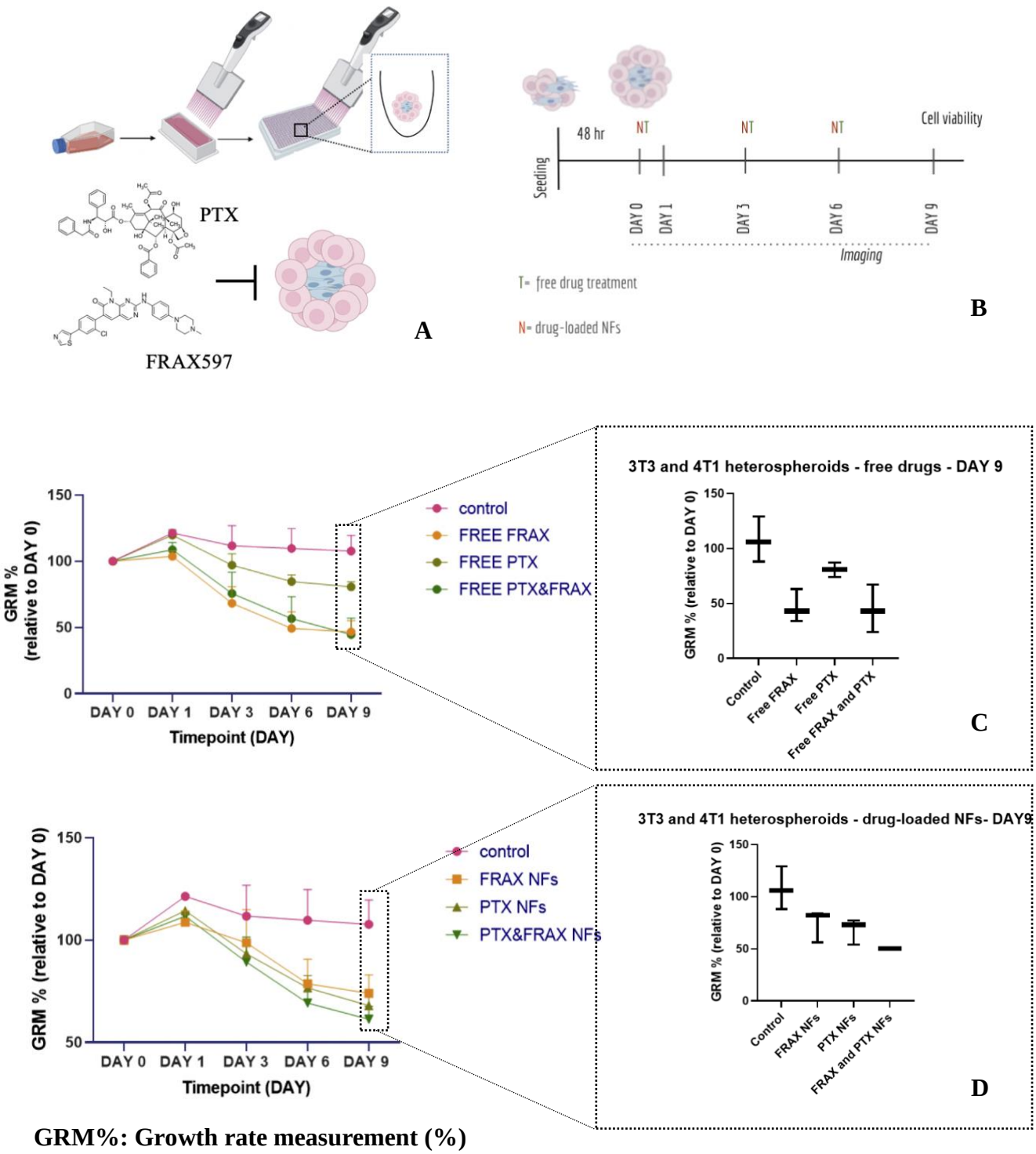

GRM%: Growth rate measurement (%)

Figure 22: *Heterospheroids treatment for 9 days, with three free drug and drug-loaded NFs doses. (A) Schematic illustration of heterospheroids formation and the chemical types of the drugs (PTX and FRAX597) which used to inhibit heterospheroids growth (B) Timeline of the first set of experiments (three free drug doses and three doses of drug-loaded NFs). (C) Growth rate measurement experiments for heterospheroids*

*treated with free drugs (FRAX597, PTX, and FRAX597 and PTX) with the boxplot analysis for DAY 9 (D) Growth rate measurement experiments for heterospheroids treated with drug-loaded NFs (FRAX597-loaded NFs, PTX-loaded NFs, and FRAX597 and PTX-loaded NFs) with the boxplot analysis for DAY 9. Data represent mean ± SEM for 3 heterospheroids' experiment. *p < 0.05, **p < 0.01, ***p < 0.001.*

5.4.2 Single dose of free drug and drug-loaded NFs

The second set of experiments includes growth rate measurement studies on heterospheroids with one drug dose and one drug-loaded NF applied for the treatment (**Figure 23B**). Although the treatments were not refreshed, the medium was refreshed every three days. The treatments were applied two days after spheroids formation, and growth measurements of the heterospheroids were observed for the next nine days.

Free drug and drug-loaded NFs treatments provide a decrease in spheroids' size compared to control (**Figure 23)**. For example, on day 6, FRAX597, FRAX597, and PTX show better size inhibitory effects than PTX, but on day 9, there was a boxplot analysis of no significant difference between the different treatments (**Figure 23B**).

Treatment with drug-loaded NFs also provided a decrease in heterospheroids' size compared to control (**Figure 23D**). Thus, drug-loaded NFs treatments on DAY 9 are comparable with the free drug treatment results, although there was no significant difference between drug-loaded NFs treatments.

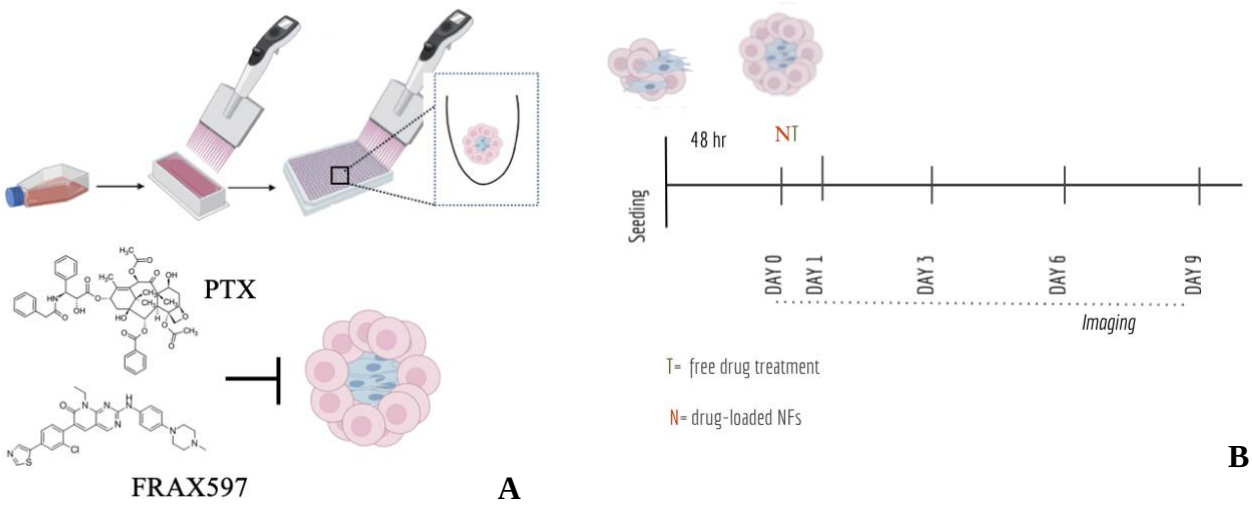

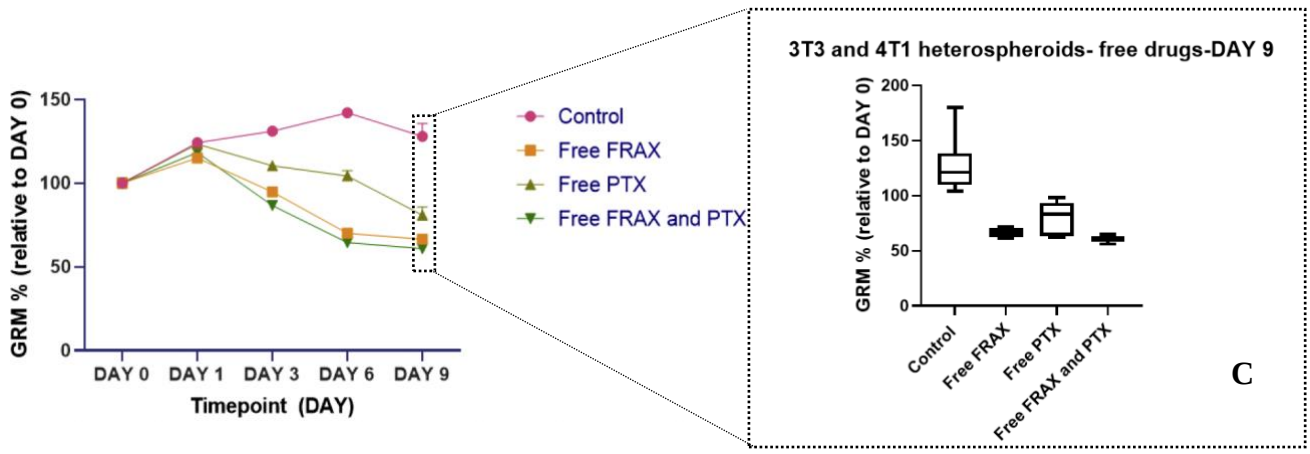

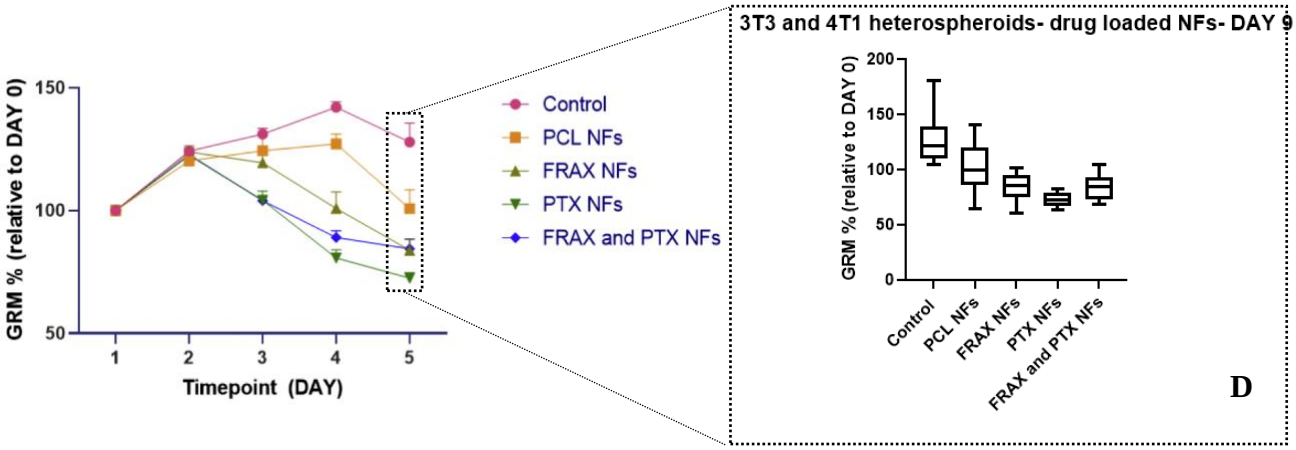

GRM%: Growth rate measurement (%)

Figure 23: *Heterospheroids treatment for 9 days, with one free drug and drug-loaded NFs dosage. (A) Schematic illustration of heterospheroids formation and the chemical types of the drugs (PTX and FRAX597) which used to inhibit heterospheroids growth (B) Timeline of the second set of experiments (one free drug dosage and one dose of drug-loaded NFs). (C) Growth rate measurement experiments for heterospheroids treated with free drugs (FRAX597, PTX, and FRAX597 and PTX) with the boxplot analysis for DAY 9 (D) Growth rate measurement experiments for heterospheroids treated with drug-loaded NFs (FRAX597-loaded NFs, PTX-loaded NFs, and FRAX597 and PTX-loaded NFs) with the boxplot analysis for DAY 9. Data represent mean ± SEM for 3 independent experiments. *p < 0.05, **p < 0.01, ***p < 0.001.*

5.4.3 Multiple doses of free drugs and a single dose of drug-loaded NFs

The third set of growth rate measurements (GRM %) includes multiple doses of free drugs and a single dose of drug-loaded NFs (**Figure 26 B**), both added on day 0. Multiple doses of free drugs were added to keep the drug that reached the cancer cells at the same level after the media refreshment every three days. This way of treatment represents the way that cancer treatment works, with multiple doses of chemotherapies. The main aim here is to examine if a single dose of drug-loaded NFs can be as much effective as multiple doses of chemotherapies and to investigate the effectiveness of co-therapy-loaded NFs compared to single-drug-loaded NFs.

Figure 24 presents images that were obtained from EVOS microscope and provides the significant difference in heterospheroids' growth between the different treatments after observation for a total of 9 days.

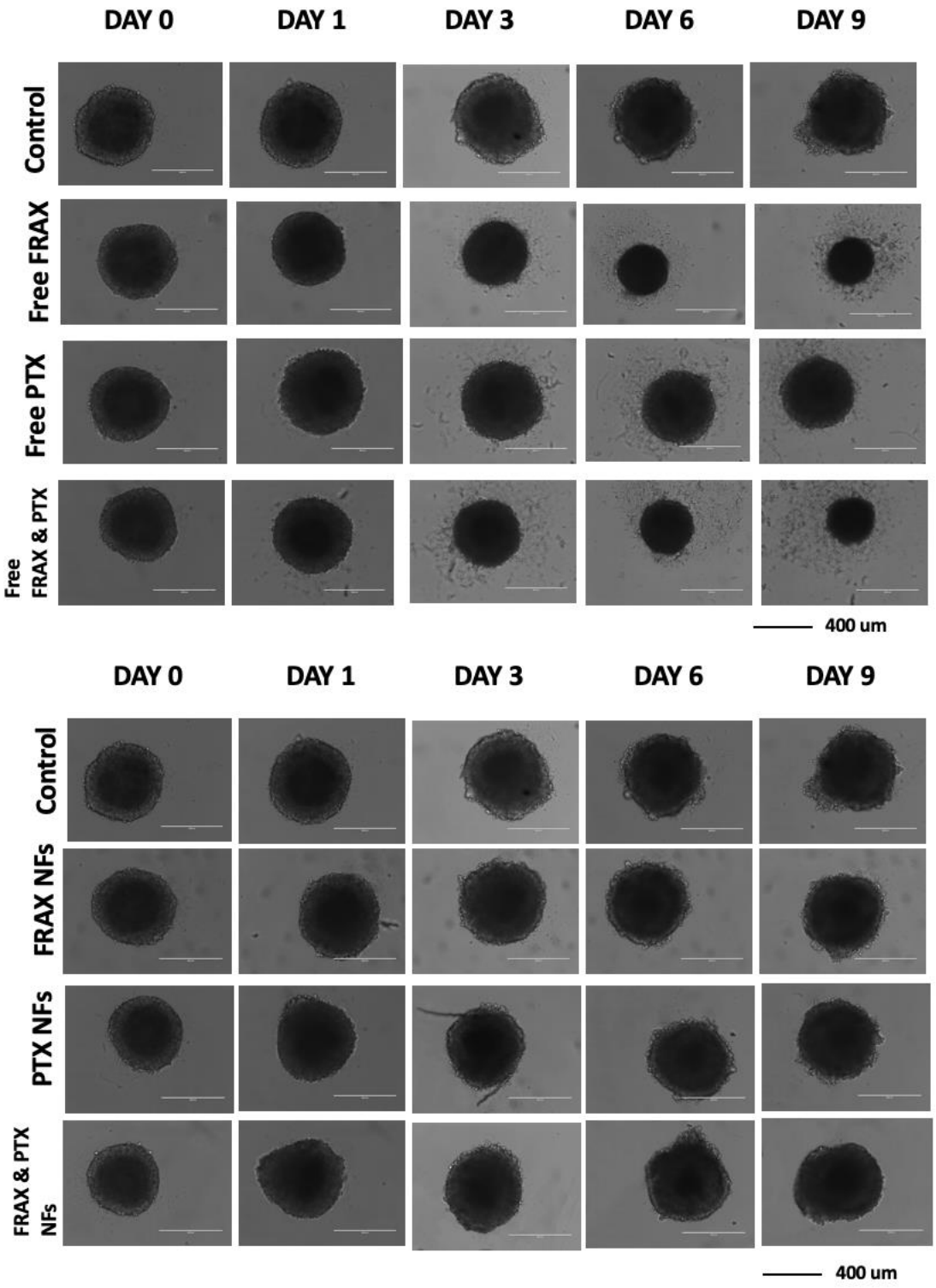

Figure 24: Images obtained from EVOS microscope for 9 days of heterospheroids treatment. *Effect of growth inhibition on 3T3 and 4T1 heterospheroids treated with free drugs (FRAX597, PTX, and FRAX597 and PTX) and drug-loaded NFs (FRAX597-, PTX-, and FRAX597 and PTX-loaded NFs).*

Free FRAX597 is observed to inhibit heterospheroids growth more than PTX or the combination therapy. Regarding **Figure 26B**, FRAX597 inhibition activity reduced the spheroids' growth to more than 50%. Free FRAX597 and PTX also seemed to inhibit growth and decrease spheroids size to almost 50 % on DAY 9 compared to DAY 1. Boxplot (**Figure 26B**) analyzed the growth rate percentage measurement on DAY 9, 12 days after spheroids seeding. It can translate into an agreement with what was observed earlier. Thus, FRAX597 inhibits heterospheroids growth rate with a significant difference from the combination therapy, while PTX shows the lower effect on the spheroids' growth.

On the other hand, heterospheroids treated with drug-loaded NFs provided different results. **Figure 26C** provides the growth rate measurement for heterospheroids treated with FRAX597-, PTX-, and FRAX597 and PTX-loaded NFs. According to the outcomes, co-therapy shows the most significant reduction in spheroids' growth. In addition, boxplot analysis on spheroids' growths at DAY 9 provides a significant difference for FRAX597 and PTX-loaded NFs in comparison with PTX-loaded NFs and FRAX597-loaded NFs.

The growth reduction for heterospheroids seemed more efficient for free drugs than drug-loaded NFs treatments (**Figure 26D**). However, co-therapy-loaded NFs provided promising results by decreasing spheroids' growth up to 50 % on DAY 9, almost the same effect with free drug treatment after three doses.

Luminescent cell viability was conducted with CellTiter-Glo assay (**Figure 25)**. The outcome shows that the cell viability of heterospheroids treated with free FRAX597 was low and probably not detectable by this method and free co-therapy of drugs provided a high reduction in heterospheroids' growth. However, regarding drug-loaded NFs, there was no significant difference between the treatments.

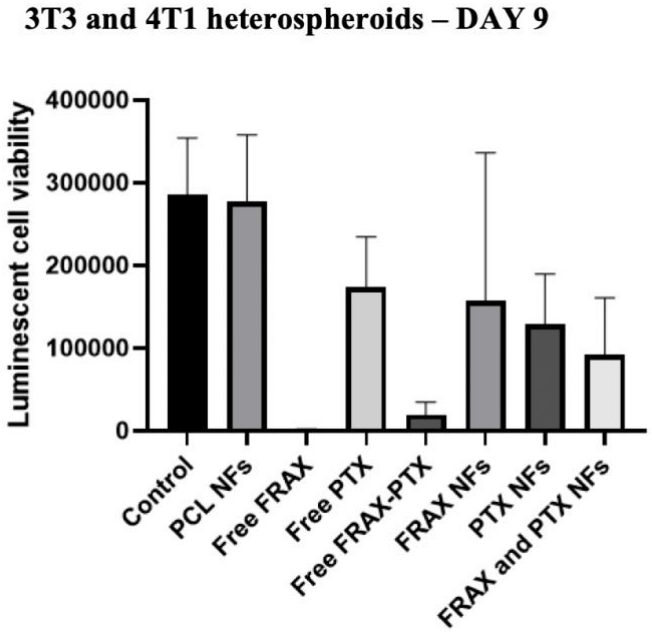

Figure 25: *Luminescent cell viability for 3T3 and 4T1 heterospheroids performed on DAY 9.*

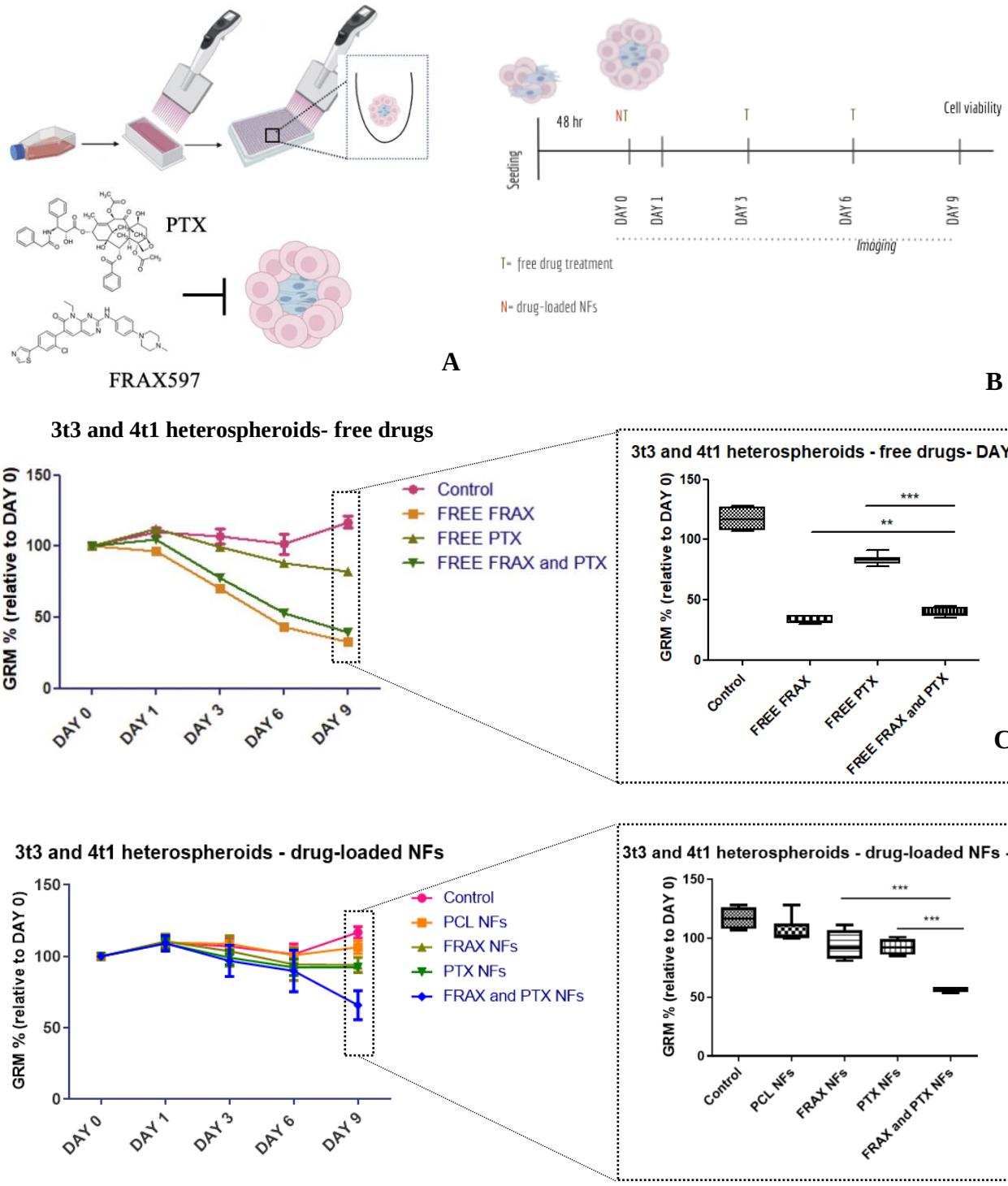

GRM%: Growth rate measurement (%)

Figure 26: *Heterospheroids treatment for 9 days, with three free drug doses and one dose of drug-loaded NFs. (A) Schematic illustration of heterospheroids formation and the chemical types of the drugs (PTX and FRAX597) which used to inhibit heterospheroids' growth. (B) Timeline of the first set of experiments (three*

*free drug doses and one dose of drug-loaded NFs). (C) Growth rate measurement experiments for heterospheroids treated with free drugs (FRAX597, PTX, and FRAX597 and PTX) with the boxplot analysis for DAY 9 (D) Growth rate measurement experiments for heterospheroids treated with drug-loaded NFs (FRAX597-loaded NFs, PTX-loaded NFs, and FRAX597 and PTX-loaded NFs) with the boxplot analysis for DAY 9. Data represent mean ± SEM for 3 independent experiments. *p < 0.05, **p < 0.01, ***p < 0.001.*

Luminescent cell viability for 4T1 homospheroids (**Figure 27**) showed that heterospheroids treated with free FRAX597 provided the lower cell viability in comparison with other treatments. Moreover, free FRAX597 and PTX also showed decreased cell viability, while between drug-loaded nanofiber treatments there is no significant difference.

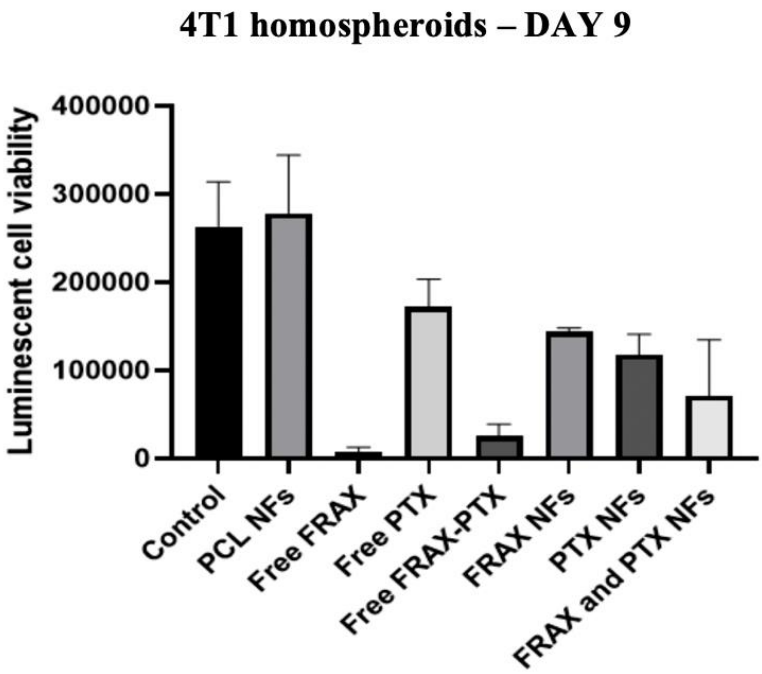

Figure 27: *Luminescent cell viability for 4T1 homospheroids performed on DAY 9.*

4T1 homospheroids treated with free drugs and drug loaded showed a decrease in comparison with control for growth rate measurement study (**Figure 28**) and the most significant difference is provided by treatments with free FRAX597 and free FRAX597 and PTX (**Figure 28A, B**).

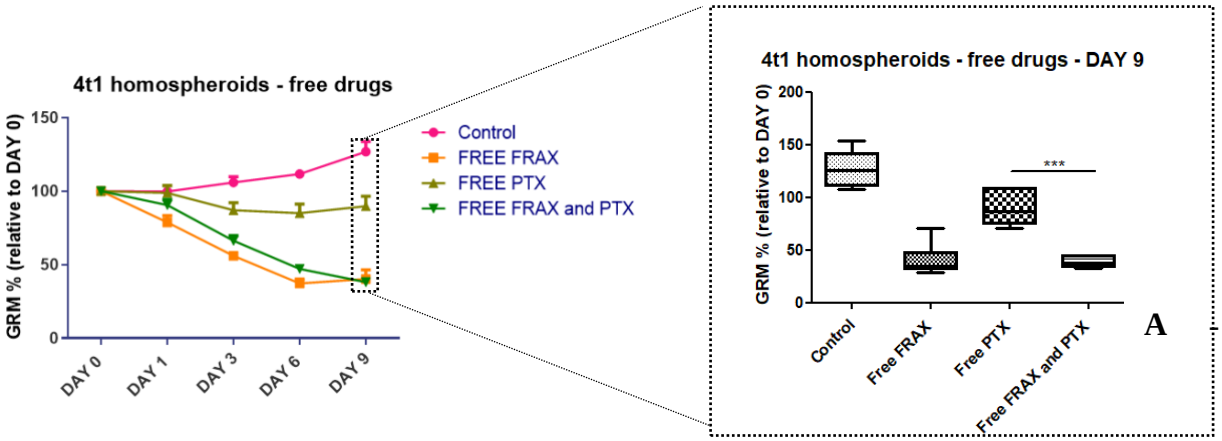

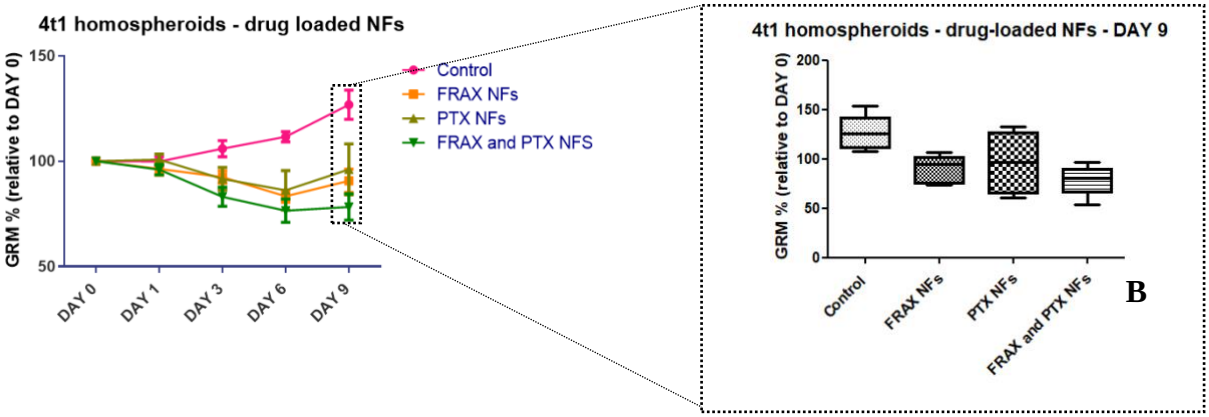

GRM%: Growth rate measurement (%)

Figure 28: *4T1 homospheroids treatment with three doses of free drugs and one dose of drug-loaded NFs. (A) Growth rate measurement experiments for homospheroids treated with free drugs (FRAX597, PTX, and FRAX597 and PTX) with the boxplot analysis for DAY 9 and (B) Growth rate measurement experiments for homospheroids treated with drug-loaded NFs (FRAX597-loaded NFs, PTX-loaded NFs, and FRAX597 and PTX-loaded NFs) with the boxplot analysis for DAY 9. Data represent mean ± SEM for 3 independent experiments. *p < 0.05, **p < 0.01, ***p < 0.001.*

6. Discussion

Cancer is the leading cause of death worldwide. In 2020, there were 19.3 million new cancer cases and almost 10 million cancer deaths. Breast cancer is the most common cancer among women, with 576,300 cases in 2020.

The current cancer treatments provide side effects and failures leading to difficulties in surgical resection, high resistance to radiation- or chemotherapy. However, the TME or stroma cells play a crucial role in the treatments' failures; they prevent the penetration of therapeutic agents to the tumor site. TME consists of cancer cells as well as non-cancerous stromal cells, endothelial cells, immune cells. Among them, cancer-associated fibroblasts are the most abundant cells within TME. TME is a promising approach to treat cancer. Targeting the tumor microenvironment means targeting tumor cells or other cells that promote the tumor progression and metastasis and provide poor drug penetration.

Local drug delivery systems enhance treatment efficacy and minimize toxicity. Their advantages relied on the controlled and extended-release, the specific targeting of the tumor, and the avoidance of surgical removal of the device as the used devices are biodegradable and can release drugs to the specific site for an extended period. Due to their high drug loading capacity, flexible conformation, large surface area, and adjustable size and shape, nanofibers are ideal for local drug delivery.

Encapsulation of chemotherapeutic agents will reduce the undesirable side effects and toxicity for normal tissues [41]. Moreover, nanofibers provide local drug delivery with an extended drug release system. In 2015, Shan et al. showed that drug-loaded nanofibers provided a better-sustained release behavior over ten days study [48].

Nanofibers have been extensively used to encapsulate single or dual drugs. For example, in 2009, Xu et al. successfully encapsulated paclitaxel and doxorubicin hydrochloride into PEG-PLA nanofibers. The release behavior of both drugs was attributed to their solubility properties and distribution of nanofibers. In vitro cytotoxicity against rat Glioma C6 cells showed that the dual drug combination showed a higher inhibition and apoptosis against C6 cells than a single drug-loaded system [49]. Farboudi et al., in 2020, synthesized a magnetic gold-coated poly (ε-caprolactone diol) based polyurethane/poly (*N*-isopropyl acrylamide)-grafted-chitosan core-shell nanofibers for controlled release of paclitaxel and 5-FU. The developed nanofibers were examined toward 4T1 breast cancer cells *in vitro* and *in vivo,* and their growth was inhibited during ten days of treatment [50].

In this study, we explored the potential of co-therapy-loaded NFs, targeting both breast cancer cells and cancer-associated fibroblasts. Targeting CAFs can lead to an increase in chemotherapeutic efficacy, enhanced penetration, and avoidance of undesirable side effects on normal cells. Co-therapy includes commonly used chemotherapy, paclitaxel, and an anti-CAFs molecule named FRAX597, which has shown significant data on reducing a-SMA expression on CAFs and tumor inhibitory activity.

The first part of this project focused on developing drug-loaded NFs after the optimization of the electrospinning variables. **Supplementary Figure S1** and **Supplementary Figure S2** summarize the experiments conducted with chloroform/methanol and DCM/DMF in different ratios and different concentrations of PCL. Moreover, **Figure 14** provides the

outcomes of different trials for the applied voltage, flow rate solution, and tip-to-collector distance. SEM was used to characterize the surface morphology of the formed NFs and compare the results to select the variables that better developed NFs, based on their morphology and reproducibility.

Seta Aynaz, in 2016, tested different concentrations of poly-ε-caprolactone (5 to 20 % w/v) dissolved in different solvents such as DMF and DCM. According to the outcomes, PCL solutions of ≤10% w/v concentration were not suitable to produce well-formed fibers in diameter, and they were short in length. That happened because of the low viscosity of PCL solutions. When the concentration was increased to 20% w/v, PCL solution could not support electrospun when dissolved in DMF and DCM [53]. That reflects that the concentration used for the nanofiber's formation should range from 10-20 wt%. This study aligns with the study of Balakrishnan et al. in 2017, in which electrospun successfully 15 wt% PCL dissolved in N, N-dimethylformamide (DMF), and dichloromethane (DCM) solvent mixture at 70:30 ratio and results in 1.5 um average diameter fibers [51]. For our electrospinning set-up and the environmental variables, 15 wt% PCL dissolved in DCM/DMF (7/3) could not provide nanofibers (**Supplementary Figure S2**). Thus, we should adjust these variables to our electrospinning system.

Can-Herrera et al., in 2021, studied the effect of the applied voltage on the morphology and the mechanical properties of electrospun PCL fibers, and they concluded that by increasing the applied voltage, larger fiber diameter could be produced [52]. That lined up with our result in **Figure 14**. Moreover, in 2021, Luraghi et al. provided a list of the variables and how these affect the electrospinning process. They mentioned that high flow rate solution crated beaded NFs while low flow rate can decrease the fiber diameter. These results also corresponded to our results in **Figure 14**, where for lower flow rate solution, beaded NFs are observed.

Furthermore, the tip-to-collector distance may also affect the NFs formation; when the distance is small, the fibers could not be formed, and when the distance is high, beaded nanofibers are formed [53]. According to Yun-Ze Long et al., a typical distance ranges from 10 to 15 cm is sufficient for the solvent to vaporize and for fiber to produce. Thus, we only tested three different distances, 10, 15, and 20 cm, and concluded that 15 cm distance provides the best-formed nanofibers' diameters (**Figure 14**) [37].

Considering all the above, we concluded the more promising electrospinning variables are 30 kV applied voltage, 3 ml/hr solution flow rate, and 15 cm distance from the tip of the syringe to the collector. Regarding the solvents and the polymer concentration, 11 wt% of PCL dissolved in DCM/DMF in a ratio of 8/2 provided the most optimistic morphology of NFs.

The diameters of PCL were observed from 0.34 to 1.56 um, according to Li et al. in 2018, where PCL nanofibers were developed for fast-dissolving drug delivery systems [54]. Moreover, Simsek et al., in 2020, showed the PCL NFs dissolved in DCM/DMF had diameters from 0.697 to 1.02 um [55]. The same study mentioned that fiber diameters decreased with increasing relative humidity in the presence of DCM/DMF. In our project, nanofibers' diameters correspond to the diameters that are mentioned in the above studies. PCL NFs diameters have an average of 0.8 to 1 um, which slightly changes when drugs are encapsulated. PCL NFs are increased in diameter to 1-1.2 um when FRAX597 is added, and decreased when PTX is added to 0.3-0.4 um. When both drugs are added, the dual drugs-loaded NFs diameters are 0.4 to 0.6 um (**Figure 16**). Although the small changes in the NFs diameters, there are no noticeable significant changes in the structure of nanofibers associated with drug absorption.

The second part of the project focused on the 2D cell culture experiments. The two drugs will be tested on 2D cell culture, 3T3 fibroblast, and 4T1 tumor cells. Different FRAX597 and PTX concentrations were tested, and the cells' metabolic activity was observed (**Figure 17**).

Cell viability of 3T3 cells treated with FRAX597 showed that concentration above 5 uM inhibited 3T3 growth, and apoptosis was induced. According to the IC50 graph in **Figure 17**,

FRAX597 induced a 50% inhibition level to 3T3 cells at a concentration of 1.566 uM. Additionally, FRAX597 inhibition properties were investigated in pancreatic cancer cells by Yeo et al. in 2016. FRAX597 inhibited the proliferation of pancreatic cells in a dose-dependent manner with IC50 values between 650 nM for BxPC-3 cells and 2 uM for PANC-1 cells. Also, they showed that FRAX597 inhibited the survival of PANC-1, MiaPaCa-2, BxPC-3, and Pano2 cells only at a concentration greater than 1 uM [27]. Considering the above, 1 uM FRAX597 could be a potential concentration to inhibit 3T3 cells activation and growing rate without inducing apoptosis of 3T3 cells completely.

The same experiment, with PTX concentrations, was examined on 4T1 breast cancer cells. In general, 4T1 cells are mice cells that mimic human breast cancer. When 4T1 cells are injected, they induced tumors that can be used as a post-operative model and a non-surgical model since they induce tumor metastasis in both models with similar kinetics[56]. Thus, the 4T1 cell line is a promising model to test the local delivery system. 4T1 cells treated with PTX showed that cancer cells were inhibited in a concentration above 100 nM (**Figure 17**). In our tested condition, the IC50 graph provided that 131.2 nM of PTX is necessary for 50% inhibition in vitro (**Figure 17**). Various studies provided comparable outcomes for IC50 for 4T1 cells treated with PTX. In 2012, Ying Ho et al. examined the cytotoxicity of paclitaxel on 4T1 breast cancer cells, and cells were exposed to a range of PTX (10-250 nM) for 24 hours. Paclitaxel induced inhibition at a range of 60-67% in the 4T1 cancer cells at a concentration up to 250 nM. They also mentioned that IC40 for PTX is 125 nM [57]. Furthermore, Chen et al., in 2016, calculated that the IC50 for 4T1.2 cancer cells was 287 nM [58], and Gupta et al., in 2019, showed that the IC50 in 4T1 cells was 50nM and only about 35 % of 4T1 cells survived after treatment with 100 nM paclitaxel [59]. In the light of those above-mentioned, 250 nM PTX could be a promising concentration to inhibit 4T1 tumor cells' growth, proliferation, and migration.

Empty PCL NFs and drug-loaded NFs were applied to 3T3 fibroblast and 4T1 breast tumor cells, and their metabolic activity was measured for 72 hr in **Figure 18**. Both cell types of treatment provided no significant difference at 72 hours. However, the cell metabolic could provide a more significant outcome if the study continued for additional days because in **Figure 18,** drug(s)-loaded NFs provided a more decreased behavior than control and empty PCL NFs.

Furthermore, immunocytochemistry staining has tested the ability of FRAX597 to stimulate collagen, resulting in slower wound healing [60]. Wound healing includes synthesizing alpha-smooth actin (a-SMA) and collagen1 production, both detected with a digital fluorescence microscope. Transforming growth factor-beta was added to activate 3T3 fibroblasts. TGF-β is a known potent inducer of collagen synthesis, and it was used as a positive control [60]. In addition, TGF-β induced the expression of a-SMA [61]. 3T3 cells and 3T3-TGF-β activated cells treated with FRAX597 provided decreased expression of a-SMA and collagen 1 (**Figure 19**). This ability of FRAX597 to decrease the amount of a-SMA and collagen could result in slower wound healing [60]. Wound healing includes the synthesis of a-SMA by fibroblasts that convert to contractile cells called myofibroblasts. These cells are essential for wound contraction [60]. **Figure 20** represents the outcomes of the migration/wound healing assay of 3T3 cells activated with TGF- β and their treatment with FRAX597 in two concentrations, 1 uM and 5 uM. Both treatments provided reduced migration/wound healing process. That could happen with the ability of FRAX597 to reduce a-SMA and collagen 1 expression.

The next part of the project includes the investigation of the effect of drug treatments on heterospheroids and homospheroids. Heterospheroids were prepared with 3T3 fibroblasts and 4T1 breast cancer cells in a ratio of 5 to 1. Homospheroids were prepare only with one type of cells and formed 3T3 homospheroids or 4T1 homospheroids. The treatments involve free

drug(s) and drug-loaded nanofibers treatments. Based on the frequency of treatments, this section can be divided into three different steps, while growth rate measurement analysis and CT-Glo assay were used to compare the outcomes.

First, the first set of experiments includes multiple doses of free drug treatments and drug-loaded nanofibers. Both treatments provide some significant decrease in the size of heterospheroids through the days of treatments; among the different treatments, there was not any significant difference (**Figure 22 C, D**). **Figure 21** provides the luminescent cell viability outcomes in which free FRAX597 and free co-therapy provide an essential decrease. Nanofibers' refreshment every three days did not provide any critical difference between nanofibers' treatment. **Supplementary Figures S5 and S6** provide the outcomes of homospheroids with multiple doses of treatments. Both treatments provided no crucial differences.

To understand the effectiveness of different treatments, we moved on to the second part of the experiments, including a single dose of free drugs and a single dose of nanofibers' treatment. This set of experiments did not provide any significant difference between the different treatments (**Figure 23 C, D)**. Still, the results are unclear, and the experiment should be further exanimated in the future with more spheroids to be tested. Here, we expected a better synergistic effect of dual-drug-loaded nanofibers as the nanofibers' treatment was conducted for 9 days. Moreover, for homospheroids' treatment, we could not also observe promising results for 3T3 homospheroids treated with FRAX597 NFs (**Supplementary Figure S7**) and 4T1 homospheroids treated with free FRAX597 and co-therapy NFs (**Supplementary Figure S8**). These outcomes provided no decrease in the growth of homospheroids, and their values were almost similar to the untreated homospheroids.

The last experiments include multiple drug doses and a single dose of the drug-loaded NFs. **Figure 24** shows the difference in heterospheroids growth by images that were obtained from the EVOS microscope. DAY 0 presents the timepoint 48 hours after the heterospheroids formation. The most notable difference in the size reduction is provided by free FRAX597(**Figure 24**). The effect of FRAX597 also caused a reduction in heterospheroids size when it is treated with free FRAX597 and PTX.

FRAX597 is a group I PAK inhibitor studied in the pancreatic cancer mouse model by Yeo et al. in 2017. Yeo and his co-workers showed that FRAX597 could improve pancreatic cancer survival by suppressing pancreatic stellate cell activation [28]. In 2016, Yeo and his co-workers also studied the synergistic effect of FRAX597 with gemcitabine on pancreatic tumor growth. They mentioned that PAK 1 was expressed in all human pancreatic cancer samples tested. They mainly showed that inhibiting PAK1, pancreatic cancer cell growth, and survival are inhibited and the sensitivity to gemcitabine treatment is increased. Moreover, they investigated that FRAX597 could inhibit the survival, proliferation, and migration of pancreatic cancer cells [27]. Christy C. Ong et al., in 2011, mentioned that PAK1 expression was significantly increased in breast cancers [62], [63] and that high expression was correlated with progression [62] and proliferation of cancer [63]. Furthermore, the same study referred that PAK1 played an essential role in cell motility and survival. In 2005, Guraraj et al. proposed that PAK1 is a common point of convergence of growth factor signaling, and in estrogen receptor (ER)-positive breast cancer, PAK1 directly interacts with ER [64], [65].

In addition, PAKs have been demonstrated to relate to drug resistance [66]. PAKs can influence various signaling pathways such as the WNT/b-catenin signaling pathway, EGFR/HER2/MAPK signaling pathway, PI3K/AKT signaling pathway, NF-kB cascades, and epithelial–mesenchymal transition (EMT) signaling pathways. The cross-talk between MAPK and P13K/AKT signaling pathways enhanced the cancer drug resistance [66].

Taking all the above into consideration, PAK inhibitors are considered to have enhanced antitumor activity. PAKs inhibitors may inhibit cancer proliferation and migration and prevent drug resistance present during chemotherapy in heterospheroids' treatment. Thus, FRAX597, which is a PAK inhibitor, can also be used for anticancer activity. That can be explained by the fact that FRAX597 works better than chemotherapy. That aligns with the results from the CellTiter-Glo assay and the heterospheroids' growth rate measurement studies. The luminescent cell viability for heterospheroids treated with free FRAX597 was so low that it was not detectable by CellTiter-Glo assay (**Figure 25**). Free FRAX597&PTX treatment also provides low cell viability (enhanced by FRAX597 activity), while free PTX treatment provided the highest level of heterospheroids viability compared with the other free drug treatments. Similar results are also provided by **Figure 26C**, in which free FRAX597 treatment showed the most significant increase in heterospheroids size following by co-therapy and paclitaxel treatments.

Drug-loaded NFs contributed to some different outcomes. In particular, in **Figure 26D**, where the results of the drug-loaded NFs on DAY 9 are given; the higher size decrease in heterospheroids is provided by the co-therapy-loaded NFs. The synergistic effect of FRAX597 and PTX encapsulated on NFs provided promising results for the co-therapy treatment that actualized this project's hypothesis. Co-therapy-loaded nanofibers decreased heterospheroids size up to 60% on day 9 (**Figure 26D**) with an essential significant difference. Homospheroids treatment could not support this outcome (**Figure 28 B, Supplementary Figure S9**) that provided no significant difference between the different ways of nanofibers' treatments. The stroma presented on heterospheroids is probably inhibited by FRAX597, leading to increased inhibition of the heterospheroids' growth.

Moreover, FRAX597 provided some increased antitumor activity against 4T1 homospheroids in **Figure 27**. Free FRAX597 following by free FRAX597&PTX treatment gave the lowest luminescent cell viability on 4T1 homospheroids. This could not be observed by FRAX597-loaded NFs treated 4T1 homospheroids or heterospheroids. Contrary to the increased heterospheroids' size inhibition of free FRAX597 treatment (**Figure 26 C**), FRAX597-loaded NFs could not work so effectively (**Figure 26 D**). The above may happen due to the FRAX597 release profile when it was encapsulated into the nanofibers. To our best knowledge, FRAX597-loaded NFs have not been studied yet, so further investigation is needed to understand their encapsulation efficacy.

7. Conclusion

To summarize, in this project, we successfully developed poly-ε-caprolactone electrospun nanofibers, which could encapsulate single and dual therapy. 11 wt % PCL dissolved in a ratio of 8/2 of DCM/DMF were electrospun with simple blend electrospinning with the optimized electrospinning variables. Furthermore, drugs (FRAX597 and paclitaxel) as an individual or in combination were incorporated into NFs. The developed nanofibers were characterized by scanning electron microscope, and their surface morphology was observed uniform, smooth without beads, and drug encapsulation did not affect the diameter of the nanofiberσ, which was ranged from 0.3 to 1.2 um.

Free drugs and drug-loaded nanofibers treatments were firstly tested on 3T3 fibroblasts and 4T1 breast cancer cells. The concentration of drugs tested and provided some promising results was 1 uM for FRAX597 and 250 nM for PTX treatment. Drug-loaded nanofibers tested on 2D cultured cells did not provide any significant difference as the experiments were conducted only for three days, and the drug release from nanofibers was not enough to inhibit cell activity. Moreover, we developed different spheroids to mimic the tumor stroma. 3T3 fibroblasts and 4T1 breast cancer homospheroids and 3T3 and 4T1 heterospheroids were formed, with heterospheroids to present a better mimic environment of the tumor microenvironment as they consisted of cancer and stromal cells. Heterospheroids showed a smaller size and higher growth due to the presence of fibroblasts. This concludes that the model is established to evaluate the effect of both chemotherapy and anti-stromal therapy. Among treatments, free FRAX597 provided the most significant decrease in spheroids' growth rate. FRAX597 is a PAK 1 inhibitor. PAKs are expressed in breast cancer and promote tumor proliferation, survival, and migration.

Additionally, PAKs are connected with increased drug resistance. Inhibiting PAKs may lead to enhanced drug penetration and antitumor activity. All the above were confirmed by heterospheroids growth rate results when treated with FRAX597. In most of the experiments conducted with spheroids, FRAX597 seemed to inhibit tumor growth more significantly than paclitaxel. Further, in heterospheroids experiments with multiple doses of free drugs and a single dose of drug-loaded nanofibers, co-therapy delivery provided promising results in inhibiting tumor activity.

In conclusion, we have developed a local drug releasing system that can deliver two drugs with different functions, simultaneously inhibiting stroma and killing tumor cells more effectively.

8. Future Perspectives

In this project, dual-drug-loaded PCL nanofibers were successfully developed with a simple blending electrospinning process. As mentioned above, blend electrospinning is easy to use, and nanofibers' fabrication could occur by mixing the polymer with the desired solvents, and the drugs diluted in solvents were added to the polymer-solvent solution. Shatil Shahriar et al., in 2019, mentioned that with blend electrospinning might occur drug enrichment on the surface of the polymer following by an initial burst release of the loaded drug, decreasing the lifetime of drug delivery. So, to have sustained release, local and controlled release, and promote the drug activity core-shell nanofibers could be a great option [41]. Coaxial electrospinning provides core-shell nanofibers formation. The inner part, where therapeutic agents are encapsulated, protects the biological activity and controls the release of these agents. In that way, many obstacles that may occur when electrospun nanofibers are developed with blend electrospinning could be avoided.

Further, multiple chemotherapies and drugs can be delivered for more significant inhibition of tumor activity. In 2020, Li et al. combined various chemotherapeutics with time programmed administration from a single tri-layered carrier for breast cancer treatment [53]. The multiple drug delivery might provide further inhibition of stromal cells, enhancing the chemotherapy's activity. Furthermore, the directional release of the therapeutic agents can be achieved. In 2021, Abdelrahman I. Rezk et al. developed a tri-layer membrane with controlled drug delivery of paclitaxel. This tri-layer membrane consists of polyurethane loaded with silver ions, which could induce drug release into a single direction and provide antimicrobial effect, polyurethane and paclitaxel in which anticancer drug was loaded poly-ε-caprolactone layer to control drug release. Following the same idea, a new design of nanofibers could be developed with the directional release of PTX and FRAX597.

Additionally, further characterization of the electrospun nanofibers could better understand the quality and efficacy of nanofibers. Some characterizations that could be applied are transmission electron microscopy (TEM) for observing the inner structural nanofibers, Fourier-transform infrared spectroscopy (FT-IR) to investigate the chemical functional groups, and the X-ray photoelectron spectroscopy (XPS) to characterize the chemical composition of the nanofibers. Furthermore, various parameters can be analyzed, such as drug loading efficacy, tensile strength, drug permeability, and degree of swelling to establish the therapeutic potential of nanofibers.

Many studies have been worked with a greater amount than what we used regarding the loaded drugs. Gamze Varan et al., in 2021, determined that the IC50 value of PTX was 3.78 uM for 4T1 cells [67]. According to that, maybe by increasing the amount of paclitaxel loaded in the electrospun nanofibers, more paclitaxel could be released, and more cancer cells could be inhibited.

It is crucial to perform *in vivo* experiments to understand the true potential of the drug-loaded electrospun nanofibers as anticancer and antistromal agents. *In vivo* models include treatment of breast tumors induced in mice, where drug-loaded nanofibers can be inserted and place next to the tumor or applied as a patch for transdermal drug delivery. Furthermore, electrospun nanofibers could be applied and tested on postoperative tumor treatment efficiency. A possible follow-up experiment of this project might be investigating how the drug-loaded electrospun nanofibers affect the expression of various cancer-associated fibroblasts and tumor markers. However, immunofluorescent staining for heterospheroids treated with FRAX597 and paclitaxel (free or loaded into nanofibers) provided not successfully results

(**Supplementary Figure S13**). **Supplementary Figure S13** provided staining for a-SMA and collagen 1 expression, both known as molecular/histopathological markers of CAFs [68]. Further staining such as Vimentin staining was also performed as vimentin is associated with cancer invasion [69], Ki-67 staining was used as a tumor marker. Hence Ki-67 is a nuclear protein associated with cellular proliferation [70] and staining of E-cadherin, a diagnostic biomarker in breast cancer [71]. The method to stain the heterospheroids sections (**Supplementary methods 9.1 and 9.2**) should be further optimized to have successfully immunofluorescent staining. We suggest that the spheroids should not be fixed with 4% formaldehyde as it is widely accepted that cross-links may occur during the fixation with formaldehyde [72].

9. Supplementary Materials

a. Supplementary Methods

9.1 In-vitro release study

The drug release study from electrospun nanofibers was measured by placing 1.5 × 1.5 cm^2 of drug-loaded NF in 100 ul of PBS. The temperature was maintained at 37 °C. The whole PBS was collected at specific time points, and fresh PBS replaced it. The samples were collected every one or two days, except for the first day, where samples were collected at 1hr, 2 hr, and 5 hr. The study was continued for one month for each NF.

9.2 Spheroids preparation for cryotome sectioning

Homospheroids (NHI3T3 and 4T1 cells) were prepared with the method that was described above. After 24 hr treatment was added, and 8 conditions were prepared. The control condition (heteropsheroids without treatment), 1 uMFRAX597 heterospheroids, 250 nM PTX heteropsheorois, 1uM FRAX597 & 250 nM PTX heterospheroids, FRAX597-loaded NFS heterospheroids, PTX-loaded NFs heterosperoids, and FRAX597&PTX-loaded NFs spheroids. For the drug-loaded NFs hetrospheroids, 2mm drug-loaded NFs were cut and placed into the wells next to the heterospheroids. The medium was refresh after 3 days, and on the sixth day, all the spheroids were collected. The heterospheroids were fixed with 100 ul of 4% paraformaldehyde (Sigma-Aldrich) for 30 min at room temperature after their media were discarded. Then, they were washed with warm DPBS and transferred into a plastic mold (1.5 x 1.5 cm^2), where extra DPBS was discarded. Afterward, the spheroids were collected and embedded in cryomatrix (Shandon Cryomatrix, Thermofisher Scientific) and directly placed on dry ice for a few minutes. Then, they were stored at – 80 ^{o}C for later experiments.

9.3 Immunofluorescent Staining- 3D heterospheoirds

Previously, the cryomatrix embedded heterospheroids were cut into 8 um thick slices using FSE Cryotome (Thermofisher Scientific) and collected on microscope slides (Superfrost Plus, Thermofisher Scientific). After drying under warm air, the slides were either stored at -20 ^{o}C or kept for further use. The heterospheroids collected on microscope slides were fixed with 100% acetone for 10 minutes. Afterward, a hydrophobic circle was made by PAP-pen/ Immedge pen (Life Technologies), and the slides were washed 3 times with PBS (5 min each). After washing, the primary antibody was diluted in PBS as instructed by the manufacturers. The slides were incubated overnight at 4 ^{o}C or for 1 hr at room temperature, depending on the used antibody. The next day, the slides were washed before the secondary fluorescent antibodies (Alexa Fluor 488 and 594) were added (diluted in PBS) and incubated for 1 h. Finally, the slides were washed three times more (5 min each), sealed with cover plate using a DAPI mounting medium (Fluoroshield with DAPI, Sigma-Aldrich, St.Louis, MO, USA) and dried overnight. Images were taken using a Nikon Eclipse E400 microscope (NIKON) equipped with fluorescent filters equipped with fluorescent filters and Hamamatsu Nanozoomer 2.0RS (Hamamatsu Photonics, Hamamatsu, JP).

b. Supplementary Figures

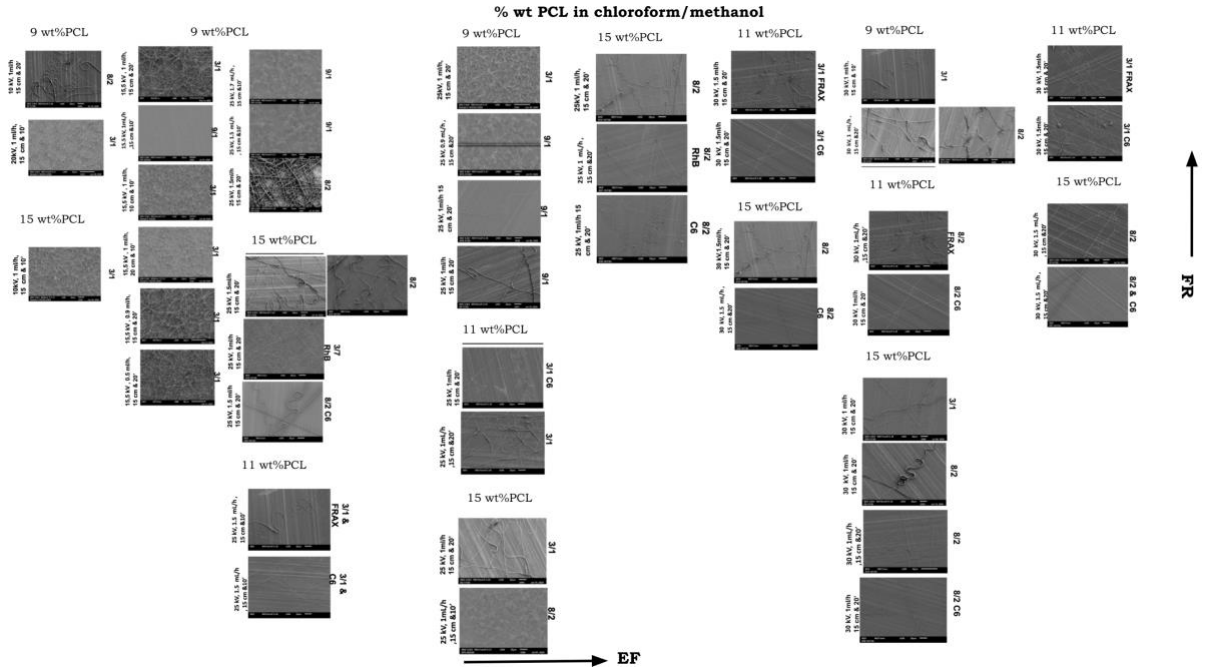

Figure S1: *Summary of developed PCL nanofibers dissolved in chloroform/methanol. Different percentages per weight of PCL were dissolved in different ratios of chloroform/methanol and several nanofibers were formed with various electrospinning variables.*

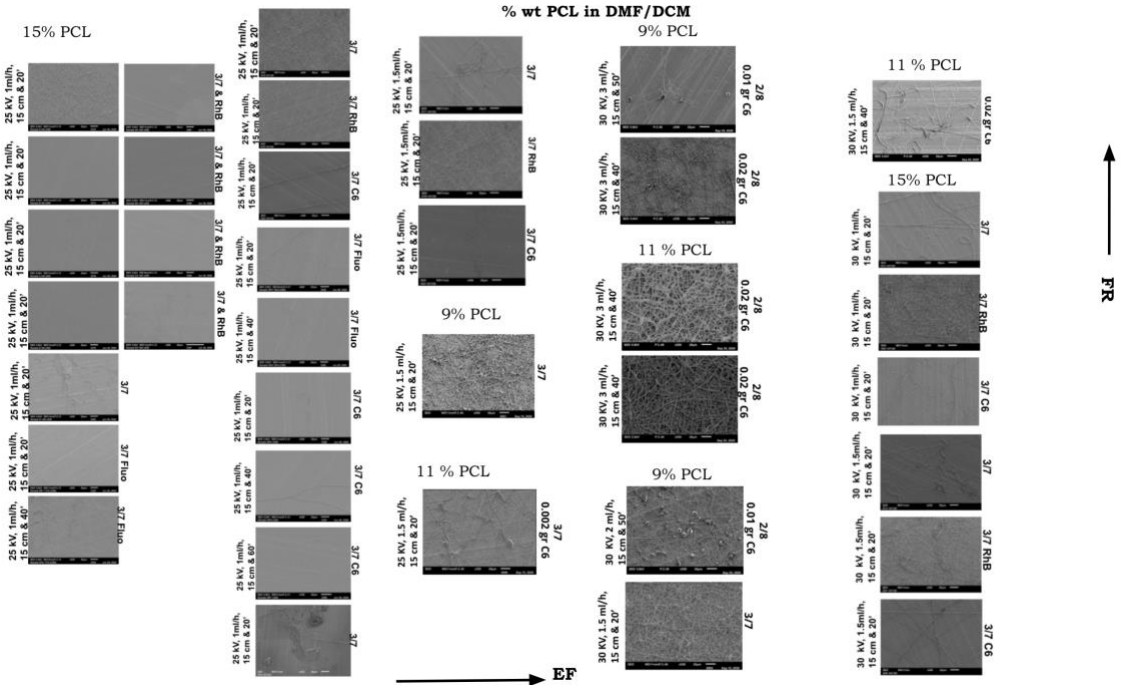

Figure S2*: Summary of developed PCL nanofibers dissolved in DMF/DCM. Different percentages per weight of PCL were dissolved in different ratios of DMF/DCM and several nanofibers were formed with various electrospinning variables*

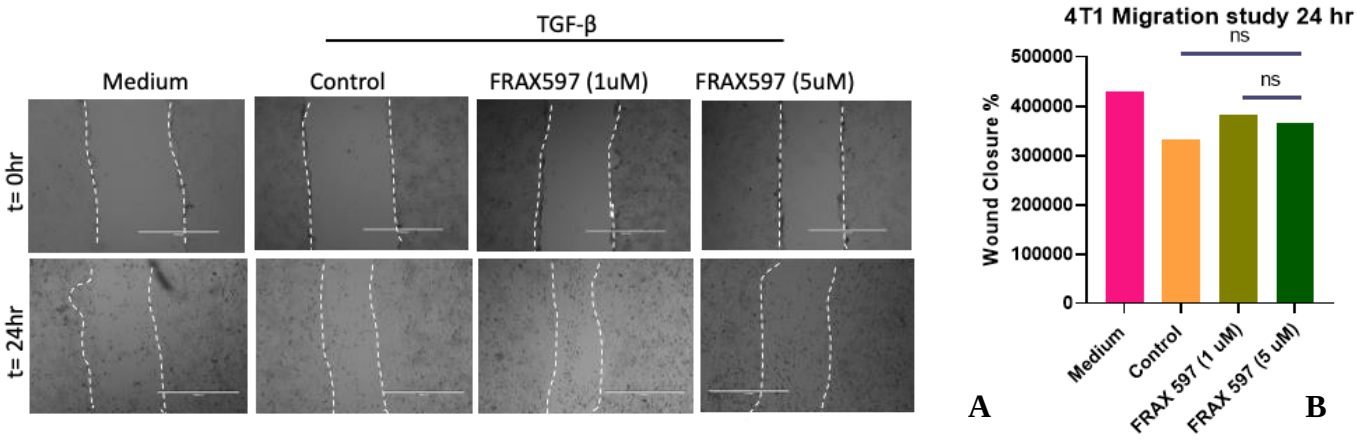

Figure S3: E*ffect of inhibition with FRAX597 (1uM and 5uM) on 4T1 activated cell migration. Microscopic images of migration/wound closure of 4T1 tumor cells. (A) Wound closure at t= 0hr and t=12hr for medium, TGF-β activated medium (control), and two treatments of FRAX597 applied on activated 4T2 tumor cells. (B) Quantitative analysis of the wound closure after 24hr incubation.*

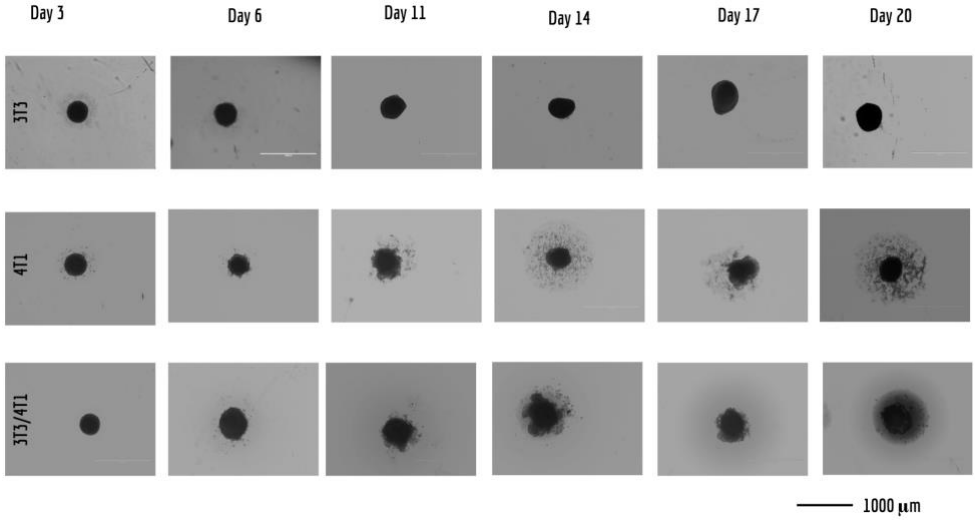

Figure S4: *3T3 and 4T1 homospheroids (60.000 cells/ml) and 3T3/4T1 heterospheroids (60.000 cells/ml in a ratio of 5/1) growth rate measurement for 20 days.*

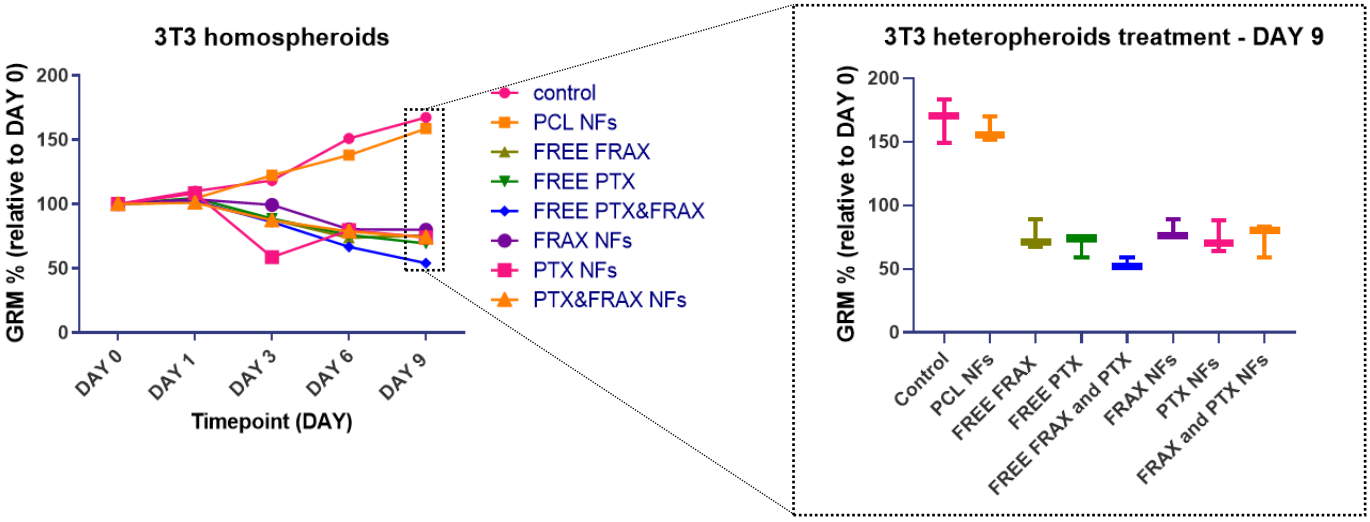

Figure S5: *Growth rate measurement study of 3T3 homospheroids treated with free drugs and drug-loaded NFs. 3T3 homospheroids were treated for 9 days with multiple doses of free drugs and drug-loaded NFs and the boxplot analysis for DAY 9 is observed.*

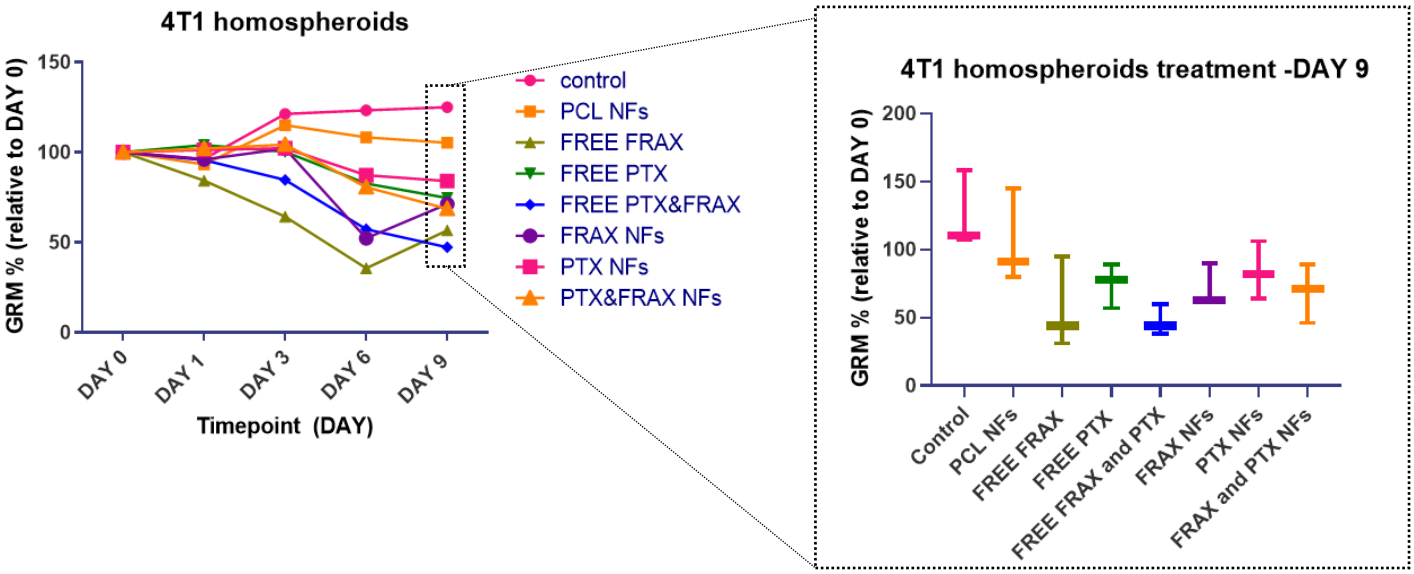

Figure S6: *1Growth rate measurement study of 4T1 homospheroids treated with free drugs and drug-loaded NFs. 4T1 homospheroids were treated for 9 days with multiple doses of free drugs and drug-loaded NFs and the boxplot analysis for DAY 9 is observed.*

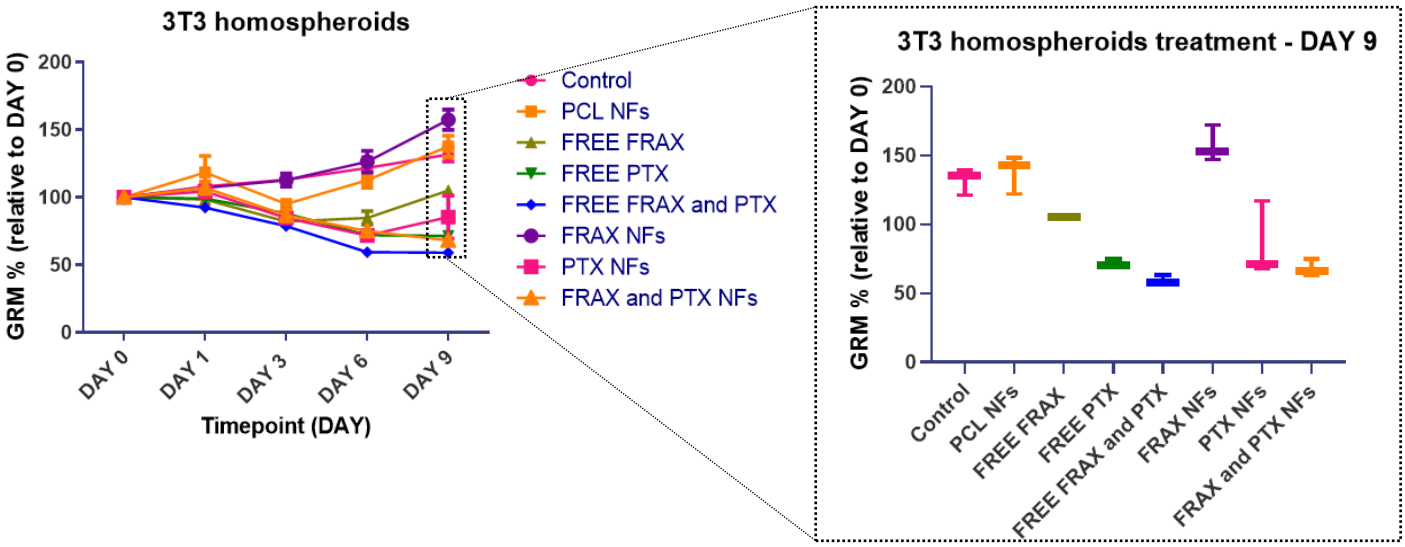

Figure S7: *2 Growth rate measurement study of 3T3 homospheroids treated with free drugs and drug-loaded NFs. 3T3 homospheroids were treated for 9 days with a single dose of free drugs and drug-loaded NFs and the boxplot analysis for DAY 9 is observed.*

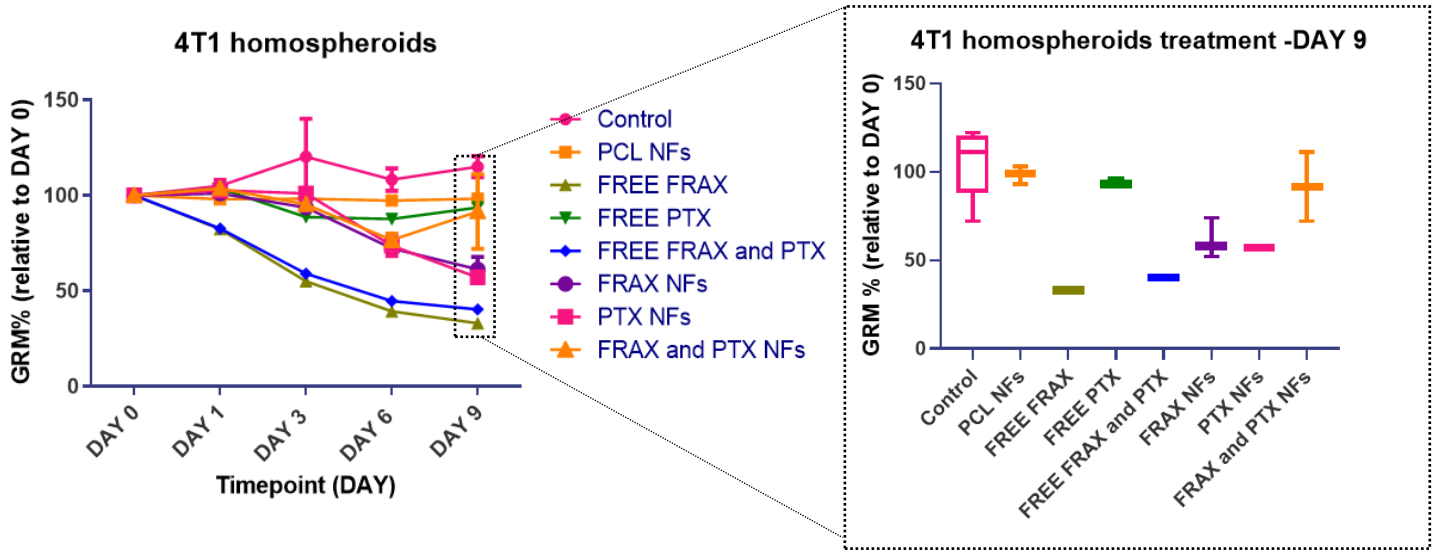

Figure S8: *Growth rate measurement study of 4T1 homospheroids treated with free drugs and drug-loaded NFs. 4T1 homospheroids were treated for 9 days with a single dose of free drugs and drug-loaded NFs and the boxplot analysis for DAY 9 is observed.*

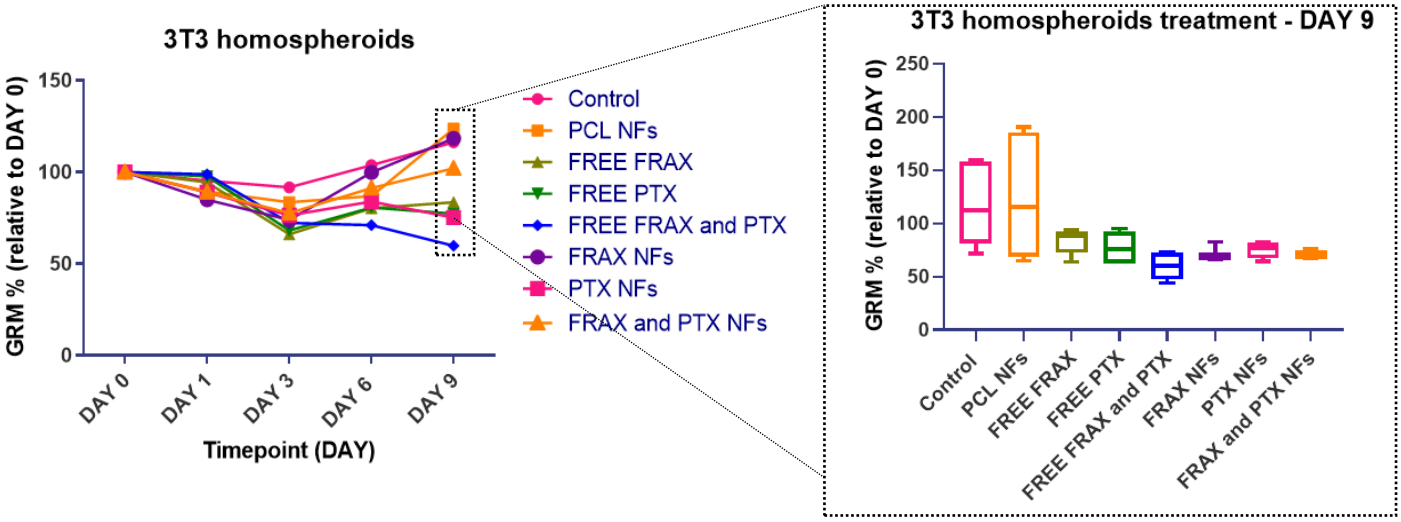

Figure S9: *Growth rate measurement study of 3T3 homospheroids treated with free drugs and drug-loaded NFs. 3T3 homospheroids were treated for 9 days with multiple doses of free drugs and a single dose of drug-loaded NFs and the boxplot analysis for DAY 9 is observed.*

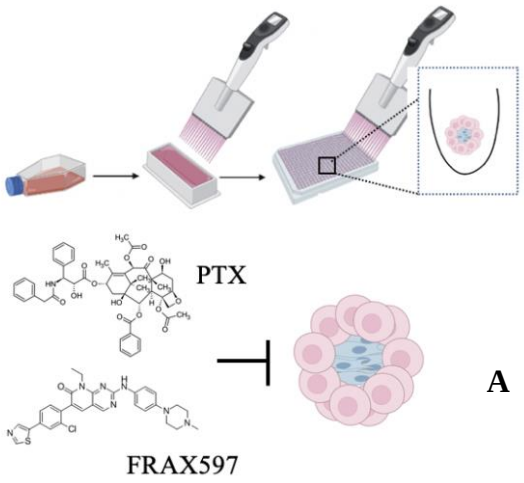

A

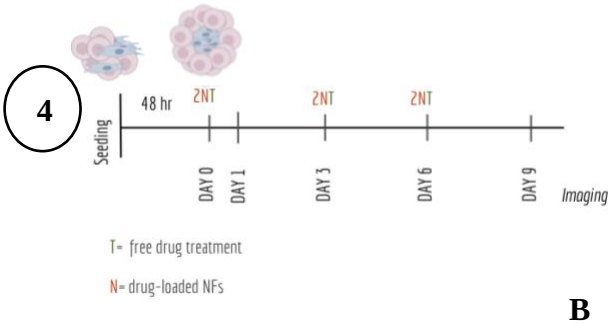

B

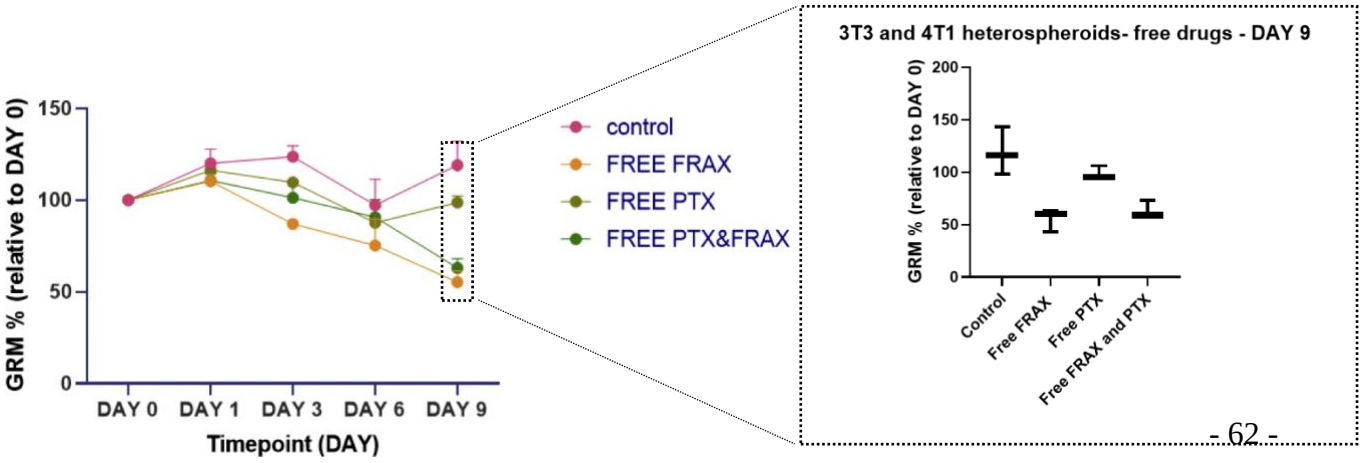

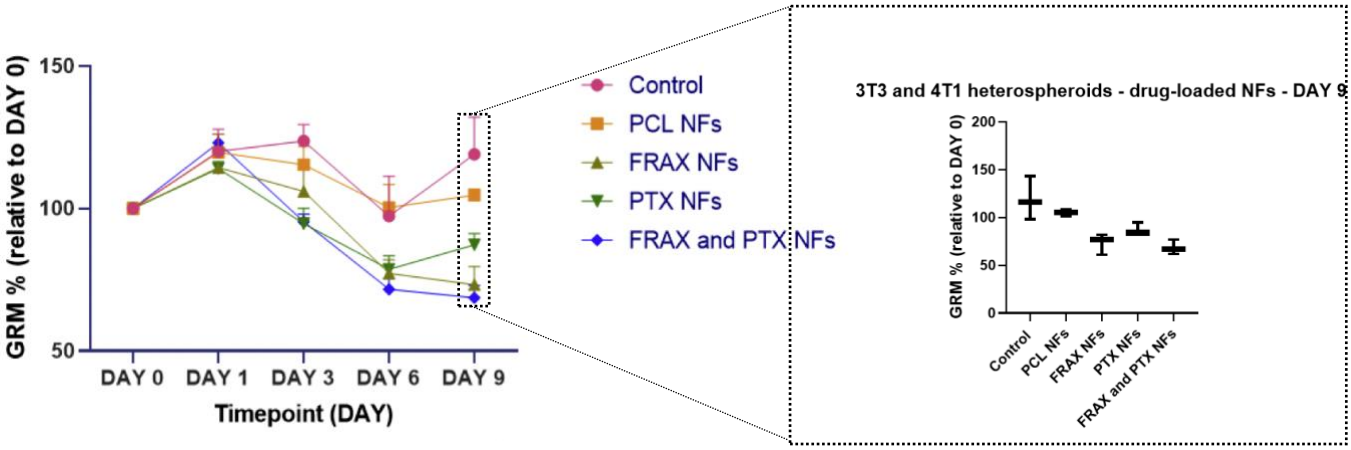

Figure S10: *Heterospheroids treatment for 9 days, with three free drug and twice drug-loaded NFs doses. (A) Schematic illustration of heterosperoids formation and the chemical types of the drugs (PTX and FRAX597) which used to inhibit heterospheroid growth (B) Timeline of the first set of experiments (three free drug doses and three doses of twice drug-loaded NFs). (C) Growth rate measurement experiments for heterospheroids treated with free drugs (FRAX597, PTX, and FRAX597 and PTX) with the boxplot analysis for DAY 9 (D) Growth rate measurement experiments for heterospheroids treated with drug-loaded NFs (FRAX597-loaded NFs, PTX-loaded NFs, and FRAX597 and PTX-loaded NFs) with the boxplot analysis for DAY 9.*

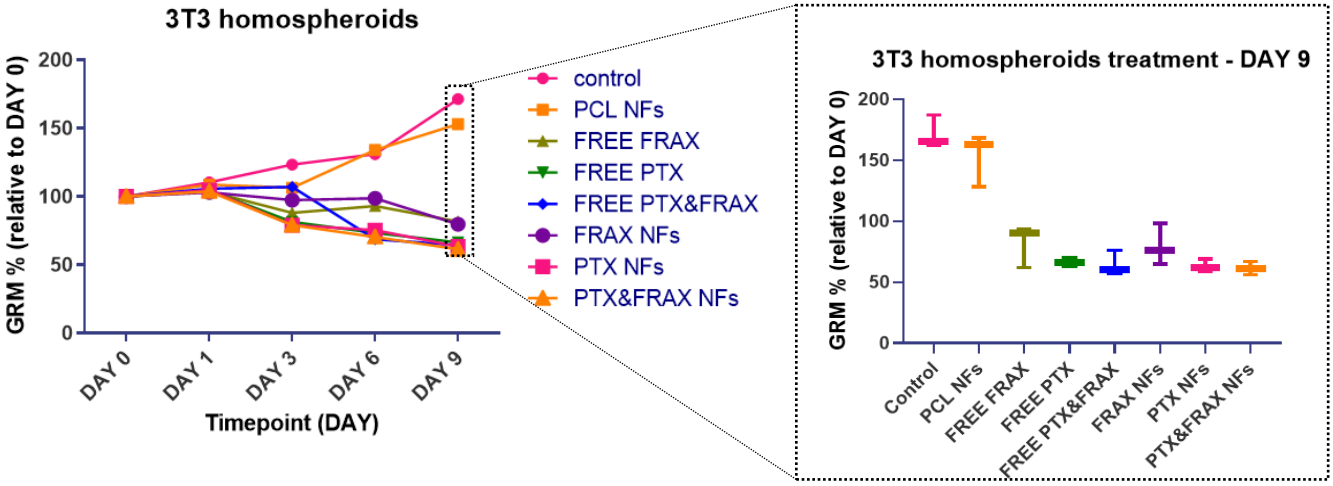

Figure S11: *Growth rate measurement study of 3T3 homospheroids treated with free drugs and drug-loaded NFs. 3T3 homospheroids were treated for 9 days with three doses of free drugs and three doses of double drug-loaded NFs and the boxplot analysis for DAY 9 is observed.*

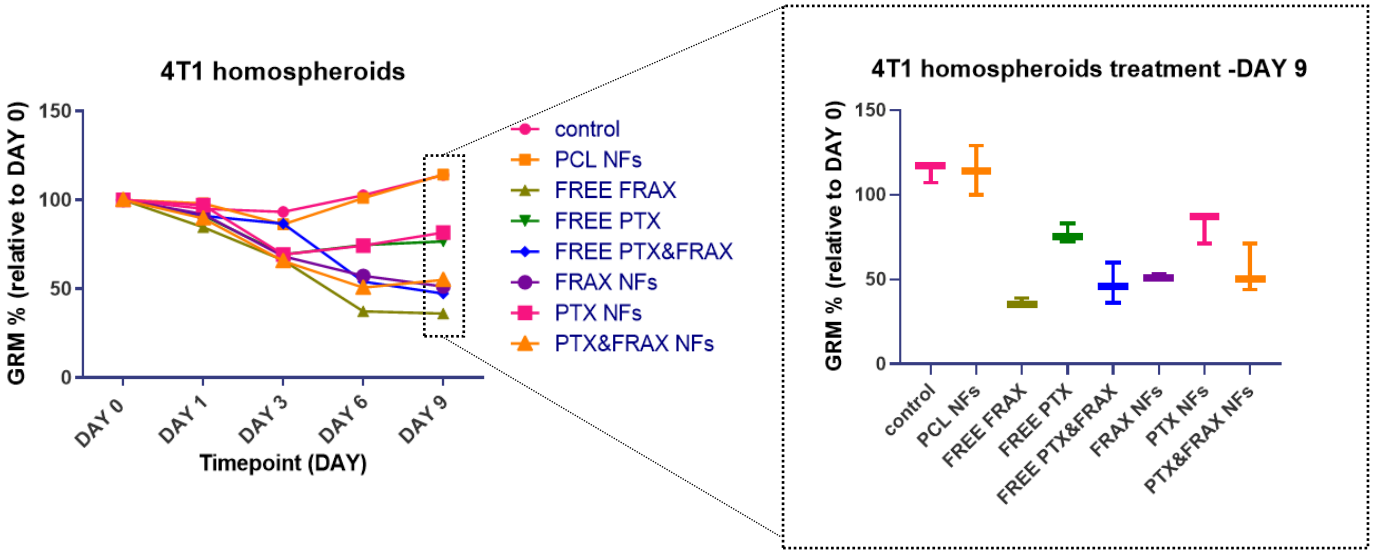

Figure S12: *Growth rate measurement study of 4T1 homospheroids treated with free drugs and drug-loaded NFs. 4T1 homospheroids were treated for 9 days with three doses of free drugs and three doses of double drug-loaded NFs and the boxplot analysis for DAY 9 is observed.*

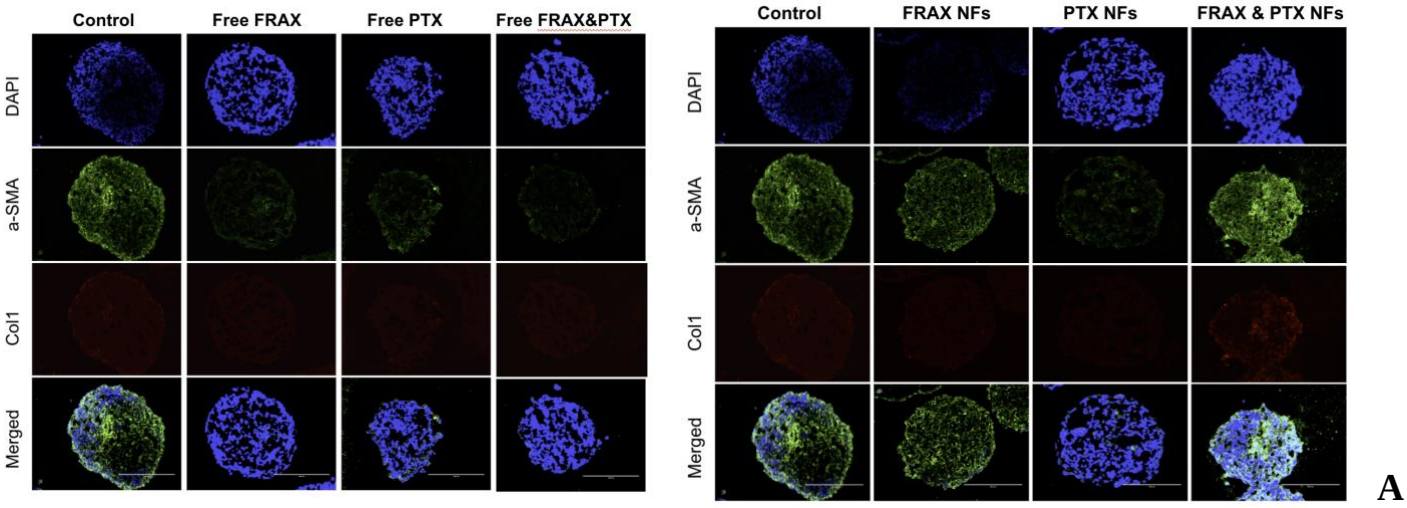

A

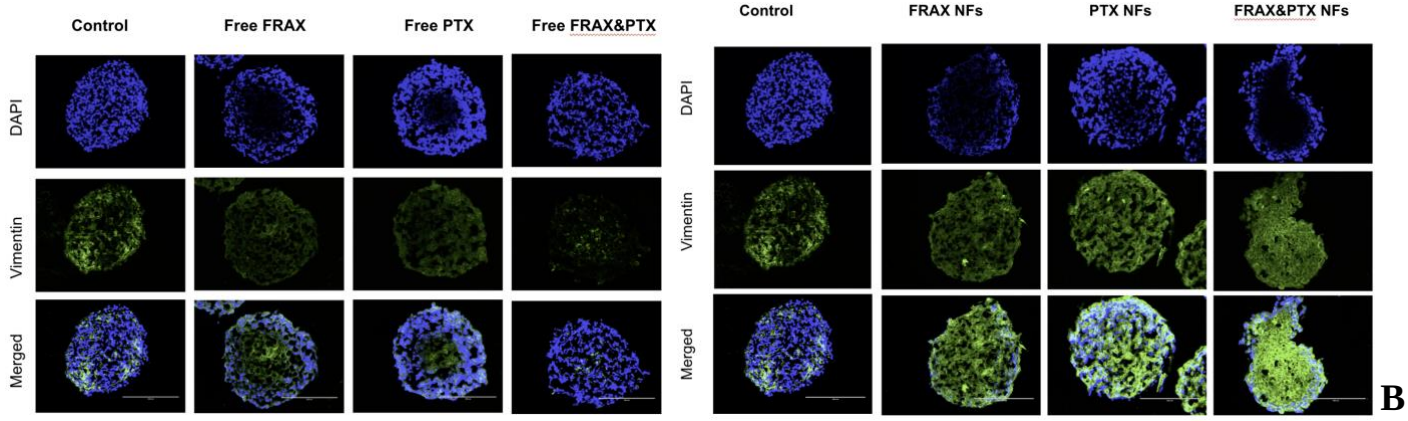

B

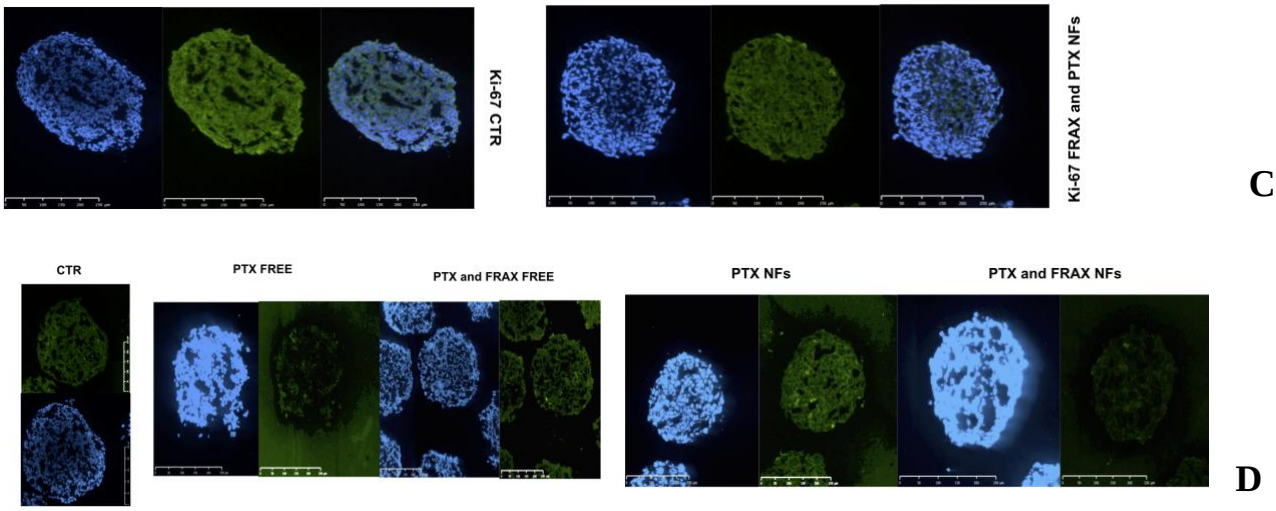

Figure S13: *Immunofluorescence (IF) staining on heterospheroids sections treated with free drug(s) or drug(s)-loaded nanofibers. (A) a-SMA/collagen1 IF staining (green: a-SMA, red: col1a and blue: DAPI for nucleus staining) , (B)Vimentin IF staining (green: Vimentin, and blue: DAPI for nucleus staining), (C) Ki-67 IF staining (green: Ki-67, and blue: DAPI for nucleus staining), and (D) E-cadherin IF staining (green: E-cadherin, and blue: DAPI for nucleus staining)*

Table S1: Used dilutions for immunocytochemistry and immunofluorescence staining.

Antibody	**Dilution ratio 1st antibody**	**Dilution ratio 2nd antibody (Fluorescent Ab)**
α-SMA (Sigma-Aldrich)	1/400	1/100 (Thermofisher Scientific, Waltham, MA, USA)
Col1a1 (Southern Biotech)	1/250	1/100 (Thermofisher Scientific, Waltham, MA, USA)
Vimentin (Santa Cruz Biotech)	1/100	1/100 (Thermofisher Scientific, Waltham, MA, USA)
Ki-67	1/200	1/100 (Thermofisher Scientific, Waltham, MA, USA)
E-cadherin	1/200	1/100 (Thermofisher Scientific, Waltham, MA, USA)

10. Bibliography

1. *World Health Organization 'Breast cancer'*. 2021 Available from: https://www.who.int/news-room/fact-sheets/detail/breast-cancer.
2. Sung, H., et al., *Global cancer statistics 2020: GLOBOCAN estimates of incidence and mortality worldwide for 36 cancers in 185 countries.* CA: a cancer journal for clinicians, 2021. **71**(3): p. 209-249.
3. Organization, W.H. *Cancer* 2021 [cited May 2021; Available from: https://www.who.int/news-room/fact-sheets/detail/cancer
4. Saria, M.G., *Overview of Cancer*, in *Your Guide to Cancer Prevention*, O.N. Society, Editor. 2017.
5. and T.A.C.S.m.a.e.c. team. *Treatment Types*. 2019 [cited 2021 May]; Available from: https://www.cancer.org/treatment/treatments-and-side-effects/treatment-types.html.
6. Gersten, T. *Cancer treatments*. Medical Encyclopedia 2021 [cited 2021 May]; Available from: https://medlineplus.gov/ency/patientinstructions/000901.htm.
7. *Treatments and Side Effects*. 2021 [cited 2021 May]; Available from: https://www.cancer.org/treatment/treatments-and-side-effects.html.
8. Liao, Z., et al., *Cancer-associated fibroblasts in tumor microenvironment–Accomplices in tumor malignancy.* Cellular Immunology, 2019. **343**: p. 103729.
9. Monteran, L. and N. Erez, *The Dark Side of Fibroblasts: Cancer-Associated Fibroblasts as Mediators of Immunosuppression in the Tumor Microenvironment.* Frontiers in Immunology, 2019. **10**(1835).
10. Sun, Q., et al., *The impact of cancer-associated fibroblasts on major hallmarks of pancreatic cancer.* Theranostics, 2018. **8**(18): p. 5072.
11. Sun, W. and S. Fu, *Role of cancer-associated fibroblasts in tumor structure, composition and the microenvironment in ovarian cancer.* Oncology letters, 2019. **18**(3): p. 2173-2178.
12. Anton, K. and J. Glod, *Tumor-Secreted Factors That Induce Mesenchymal Stromal Cell Chemotaxis.* Mesenchymal Stromal Cells as Tumor Stromal Modulators, 2016: p. 193.
13. Aalbersberg, I., et al., *Bringing Digital Science Deep Inside the Scientific Article: the Elsevier Article of the Future Project.* Liber Quarterly, 2014. **23**(4).
14. Liu, T., et al., *Cancer-associated fibroblasts: an emerging target of anti-cancer immunotherapy.* Journal of hematology & oncology, 2019. **12**(1): p. 1-15.
15. Liu, T., et al., *Cancer-associated fibroblasts build and secure the tumor microenvironment.* Frontiers in cell and developmental biology, 2019. **7**: p. 60.
16. Houthuijzen, J. and J. Jonkers, *Cancer-associated fibroblasts as key regulators of the breast cancer tumor microenvironment.* Cancer and Metastasis Reviews, 2018. **37**(4): p. 577-597.
17. Prakash, J., *Cancer-associated fibroblasts: perspectives in cancer therapy.* Trends in cancer, 2016. **2**(6): p. 277-279.
18. Sahai, E., et al., *A framework for advancing our understanding of cancer-associated fibroblasts.* Nature Reviews Cancer, 2020. **20**(3): p. 174-186.
19. Roma-Rodrigues, C., et al., *Targeting tumor microenvironment for cancer therapy.* International journal of molecular sciences, 2019. **20**(4): p. 840.
20. Bu, L., et al., *Functional diversity of cancer-associated fibroblasts in modulating drug resistance.* Cancer science, 2020. **111**(10): p. 3468.

21. Joyce, J.A., *Therapeutic targeting of the tumor microenvironment.* Cancer cell, 2005. **7**(6): p. 513-520.
22. Abu Samaan, T.M., et al., *Paclitaxel's mechanistic and clinical effects on breast cancer*. Biomolecules, 2019. **9**(12): p. 789.
23. Mitri, Z., T. Constantine, and R. O'Regan, *The HER2 receptor in breast cancer: pathophysiology, clinical use, and new advances in therapy.* Chemotherapy research and practice, 2012. **2012**.
24. Bejarano, L., M.J. Jordão, and J.A. Joyce, *Therapeutic Targeting of the Tumor Microenvironment.* Cancer Discovery, 2021. **11**(4): p. 933-959.
25. Hou, L., et al., *Nano-delivery of fraxinellone remodels tumor microenvironment and facilitates therapeutic vaccination in desmoplastic melanoma.* Theranostics, 2018. **8**(14): p. 3781.
26. Liu, M., W. Song, and L. Huang, *Drug delivery systems targeting tumor-associated fibroblasts for cancer immunotherapy.* Cancer letters, 2019. **448**: p. 31-39.
27. Yeo, D., et al., *FRAX597, a PAK1 inhibitor, synergistically reduces pancreatic cancer growth when combined with gemcitabine.* BMC cancer, 2016. **16**(1): p. 1-12.
28. Yeo, D., et al., *Inhibition of group 1 p21-activated kinases suppresses pancreatic stellate cell activation and increases survival of mice with pancreatic cancer.* International journal of cancer, 2017. **140**(9): p. 2101-2111.
29. Licciulli, S., et al., *FRAX597, a small molecule inhibitor of the p21-activated kinases, inhibits tumorigenesis of neurofibromatosis type 2 (NF2)-associated Schwannomas.* Journal of Biological Chemistry, 2013. **288**(40): p. 29105-29114.
30. Coleman, S.L., *Unsaturated Fatty Acids Repress the Expression of Adipose Fatty Acid-binding Protein, AP2, in Raw 264.7 Macrophage.* Nutrition & Health Sciences Dissertations & Theses, 2010: p. 5.
31. Wu, X.-F., et al., *Suppression of NF-κB signaling and NLRP3 inflammasome activation in macrophages is responsible for the amelioration of experimental murine colitis by the natural compound fraxinellone.* Toxicology and applied pharmacology, 2014. **281**(1): p. 146-156.
32. Roy, A. and S. Saraf, *Limonoids: overview of significant bioactive triterpenes distributed in plants kingdom.* Biological and Pharmaceutical Bulletin, 2006. **29**(2): p. 191-201.
33. Khodadadi, M., et al., *Recent advances in electrospun nanofiber-mediated drug delivery strategies for localized cancer chemotherapy.* Journal of Biomedical Materials Research Part A, 2020. **108**(7): p. 1444-1458.
34. Aquib, M., et al., *Advances in local and systemic drug delivery systems for post-surgical cancer treatment.* Journal of Materials Chemistry B, 2020. **8**(37): p. 8507-8518.
35. Asghari, S., Z. Rezaei, and M. Mahmoudifard, *Electrospun nanofibers: a promising horizon toward the detection and treatment of cancer.* Analyst, 2020. **145**(8): p. 2854-2872.
36. Cavo, M., et al., *Electrospun nanofibers in cancer research: from engineering of in vitro 3D cancer models to therapy.* Biomaterials Science, 2020. **8**(18): p. 4887-4905.
37. Long, Y.-Z., et al., *Electrospinning: the setup and procedure*, in *Electrospinning: nanofabrication and applications*. 2019, Elsevier. p. 21-52.
38. Sun, Y., et al., *Electrospun fibers and their application in drug controlled release, biological dressings, tissue repair, and enzyme immobilization.* RSC advances, 2019. **9**(44): p. 25712-25729.

39. Manuel, C.B.J., V.G.L. Jesús, and S.M. Aracely, *Electrospinning for drug delivery systems: Drug incorporation techniques.* Electrospinning-Material, Techniques, and Biomedical Applications, 2016: p. 14.
40. Hosne Ara Begum, M.K.R.K., *Study on the Various Types of Needle Based and Needleless Electrospinning System for Nanofiber Production.* International Journal of Textile Science, 2017: p. 110-117.
41. Shahriar, S., et al., *Electrospinning nanofibers for therapeutics delivery.* Nanomaterials, 2019. **9**(4): p. 532.
42. Nikmaram, N., et al., *Emulsion-based systems for fabrication of electrospun nanofibers: Food, pharmaceutical and biomedical applications.* RSC advances, 2017. **7**(46): p. 28951-28964.
43. Nagam Hanumantharao, S. and S. Rao, *Multi-functional electrospun nanofibers from polymer blends for scaffold tissue engineering.* Fibers, 2019. **7**(7): p. 66.
44. Bhattarai, R.S., et al., *Biomedical applications of electrospun nanofibers: Drug and nanoparticle delivery.* Pharmaceutics, 2019. **11**(1): p. 5.
45. Guarino, V., et al., *Polycaprolactone: synthesis, properties, and applications.* Encyclopedia of polymer science and technology, 2002: p. 1-36.
46. Torres-Martínez, E., et al., *Drugs loaded into electrospun polymeric nanofibers for delivery.* Journal of Pharmacy and Pharmaceutical Sciences, 2019. **22**: p. 313-331.
47. Mochane, M.J., et al., *Morphology and properties of electrospun PCL and its composites for medical applications: A mini review.* Applied Sciences, 2019. **9**(11): p. 2205.
48. Xiaoqian Shan, C.L., Fengqian Li, Chunfa Ouyang, Qun Gao & Kangsheng Zheng *Nanoparticles vs. nanofibers: a comparison of two drug delivery systems on assessing drug release performance in vitro.* Designed Monomers and Polymers, 2015: p. 678-689.
49. Xu, X., et al., *Ultrafine PEG–PLA fibers loaded with both paclitaxel and doxorubicin hydrochloride and their in vitro cytotoxicity.* European Journal of Pharmaceutics and Biopharmaceutics, 2009. **72**(1): p. 18-25.
50. Farboudi, A., et al., *Synthesis of magnetic gold coated poly (ε-caprolactonediol) based polyurethane/poly (N-isopropylacrylamide)-grafted-chitosan core-shell nanofibers for controlled release of paclitaxel and 5-FU.* International journal of biological macromolecules, 2020. **150**: p. 1130-1140.
51. Balakrishnan, P.B., et al., *Star poly (ε-caprolactone)-based electrospun fibers as biocompatible scaffold for doxorubicin with prolonged drug release activity.* Colloids and Surfaces B: Biointerfaces, 2018. **161**: p. 488-496.
52. Can-Herrera, L., et al., *Morphological and Mechanical Properties of Electrospun Polycaprolactone Scaffolds: Effect of Applied Voltage.* Polymers, 2021. **13**(4): p. 662.
53. Luraghi, A., F. Peri, and L. Moroni, *Electrospinning for drug delivery applications: A review.* Journal of Controlled Release, 2021.
54. Li, J.-J., et al., *Fast dissolving drug delivery membrane based on the ultra-thin shell of electrospun core-shell nanofibers.* European Journal of Pharmaceutical Sciences, 2018. **122**: p. 195-204.
55. Şimşek, M., *Tuning surface texture of electrospun polycaprolactone fibers: Effects of solvent systems and relative humidity.* Journal of Materials Research, 2020. **35**(3): p. 332-342.
56. ATCC. *4T1*
. Cell Products 2021 [cited 2021 June]; Available from: https://www.atcc.org/products/crl-2539.

57. Ho, B.-Y., et al., *Silibinin and paclitaxel cotreatment significantly suppress the activity and lung metastasis of triple negative 4T1 mammary tumor cell in mice.* Journal of traditional and complementary medicine, 2012. **2**(4): p. 301-311.
58. Chen, Y., et al., *An immunostimulatory dual-functional nanocarrier that improves cancer immunochemotherapy.* Nature communications, 2016. **7**(1): p. 1-12.
59. Gupta, N., P. Gupta, and S.K. Srivastava, *Penfluridol overcomes paclitaxel resistance in metastatic breast cancer.* Scientific reports, 2019. **9**(1): p. 1-14.
60. Woodroof, E.A., et al., *The search for an ideal temporary skin substitute: AWBAT Plus, a combination product wound dressing medical device.* Eplasty, 2010. **10**.
61. Sun, Q., et al., *TGF-β upregulated mitochondria mass through the SMAD2/3→ C/EBPβ→ PRMT1 signal pathway in primary human lung fibroblasts.* The Journal of Immunology, 2019. **202**(1): p. 37-47.
62. Ong, C.C., et al., *Targeting p21-activated kinase 1 (PAK1) to induce apoptosis of tumor cells.* Proceedings of the National Academy of Sciences, 2011. **108**(17): p. 7177-7182.
63. Lu, W., et al., *Overexpression of p21-activated kinase 1 promotes endometrial cancer progression.* Oncology reports, 2013. **29**(4): p. 1547-1555.
64. Gururaj, A.E., S.K. Rayala, and R. Kumar, *p21-activated kinase signaling in breast cancer.* Breast Cancer Research, 2004. **7**(1): p. 1-8.
65. Kumar, R. and M.-C. Hung, *Signaling intricacies take center stage in cancer cells.* Cancer research, 2005. **65**(7): p. 2511-2515.
66. Liu, H., K. Liu, and Z. Dong, *The Role of p21-Activated Kinases in Cancer and Beyond: Where Are We Heading?* Frontiers in cell and developmental biology, 2021. **9**: p. 325.
67. Varan, G., et al., *Therapeutic Efficacy and Biodistribution of Paclitaxel-Bound Amphiphilic Cyclodextrin Nanoparticles: Analyses in 3D Tumor Culture and Tumor-Bearing Animals In Vivo.* Nanomaterials, 2021. **11**(2): p. 515.
68. Nishishita, R., et al., *Expression of cancer-associated fibroblast markers in advanced colorectal cancer.* Oncology letters, 2018. **15**(5): p. 6195-6202.
69. Liu, C.-Y., et al., *Vimentin contributes to epithelial-mesenchymal transition cancer cell mechanics by mediating cytoskeletal organization and focal adhesion maturation.* Oncotarget, 2015. **6**(18): p. 15966.
70. Inwald, E., et al., *Ki-67 is a prognostic parameter in breast cancer patients: results of a large population-based cohort of a cancer registry.* Breast cancer research and treatment, 2013. **139**(2): p. 539-552.
71. Singhai, R., et al., *E-Cadherin as a diagnostic biomarker in breast cancer.* North American journal of medical sciences, 2011. **3**(5): p. 227.
72. Eltoum, I., J. Fredenburgh, and W.E. Grizzle, *Advanced concepts in fixation: 1. Effects of fixation on immunohistochemistry, reversibility of fixation and recovery of proteins, nucleic acids, and other molecules from fixed and processed tissues. 2. Developmental methods of fixation.* Journal of Histotechnology, 2001. **24**(3): p. 201-210.